



저작자표시-비영리-변경금지 2.0 대한민국

이용자는 아래의 조건을 따르는 경우에 한하여 자유롭게

- 이 저작물을 복제, 배포, 전송, 전시, 공연 및 방송할 수 있습니다.

다음과 같은 조건을 따라야 합니다:



저작자표시. 귀하는 원저작자를 표시하여야 합니다.



비영리. 귀하는 이 저작물을 영리 목적으로 이용할 수 없습니다.



변경금지. 귀하는 이 저작물을 개작, 변형 또는 가공할 수 없습니다.

- 귀하는, 이 저작물의 재이용이나 배포의 경우, 이 저작물에 적용된 이용허락조건을 명확하게 나타내어야 합니다.
- 저작권자로부터 별도의 허가를 받으면 이러한 조건들은 적용되지 않습니다.

저작권법에 따른 이용자의 권리는 위의 내용에 의하여 영향을 받지 않습니다.

이것은 [이용허락규약\(Legal Code\)](#)을 이해하기 쉽게 요약한 것입니다.

[Disclaimer](#)

공학석사 학위논문

**Punching Shear Strength of RC
Interior Slab-Column Connections
Retrofitted by UHPC overlay**

초고성능 콘크리트로 보강된 RC 내부 슬래브-
기둥 접합부의 뚫림 전단 강도

2017 년 8 월

서울대학교 대학원

건축학과

염 현 수

Punching Shear Strength of RC Interior Slab-Column Connections Retrofitted by UHPC overlay

지도 교수 홍 성 결

이 논문을 공학석사 학위논문으로 제출함
2017 년 8 월

서울대학교 대학원
건축학과
염 현 수

염현수의 공학석사 학위논문을 인준함
2017 년 8 월

위 원 장 _____ (인)

부위원장 _____ (인)

위 원 _____ (인)

Abstract

Punching Shear Strength of RC Interior Slab-Column Connections Retrofitted by UHPC overlay

Youm, Hyun Soo

Department of Architecture and Architectural Engineering
College of Engineering
Seoul National University

The flat plate system is subjected to the combination of locally high negative bending moments and shear forces around the columns, which increases the susceptibility of this zone to brittle punching shear failure. The punching shear failure, in other words, two-way shear failure, is one of the most widely reported types of failure in buildings with flat plate system. As can be observed in many collapse accidents, it may eventually lead to a hazardous progressive collapse of the entire structure, accompanied by a truncated cone above the column. Therefore, various retrofitting strategies have been investigated and can be applied to it to improve its performance. The topping a layer of cementitious composite material is one of the retrofitting strategy generally used in working place due to its economic efficiency and ease of construction. The insufficiency of punching shear capacity can be retrofitted by adding a thin layer of UHPC with or without steel re-bars over existing RC section.

Ultra-High Performance Concrete (UHPC), developed in the mid-1990s, is a new material which has attracted many researchers and engineers for practical construction applications in structures owing to its splendid mechanical performances. Additionally, it was demonstrated by previous study that the UHPC overlay increases structural rigidity, and bending and shear strength of RC slab-column connections. However, the punching shear strength of such composite members is not defined in current design codes.

The present study, thus, focusing on how the UHPC overlay contributes to the structural response of the UHPC-RC composite slab, a set of concentric loading tests was conducted to evaluate the punching shear resistance of the RC slab-column connections retrofitted by the UHPC overlay. Five specimens were constructed on half scale and designed to be failed in punching shear mode. The test variables are the UHPC overlay thickness (0mm, 30mm, and 50mm) and the amount of steel re-bars in it (0, D10@180mm, and D10@90mm). Before casting the UHPC overlay, surface of all retrofitting targets was roughened by sand-blasting method. The test results showed that by adding a thin layer of UHPC over the RC substrates, considerable increases in global punching shear resistance and structural rigidity were achieved. Furthermore, two governing failure modes based on the cracking patterns were observed: 1) diagonal shear failure in RC section (Mode 1) and 2) debonding failure at the interface (Mode 2). For verifying applicability of current design expressions, refined design expressions by reflecting the retrofitting effect in the form of effective flexural depth and effective reinforcement ratio were discussed, however, were still conservative.

Based on the test results, an analytical method to evaluate the structural response of the UHPC-RC composite slab was proposed based on CSCT with slight modification. To estimate each contribution of the UHPC overlay and the RC substrate to the global punching shear resistance, two free body

diagrams were formulated from a slab portion. Additionally, focusing on the observed governing failure modes, two capacity curves were proposed. The predicted failure mode and maximum punching shear resistance, then, were determined by the intersection point of the demand curve and one of the capacity curves occurring at smaller slab rotation. For the validation, the experimental results were compared with the predicted results by the proposed method. The predictions show a good agreement with the test results with a small value of COV(=2.26%) and the closest average to 1.0(=1.003).

Keywords : CSCT; Punching shear strength; Retrofit; Slab-column connection; UHPC overlay

Student Number : 2015-22846

Contents

Abstract	i
Contents	iv
List of Tables.....	vii
List of Figures	viii
List of Symbols	xii
Chapter 1. Introduction	1
1.1 General.....	1
1.2 Necessity.....	4
1.3 Scope and Objectives	6
1.4 Outline of Thesis	7
Chapter 2. Literature Review	9
2.1 Overview.....	9
2.2 UHPC (Ultra-High Performance Concrete), As a Repair Material	9
2.2.1 General and composition of UHPC	9
2.2.2 Material properties of UHPC.....	10
2.2.3 Curing of UHPC	11
2.2.4 Advantages of the use of UHPC	12
2.3 Punching Shear Strength	14

2.3.1 Kinnunen and Nylander (1960)	14
2.3.2 Muttoni (2008).....	16
2.4 Interfacial Bond Strength between UHPC and Concrete	19
2.4.1 Tayeh et al. (2013)	19
2.4.2 Carbonell Muñoz et al. (2014).....	20
2.4.3 Lim and Hong (2016).....	20
2.5 RC Members Retrofitted by Cement-Based overlay.....	22
2.5.1 Rocha (2012)	22
2.5.2 Hable et al. (2006)	23
2.5.3 Noshiravani and Brühwiler (2013, 2014).....	24
2.5.4 Bastien-Masse (2015)	25
Chapter 3. Current Code Provisions	28
3.1 ACI 318-11 (2011)	28
3.2 KCI 2012 (2012)	29
3.3 Eurocode 2 (2004).....	32
3.4 JSCE (2010).....	34
Chapter 4. Specimen Design and Test Set-up	37
4.1 Introduction.....	37
4.2 Design Concept	37
4.3 Construction and Detail of Test Specimens	40
4.4 Test Set-up	48
4.5 Materials	53
Chapter 5. Concentric Loading Test of UHPC-RC Composite Slab	60
5.1 Introduction.....	60
5.2 Test Results	63

5.2.1 Load vs displacement relationships	63
5.2.2 Cracking patterns	73
5.2.3 Thickness variation	81
5.2.4 Crack opening in tension surface.....	83
5.2.5 Strain in steel re-bars.....	86
5.2.6 Strain in concrete compressive surface	89
5.3 Punching Shear Strength Predictions	93
5.4 Discussion.....	105
Chapter 6. Theoretical Analysis.....	108
6.1 Failure Mechanism	108
6.2 Proposed Analytical Method.....	110
6.2.1 Overview	110
6.2.2 Moment-curvature relationship of UHPC-RC composite section	116
6.2.3 Load-rotation behavior of UHPC-RC composite slab	127
6.2.4 Proposed capacity curves	136
6.3 Validation of the Proposed Method.....	142
6.4 Limitation of the Proposed Method	144
Chapter 7. Concluding Remarks	146
References.....	150
국문초록.....	155

List of Tables

Table 2-1. Durability results of UHPC subjected to different curing (Graybeal, 2006).....	11
Table 4-1. Dimensions and reinforcement details of specimens.....	46
Table 4-2. Design parameters of test specimens	47
Table 4-3. Material composition of NSC.....	53
Table 4-4. Material properties of NSC	54
Table 4-5. Material composition of UHPC.....	54
Table 4-6. Material properties of UHPC.....	55
Table 4-7. Material properties of steel reinforcements.....	56
Table 5-1. Comparison of increasing ratios between strength and self weight.....	61
Table 5-2. Experimental test results	62
Table 5-3. Effective flexural depth and reinforcement ratio of specimens	95
Table 5-4. Effective flexural depth and effective reinforcement ratio of specimens of previous studies	97
Table 5-5. Comparison of strength ratios of specimens predicted by refined code provisions (strategy 1).....	99
Table 5-6. Comparison of strength ratios of specimens predicted by refined code provisions (strategy 2).....	100
Table 6-1. Collapse mechanisms.....	109
Table 6-2. Collected test data from four literatures on interface performance.....	138
Table 6-3. Comparison between experimental test results and predictions	142

List of Figures

Fig 1-1. Flat plate system.....	1
Fig 1-2. Failure of slab-column connections due to punching shear	2
Fig 1-3. Different shear resistance mechanism of FRP and UHPC overlay.....	5
Fig 2-1. Classification of UHPC	11
Fig 2-2. Mechanical model of Kinnunen/Nylander (Kinnunen and Nylander, 1960)	16
Fig 2-3. Concept of CSCT (Muttoni, 2008).....	18
Fig 2-4. Description of configuration and the analytical model of UHPFRC-concrete elements (Hable et al., 2006).....	23
Fig 2-5. Fictitious Composite Hinge model (Noshiravani and Brühwiler, 2014)	24
Fig 2-6. UHPFRC resisting mechanism (a) out-of-plane bending mechanism; (b) efforts in the UHPFRC sector element (Bastien-Masse, 2015)	27
Fig 3-1. Critical section according to ACI 318-11 and KCI 2012.....	32
Fig 3-2. Typical basic control perimeters (EC2, 2004).....	32
Fig 3-3. Typical design cross section (JSCE, 2010).....	35
Fig 4-1. Proto type of the study.....	38
Fig 4-2. Specimen modelling for test	39
Fig 4-3. Specification of retrofitting target	40
Fig 4-4. Casting sequence of RC specimen	41
Fig 4-5. Machine and comparison of surfaces before and after sandblasting	43
Fig 4-6. Casting sequence of UHPC overlay	44
Fig 4-7. Photo of test set-up.....	49

Fig 4-8. Test set-up and disposition of LVDTs.....	50
Fig 4-9. Disposition of PI-type and strain gauges at concrete surfaces	51
Fig 4-10. Disposition of strain gauges at steel reinforcement in RC section	52
Fig 4-11. Test set-ups for compressive and tensile strength of UHPC .	55
Fig 4-12. Test set-ups for tensile strength of steel re-bars	56
Fig 4-13. NSC compressive strength used in tests	57
Fig 4-14. UHPC compressive and tensile strength used in tests.....	58
Fig 4-15. Steel rebar yield and tensile strength used in tests	59
Fig 5-1. Load-displacement relationship (a) and deformed shapes (b) of R.....	64
Fig 5-2. Load-displacement relationship (a) and deformed shapes (b) of U30.....	67
Fig 5-3. Load-displacement relationship (a) and deformed shapes (b) of U50.....	68
Fig 5-4. Load-displacement relationship (a) and deformed shapes (b) of U50S.....	69
Fig 5-5. Load-displacement relationship (a) and deformed shapes (b) of U50L	70
Fig 5-6. Load-deformation relationships of specimens	71
Fig 5-7. Fully developed cracking patterns of R specimen.....	75
Fig 5-8. Fully developed cracking patterns of U30 specimen	76
Fig 5-9. Fully developed cracking patterns of U50 specimen	77
Fig 5-10. Fully developed cracking patterns of U50S specimen	78
Fig 5-11. Fully developed cracking patterns of U50L specimen.....	79
Fig 5-12. Typical failure cracks developed in UHPC-RC composite slabs.....	80
Fig 5-13. Change of thickness in two locations (south and north).....	82
Fig 5-14. Crack opening in radial (left) and tangential (right) directions	84

Fig 5-15. Relationship between tensile behavior of UHPFRC and crack openings	85
Fig 5-16. Measured strains of re-bars in RC section of R	86
Fig 5-17. Measured strains of re-bars in RC section of U30	87
Fig 5-18. Measured strains of re-bars in RC section of U50	87
Fig 5-19. Measured strains of re-bars in RC section of U50S	88
Fig 5-20. Measured strains of re-bars in RC section of U50L	88
Fig 5-21. Comparison of measured strain of top re-bars in RC section	89
Fig 5-22. Measured compressive strain in R.....	90
Fig 5-23. Measured compressive strain in U30.....	91
Fig 5-24. Measured compressive strain in U50.....	91
Fig 5-25. Measured compressive strain in U50S.....	92
Fig 5-26. Measured compressive strain in U50L	92
Fig 5-27. Two strategies for application of code design expressions ...	93
Fig 5-28. Comparisons of test results with strengths provided by design expressions	98
Fig 5-29. Experimental values dependent on critical parameters	101
Fig 5-30. Strength ratios of specimens predicted by refined ACI 318-11	103
Fig 5-31. Strength ratios of specimens predicted by refined KCI 2012	103
Fig 5-32. Strength ratios of specimens predicted by refined Eurocode2	104
Fig 5-33. Strength ratios of specimens predicted by refined JSCE	104
Fig 6-1. Two governing failure modes.....	109
Fig 6-2. Typical demand and capacity curves for RC and UHPC-RC composite slabs.....	111
Fig 6-3. Proposed method by Bastien-Masse (2015)	112
Fig 6-4. Strength ratios of test strength to prediction by proposed	

method by Bastein-Masse (2015)	113
Fig 6-5. Proposed flow chart to analyze UHPC-RC composite slab..	115
Fig 6-6. Modelling of material constitutive laws	118
Fig 6-7. Moment-curvature relationship of UHPC-RC composite section	125
Fig 6-8. Calculated moment-curvature relationship of retrofitted specimens	126
Fig 6-9. Idealized slab under simply supported conditions	127
Fig 6-10. Prediction of load-rotation behavior of R through assumed rs and rq	128
Fig 6-11. Uncracked and cracked stage of UHPC-RC composite slab portion	129
Fig 6-12. Two sets of free body diagram of UHPC-RC composite slab	130
Fig 6-13. Computation of two-dimensional interface shear stress under pure shear	131
Fig 6-14. Modelling the interface as Mohr-Coulomb material	139
Fig 6-15. Typical load-rotation behavior and capacity curves depending on governing failure modes	141
Fig 6-16. Comparison between load-rotation curves and predictions	143
Fig 6-17. Moment at column face depending on discontinuity.....	145

List of Symbols

- $V_R(\psi)$ = total punching shear force
 $V_c(\psi)$ = concrete contribution to punching shear resistance
 V_U = UHPFRC contribution to punching shear resistance
 b_0 = Critical perimeter for punching shear set at $d_{sc}/2$ from the column face
 d_{sc} = flexural depth for tensile reinforcement in RC section
 f_c' = concrete compressive strength
 f_{ct} = concrete tensile strength
 E_c = young's modulus of normal strength concrete
 ψ = slab rotation
 d_{g0} = reference aggregate size set at 16mm
 d_g = Maximum diameter of aggregate
 h_c = height of RC section
 d_U = height of UHPFRC overlay
 r_U = radius of tip of inclined crack at the top of the slab located at $h_c + h_U$ from the column side
 V_n = nominal shear strength
 V_c = nominal shear strength provided by concrete
 λ = modification factor reflecting the reduced mechanical properties of lightweight concrete
 β = ratio of long to short sides of column, concentrated load or reaction area
 b_0 = critical perimeter
 d = distance from extreme compression fiber to centroid of longitudinal tension reinforcement
 α_s = Constant used to compute V_c in slabs and footings, take 40 for interior columns, 30 for edge columns, and 20 for corner columns

λ	=	modification factor reflecting the reduced mechanical properties of lightweight concrete
v_c	=	nominal shear stress of concrete
b_0	=	critical perimeter
d	=	distance from extreme compression fiber to centroid of longitudinal tension reinforcement
k_s	=	size effect factor
k_{bo}	=	aspect ratio factor
f_{te}	=	effective tensile strength reduced by the transverse compressive stress
Ψ	=	crack angle of slab in flexure zone
c_u	=	depth of compression zone, neglecting compressive reinforcement
f_{cc}	=	mean value of compressive stress applying to compression zone at critical section
α_s	=	coefficient factor when deciding V_c in two-way slab or footing slab; take 1.0 for interior columns, 1.33 for edge columns, and 2.0 for corner columns
ρ	=	the ratio of flexural tensile reinforcement
$v_{Rd,c}$	=	design value of the punching shear resistance of a slab without punching shear reinforcement along the control section considered
f_{ck}	=	characteristic compressive cylinder strength of concrete at 28 day
k	=	coefficient considering size effect
k_1	=	0.1
σ_{cp}	=	compressive stress in the concrete from axial load or prestressing, MPa
ρ_l	=	reinforcement ratio for longitudinal reinforcement
ρ_{ly}, ρ_{lz}	=	reinforcement ratio for longitudinal reinforcement in y- and z- directions respectively, within a slab width equal to the column width plus 3d each side
d	=	effective depth of the cross section
f'_{pcd}	=	design compressive strength of concrete
u	=	peripheral length of loaded area

List of Symbols

- u_p = peripheral length of the design cross section located at a distance $d/2$ from the loaded area
- d = effective depth defined as the average values for the reinforcement in two directions
- p = reinforcement ratio defined as the average values for the reinforcement in two directions
- γ_b = member factor, may generally be taken as 1.3
- B = side length of slab specimen
- r_q = radius of supports from force introduction
- C = side length of column
- h_c = thickness of RC section
- h_U = thickness of UHPC overlay
- d_{sc} = effective flexural depth from the extreme compression fiber to the centroid of tension steel rebars in RC section
- d_{sU} = effective flexural depth from the extreme compression fiber to the centroid of steel rebars in UHPC overlay
- l_f = length of steel fiber
- d_f = diameter of steel fiber
- V_f = volume fraction of steel fiber
- f_{cU} = UHPFRC compressive strength
- f_{Ute} = maximum tensile elastic strength of UHPFRC
- f_{Uu} = tensile strength of UHPFRC
- E_U = young's modulus of UHPFRC, calculated as specified in K-UHPC 2012
- V_{flex} = flexural strength
- α = average of diagonal shear crack angle
- α_N = diagonal shear crack angle at north direction
- α_S = diagonal shear crack angle at south direction
- Δ_{cr} = center displacement at cracking load stage
- Δ_u = center displacement at ultimate load stage
- $\Delta_{failure}$ = center displacement at failure load stage

V_{cr}	=	cracking load
V_u	=	ultimate load
$V_{failure}$	=	failure load
d_{eff}	=	effective flexural depth considering the existence of UHPC overlay
ρ_{eff}	=	effective reinforcement ratio considering the existence of UHPC overlay
ρ_U	=	reinforcement ratio of UHPC overlay
d_U	=	flexural depth of UHPC overlay
$f_{sc, sy}$	=	yield strength of tensile steel rebars in RC section
$f_{sU, sy}$	=	yield strength of tensile steel rebars in UHPC overlay
E_s	=	young's modulus of steel rebars in RC section
E_{sU}	=	young's modulus of steel rebars in UHPC overlay
V_{pcd}	=	design punching shear strength of UHPC slab, N
ϕ_b	=	member reduction factor, generally 0.77
f_{vd}	=	design average tensile strength in the direction perpendicular to the diagonal tensile crack of UHPC
w_v	=	$\max (w_u, 0.3\text{mm})$
ϕ_c	=	material reduction factor considering the orientation of the steel fibers, 0.8
$\sigma_k(w)$	=	tension-softening curve of UHPC as defined in K-UHPC
u_p	=	circumferential length of design cross section, computed at the position located at a distance $d/2$ from the loaded face
d	=	effective depth, which can be assumed to be 80% of the thickness of the deck
$V_{d, strategy1}$	=	design punching shear strength calculated by strategy 1
$V_{d, strategy2}$	=	design punching shear strength calculated by strategy 2
V_{test}	=	punching shear force obtained by test results
V_{ACI}	=	design punching shear strength calculated by ACI 318-11 code provisions
V_{KCI}	=	design punching shear strength calculated by KCI 2012 code provisions

List of Symbols

V_{EC2}	=	design punching shear strength calculated by Eurocode 2 code provisions
V_{JSCE}	=	design punching shear strength calculated by JSCE code provisions
ε_{Utu}^{RU}	=	strain corresponding to tensile strength of R-UHPC tension chord
ε_{Ute}	=	strain corresponding to maximum tensile elastic strength of UHPC
w_{Ulim}	=	crack mouth opening at limit state ($=l_f / 2$)
w_{Utu}^{RU}	=	crack mouth opening at ε_{Utu}^{RU}
E_U^{RU}	=	young's modulus of R-UHPC tension chord at elastic stage
E_{Ush}^{RU}	=	young's modulus of R-UHPC tension chord at strain-hardening stage
E_{Uss}^{RU}	=	young's modulus of R-UHPC tension chord at strain-softening stage
x_{el}	=	compression depth at elastic stage
x_{sh}	=	compression depth at strain-hardening stage
x_{Ut}	=	compression depth at cracked-hardening stage
x_{sy}	=	compression depth at cracked-hardening 2 stage
x_{end}	=	compression depth at softening-yielding stage
χ_{sh}	=	strain-hardening curvature
χ_{cr}	=	concrete cracking curvature
χ_{ts}	=	decrease in curvature due to tension stiffening
χ_1	=	stabilized cracking curvature
χ_{Ut}	=	cracked-hardening curvature
χ_{sy}	=	cracked-hardening 2 curvature
χ_{end}	=	softening-yielding curvature
m_{sh}	=	strain-hardening moment per unit width
m_{cr}	=	cracking moment per unit width
m_1	=	m_{cr}
m_{Ut}	=	cracked-hardening moment per unit width

- m_{sy} = cracked-hardening 2 moment per unit width
- m_{end} = softening-yielding moment per unit width
- EI_0 = elastic flexural rigidity
- $EI_{0,1}$ = flexural rigidity after UHPC cracking
- EI_1 = flexural rigidity after concrete cracking
- EI_2 = flexural rigidity after tensile strength of UHPC is reached
- EI_3 = flexural rigidity after steel in RC section yields
- β = factor considering orthogonal reinforcement(0.6~0.75)

Chapter 1. Introduction

1.1 General

In the 1950s, reinforced concrete (hereinafter referred to as RC) flat plate systems started to become prevalent because of its simplicity, functional benefits than other structural systems. The flat plate system is a simple structural system consisting only of slab and columns without any beams, drop panels, or column capitals as shown in **Fig 1-1**. Nowadays, this construction system has been widely used around the world, thanks to these economic and functional benefits; flexible floor plan, relatively smaller floor to floor height, larger available space and ease of construction. In addition to parking garages, medium height residential and office buildings have been constructed in the form of the flat plate systems (Muttoni, 2008). Despite its simple appearance, a flat plate system has a complex shear behavior, which is still under debate.



Fig 1-1. Flat plate system

The flat plate systems are subjected to the combination of locally high negative bending moments and shear forces around the slab-column

connections, which increases the susceptibility of this zone to brittle punching shear failure. The punching shear or two-way shear is often the critical failure mode for the design of RC floor and deck slabs. This failure mechanism forms a truncated cone or a truncated pyramid separated from the rest of the slab by the shear crack. Therefore, as can be seen in many collapse accidents, punching shear failure can eventually trigger to a hazardous progressive collapse of the entire structures, reported as shown in **Fig 1-2**.



Fig 1-2. Failure of slab-column connections due to punching shear

Additionally, many existing buildings constructed with the flat plate systems are becoming obsolete. In this trend, it is significantly emphasized to investigate reinforcing the RC slab-column connections against punching shear failure.

To date, various methods have been proposed and used for strengthening existing slab-column connections against punching shear failure: 1) enlargement of the column section and slab thickness, or use a shear capital and a drop panel, 2) post-installed shear reinforcement such as stirrups or shear bands, 3) pre-stressing and 4) increasing of the amount of flexural reinforcement. This last method has been widely investigated to increase the punching shear resistance of slab-column connections by attaching CFRP (Carbon Fiber-Reinforced Polymer), GFRP (Glass Fiber-Reinforced Polymer), and steel plate, etc. to the tensile surface. However, these methods have a long

construction process and need a lot of labor. In addition, these methods are not capable of reducing permeability that causes cracks and corrosion of steel re-bars placed in RC structures.

Alternatively, placing a thin layer of cementitious composite material on top surface of RC members can be one of the most efficient, and practical method for field application among several retrofitting methods. Previous studies have carried out several experimental campaigns on normal strength concrete overlay (Rocha, 2012). Although, the existing normal strength concrete overlay method is actually ineffective method in architectural viewpoint. It is because not only several transverse reinforcements have to be arranged in the enlarged section, which may cause additional damage to existing buildings, but also the existing buildings' self-weight considerably increases due to thick overlay thickness to improve load carrying capacity of the slab-column connections. To resolve this problem, a new material comes to the fore; Ultra-High Performance Concrete (UHPC). Its high performance material properties can reduce the thickness of the retrofitting overlay, and be expected that the steel fibers mixed in the UHPC can play a significant role of the reinforcements. In addition, it is possible to cast the UHPC overlay directly on the suitably prepared existing concrete surface without any mechanical shear connectors or bonding materials, such as epoxy resin used to attach steel plates or FRP sheets. According to the previous researches (Hable et al, 2006, Noshiravani and Brühwiler, 2013, Bastien-Masse, 2015), the UHPC overlay greatly improves the shear resistance, as well as the flexural rigidity by acting as a two-dimensional reinforcement. From an economical view point, this advantage attributed to the material outstanding properties ultimately leads to lower consuming of material, money and time. However, there exist very little researches related to the retrofitting effect of the UHPC overlay method.

1.2 Necessity

As described in previous paragraphs, the punching shear failure is one of the most devastating failure aspects, which is known to be abrupt and able to trigger a progressive collapse of the whole structures, leading to an enormous material loss and a large number of casualties. Therefore, not only because of these failures but also generally due to the increasing number of aging structures, the need for the strengthening of existing concrete slabs against punching shear is significantly increasing. Many methods to strengthen and rehabilitate existing RC slab-column connections have been developed to overcome the deficient punching shear resistance, especially in the way of increasing the amount of flexural tensile reinforcement; FRP sheets, steel plate, concrete overlay with shear connectors and recently, UHPC overlay.

The use of FRP sheets to increase the punching shear resistance has been widely investigated by various authors. As expected, the slabs with FRP attached on the tension side have a stiffer behavior. The FRP sheet also delays and controls the development of inclined cracking in the RC slab. However, even though the punching shear resistance of the slab reinforced with FRP is higher, smaller deformations at maximum resistance and no yielding of external reinforcement are noticed, which means ductility is reduced contrary to the original intention. On the other hand, it has been reported that an additional UHPC overlay can not only greatly increase the maximum punching shear strength, but also almost maintain rotational capacity of reference RC slab. It can be attributed to different shear resistance mechanism of the UHPC overlay from that of conventional FRP sheets as roughly described in **Fig 1-3**, which makes it an unusual and exclusive method to use of the UHPC overlay. Thus, an experimental campaign on UHPC-RC composite slabs is necessary to understand how the UHPC overlay acts as a

two-dimensional reinforcement and how it modifies the structural behavior and load carrying capacity of the two-way slab-column connections.

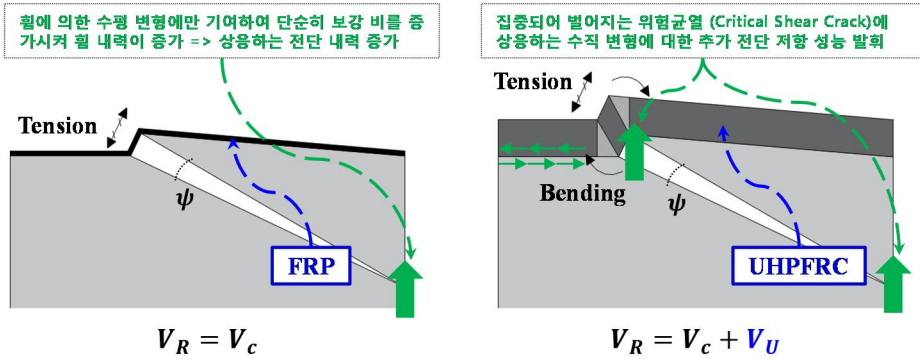


Fig 1-3. Different shear resistance mechanism of FRP and UHPFRC overlay

1.3 Scope and Objectives

The primary objectives of this thesis are to verify the applicability of a thin layer of UHPC acting as a two-dimensional tensile reinforcement over RC slab-column connections for shear design, and ultimately, to propose an analytical method to evaluate the structural behavior of the UHPC-RC composite slab. To achieve the objective, monotonic loading tests of RC slab-column connections with UHPC overlay with or without steel re-bars were performed. The test results were thoroughly investigated focusing on load-deformation behavior, cracking patterns and failure modes. Based on the efforts, the following objectives can be achieved.

As a study of the applicability of a thin layer of UHPC acting as a two-dimensional tensile reinforcement over RC slab-column connections, the first objective of this thesis is to discuss to use refined design expressions of current code provisions considering the effective flexural depth and the effective reinforcement ratio. Through this process, not only the applicability of the refined design expressions was discussed, but also demand for further evaluation about the contribution of the UHPC overlay was emphasized.

Next, on the basis of test results, especially focusing on cracking patterns and failure modes, the second objective of this thesis is to propose a new analytical method to estimate contribution of the UHPC overlay and the RC substrate to global shear resistance. In the present study, thus, a physically sound model, CSCT was adopted and slightly modified to derive an analytical model. To validate the proposed analytical method, the experimental results were compared with the predicted results by the proposed method.

1.4 Outline of Thesis

The present thesis is an attempt to estimate the punching shear capacity of RC slab-column connections retrofitted by a thin layer of UHPC with or without steel re-bars under monotonic loading at centrally located column. Therefore, to achieve the goal, this thesis is organized into six main chapters.

In **Chapter 2**, review of previous studies, which derived analytical models performed on evaluating punching shear strength of RC slab was conducted. Also, studies on interfacial bond strength between UHPC and concrete were researched, since the performance level of the interface may determine the overall behavior and maximum resistance of UHPC-RC composite members. Lastly, experiential studies and previously proposed analytical methods for analyzing structural behavior of UHPC-RC composite members were thoroughly investigated.

In **Chapter 3**, current design expressions for punching shear capacity of conventional RC slab were reviewed especially focusing on which parameters are dominant in determining the punching shear strength.

In **Chapter 4**, design purpose and manufacturing process of test specimens were explained in detail. Furthermore, test set-up and material characteristics used in the present study were also discussed.

In **Chapter 5**, a set of experimental study on punching shear resistance of RC slab-column connections retrofitted by UHPC overlay with or without steel re-bars was performed, focusing on the effect of the UHPC overlay on global punching shear resistance. The major test variables were the UHPC overlay thickness (0mm, 30mm, and 50mm), and the amount of steel re-bars

placed in it (0, D10@180mm, and D10@90mm). The test results were compared with the predicted results by using refined design expressions considering the effective flexural depth and the effective reinforcement ratio. Based on the comparison of the results, it was confirmed that the UHPC overlay contributes to the improvement of the global punching shear resistance by additional load-carrying mechanism.

In **Chapter 6**, an analytical method for predicting the behavior and maximum shear resistance of the UHPC-RC composite slab was proposed based on the modified CSCT. For validation, the test results were compared with the predicted results by the proposed method

Finally, summary and conclusions were presented in **Chapter 7**.

Chapter 2. Literature Review

2.1 Overview

This section provides a review of the UHPC, as a new rehabilitating material and the literature on experimental studies of slab retrofitted with cement-based overlay designed to fail in brittle punching shear. Also, the literature on experimental studies of interface shear transfer between different concrete, or different casting time, which should be mentioned to suitably understand the shear carrying mechanisms of UHPC-RC composite slabs. Punching shear capacities and interface shear capacities treated in several design codes of practice will also be covered.

2.2 UHPC (Ultra-High Performance Concrete), As a Repair Material

General, material composition and material properties of UHPC are characterized in this section. Also, curing condition for UHPC, which is considerably different from that of normal concrete will be introduced. Lastly, advantages of the use of the UHPC as a rehabilitating material will be focused from economic and environmental view points.

2.2.1 General and composition of UHPC

The UHPC fundamentally consists of very fine particles to improve homogeneity of the mix, compare to concrete, by eliminating all coarse aggregates. The UHPC consists of cement, silica fume, silica powder, sand,

water, and additional superplasticizer. Typical wayer/cement ratios are 0.2 to 0.25 with 20 to 30% of silica fume. Silica fume which is the smallest particle used in the UHPC, fills voids between cement grains, leading to enhancement of the rheological characteristics and forms hydration products by pozzolanic activity. To reduce water content and increase material properties at the same time, additional superplasticizer is essential for workability of UHPC. With low w/c ratios, UHPC can exhibit higher mechanical properties such as compressive and tensile strength, and flexural toughness caused by low porosity. Addition of short slender steel fibers with a diameter of 0.2mm and length of 9-17mm is necessary to improve tensile behavior and ductility.

2.2.2 Material properties of UHPC

UHPC, as part of the group of HPCFRCC demonstrated in **Fig 2-1**, is one of the breakthroughs in the 21st century in the field of concrete technology where this cementitious composite material providing an significant improvement in strength, workability, low porosity, tightness without any intentional mechanical vibration, ductility and durability when compared with normal strength concrete (NSC). These improved properties are achieved by using different material composition from NSC. Furthermore, by adding various volume fractions of steel fiber (0~3%) into UHPC, called as Ultra-High Performance Fiber-Reinforced Concrete (UHPCFRCC), UHPCFRCC is an advanced cementitious material which has exceptional mechanical and chemical properties including a very high tensile strength, strain hardening behavior and a density leading to a very low permeability making it ideal for the rehabilitation and modification of existing structures.

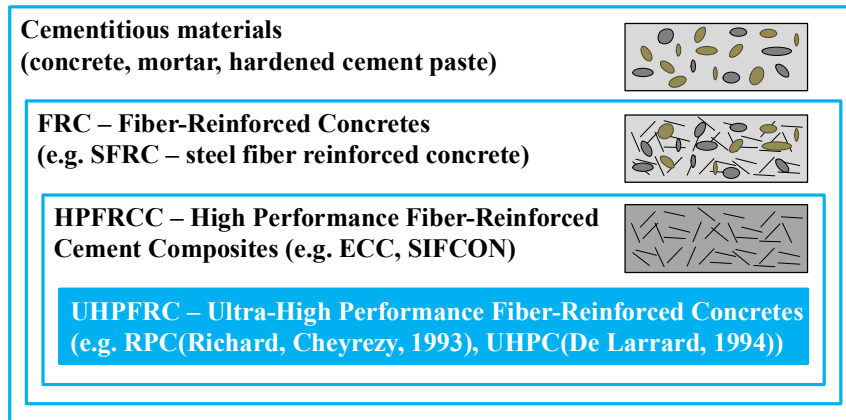


Fig 2-1. Classification of UHPC

2.2.3 Curing of UHPC

The UHPC may be subjected to high temperature steam or pressure treatment after curing in a mold for 24h at room temperature ($20\pm 2^{\circ}\text{C}$). Pressure treatment of the fresh material increases the density by reducing the entrapped air, by removing excess water and by accelerating chemical shrinkage. Post-set high temperature steam curing of about $90\pm 5^{\circ}\text{C}$ for 48h accelerates the pozzolanic reaction and modifies the microstructure of the hydrates, after which no more hydration takes place. In the FHWA report (Graybeal, 2006) on material characteristics of UHPC subjected to different curing treatment, the superiority of the steam curing is well demonstrated. Some of the experimental results are listed in **Table 2-1**.

Table 2-1. Durability results of UHPC subjected to different curing (Graybeal, 2006)

Material Characteristic	Steam	Untreated	Tempered Steam	Delayed Steam	Supplemental Description
Compressive strength (ksi)	28.0	18.3	24.8	24.8	ASTM C 39; 28 days strength
Modulus of elasticity (ksi)	7600	6193	7397	7295	ASTM C 469; 28 days modulus

Flexural strength (psi)	1305	1305	1494	1407	ASTM C1018; 12 inch span; corrected span
Tensile strength (psi)	1407 - 1595	798 - 1001	1102 - 1305	1305 - 1595	Axial tensile load
Chloride ion penetrability (coulombs)	18	360	39	18	ASTM C1202; 28 days test
Chloride ion permeability (lb/in ³)	< 0.21 × 10 ⁵	< 0.21 × 10 ⁵	< 0.21 × 10 ⁵	< 0.21 × 10 ⁵	AASHTO T259; 0.5 inch depth
Abrasion resistance	0.17	0.73	0.20	0.13	ASTM C944 2xweight; ground surface
Freeze-Thaw resistance	96%	112%	100%	99%	ASTM C666A; 600 cycles

However, the high temperature steam curing treatment is very difficult to apply in case of composite UHPC-RC elements and in-situ applications, and would present major drawbacks such as the limited capacity to heat the limited area of steam boiler and significant resource consumption. Though UHPC cured only under the room temperature condition without heat treatment was proposed and used in the recent studies (Kang and Hong, 2014), in the present study, 90°C steam curing was applied for all specimens retrofitted by UHPC overlay.

2.2.4 Advantages of the use of UHPC

As described in previous sections, the benefits of UHPC are quite substantial, but are offset by high cost of the material. With the material being relatively new, there have only been a limited number of structural applications and the costs have remained high because the material is still considered to be a specialty product (Hussein, 2014). Nevertheless, the lower energy and raw materials consumption of UHPC are required in comparison with normal and

high strength concrete, and it can lead to possibility to use larger space that can be achieved in a building, as a result of smaller compound units. There is also the factor of the optimized durability of UHPC, which generates altogether lower life-cycle costs than the existing standard concrete (Yoo & Yoon, 2016). Furthermore, as UHPC mixes do not need to be mechanically vibrated when placed in-situ, UHPC necessitates fewer workers for its placement and the environmental impact of the vibration is eliminated. In short, UHPC can be characterized as the more ecologically sustainable and cost-efficient rehabilitating material.

2.3 Punching Shear Strength

Design of shear and punching shear strengths of slabs without transverse reinforcement has been a global concern that many researchers have devoted significant efforts in the past. For several decades since 1960, among many other approaches, Kinnunen/Nylander model seems to be the most rational mechanical model for predicting the punching shear failure of slab-column connections, yielding good agreement with existing test results. This model has even been used and modified to account for different types of situations on a rational basis by many researchers until now, like e.g. Hallgren (1996), Broms (2006) and recently Muttoni (2008). In this chapter, the Kinnunen/Nylander model and especially, an advanced model by Muttoni (2008) will be covered.

2.3.1 Kinnunen and Nylander (1960)

With respect to punching of slabs without transverse reinforcement, the first rational approach developed with a certain success was that of Kinnunen and Nylander (Kinnunen and Nylander, 1960) in Royal Technical University (1960), which inspired the work of other researchers (Hallgren, 1996, Broms, 2006 and Muttoni, 2008). Kinnunen and Nylander carried out an experimental study on 61 circular slabs with circular column stubs in a symmetric scheme, varying the amount of flexural reinforcement in the slab. Based on their test results, Kinnunen and Nylander formulate a mechanical model, considering the formation of shear cracks, the deformation of the sector elements and the strain of the concrete and steel.

This model assumed that a slab consists of a centrally truncated cone within boundary lines made by the tangential shear crack and segmental slab

sector elements, divided by radial flexural cracks, as schematically described in **Fig 2-2**. The basic idea of this model, then, is to create forces and moment equilibrium acting on the sector element.

According to the proposed model by Kinnunen and Nylander, the punching shear failure occurs when the compressive strain in tangential direction in the slab at the column edge reaches a certain critical value. The cracking at a critical tangential flexural strain softens the concrete at the column edge. Subsequently, at the ultimate stage the compressive strain always exceeds the strain corresponding to the concrete strength. Thus, when the flexural tangential strain in the bottom of the slab reaches the critical value, the concrete loses the interface bond resulting in a vertical crack. It has been observed that the radial compressive strain at the bottom surface of the slab in the vicinity of the column suddenly decreases to zero when the load almost reaches the ultimate punching shear load. Therefore, the inclined compression strut cannot resist the support reaction, resulting progressively in the column collapse. Thus, the crack propagation takes place in combination with the shear deformation of the compression zone. Due to the shear deformation, the radial flexural strain in the bottom of the slab stops increasing while the load increases.

Conclusively, the failure mode is governed more by the circumferential crack at the slab-column connection rather than by propagation of an inclined flexural crack.

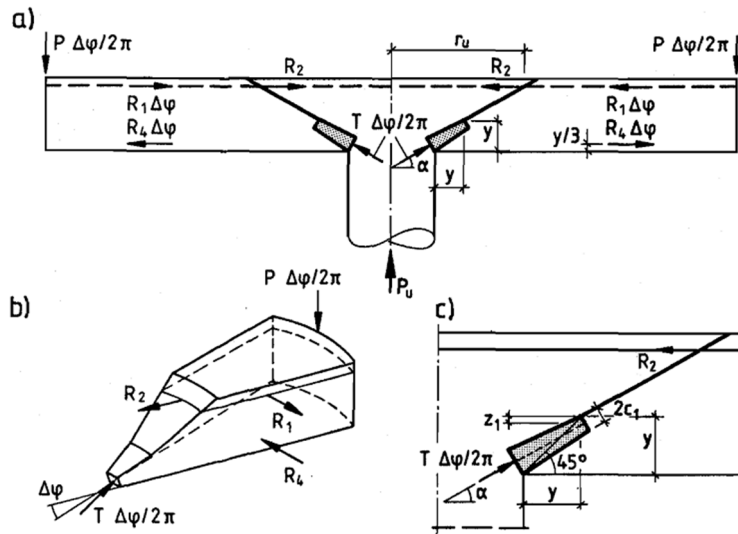


Fig 2-2. Mechanical model of Kinnunen/Nylander (Kinnunen and Nylander, 1960)

2.3.2 Muttoni (2008)

Muttoni (Muttoni, 2008) also accepted the Kinnunen/Nylander model, and based on the model, proposed the Critical Shear Crack Theory (CSCT). The CSCT is a theory whose fundamental was first presented in 1991 (Muttoni and Schwartz, 1991) and that can be applied for shear design of one- and two-way slabs. With respect to beams and one-way slabs without transverse reinforcement, currently most design approaches are based on empirical models (ACI 318-11, Eurocode 2). Whereas, CSCT was developed concerning members subjected to shear like beam or one- and two-way slab without transverse reinforcement.

The theory is based on the assumption that the shear strength in members without transverse reinforcement is governed by the critical shear crack width and the roughness of the lips of a shear crack which develops through the inclined compression strut carrying shear. Based on the assumption, to evaluate the shear strength, Muttoni suggested a failure criterion validated by

a large set of test data based on fracture mechanics, which considers aggregate interlocking effect and size effect also, as expressed in Eq.(2-1).

$$\frac{V_R}{b_0 d} = \sqrt{f'_c} \cdot f(w, d_g) \quad (2-1)$$

According to the CSCT, the punching shear strength can be expressed as a function of slab rotation, which has a proportional relationship with the width of a critical shear crack as described in Eq.(2-2), where w is width of a critical shear crack, ψ is the slab rotation and d is the effective depth of the member. Thus, based on the assumed relationship, Muttoni proposed a failure criterion of the punching shear strength of a two-way slab as expressed in Eq.(2-3). The failure criterion has been experimentally proven to predict very well the maximum punching shear capacity of a two-way slab, with high correlation.

$$w \propto \psi d \quad (2-2)$$

$$\frac{V_R}{b_0 d \sqrt{f'_c}} = \frac{3/4}{1 + 15 \frac{\psi d}{d_{g0} + d_g}} \quad (2-3)$$

where V_R is the shear strength, b_0 is a critical perimeter (equal to the width of the member (b) in beams and set at $d/2$ of the border of a column for punching-shear), d_{g0} is the reference aggregate size set at 16mm, f'_c is the compressive strength of the concrete, and d_g is the maximum size of the aggregate (accounting for the roughness of the lips of the cracks).

The CSCT models the RC section having a quadrilinear moment-curvature relationship as shown in **Fig 2-3(b)**. Then, equilibrium equation,

which is also expressed as a function of slab rotation, is solved for a slab portion set up as a free body diagram to obtain the load-rotation relationship of the slab. The point at which this demand curve intersects the capacity curve, that is, the failure criterion previously mentioned is determined as the performance point and the maximum load-carrying capacity of the slab.

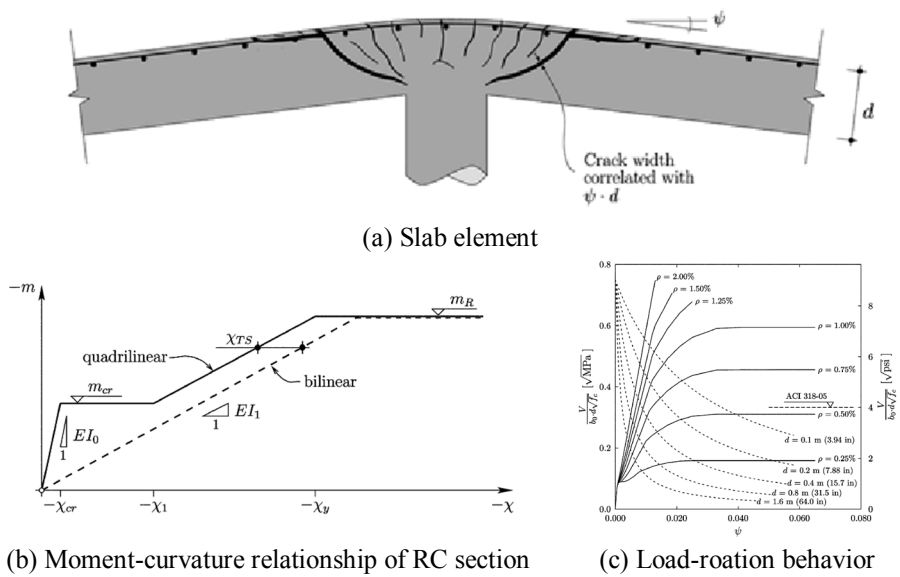


Fig 2-3. Concept of CSCT (Muttoni, 2008)

2.4 Interfacial Bond Strength between UHPC and Concrete

Experimental studies conducted on performance level of interface between UHPC and concrete are reviewed in this section. Most of the studies showed that only by surface roughening, the interface between UHPC and concrete has sufficient interfacial bond strength without any shear connectors.

2.4.1 Tayeh et al. (2013)

Tayeh et al. (2013) performed a set of slant shear and tensile splitting strength tests according to ASTM C 882 and ASTM C 496, respectively, to assess the interfacial bond characteristics between normal concrete substrate as old concrete and ultra high performance fiber concrete as repair material. The main test parameter was surface roughness. In the study, for surface roughening, five types of surface roughened method were used: no roughness (AC), sand blasted (SB), wire brushed (WB), with drilled holes (DH), and with grooves (GR). Before casting the UHPFC over the concrete substrate, the roughened surface was moistened for 10 minutes and wiped dry with a damp cloth to retain the saturated surface-dry (SSD) condition.

According to the test results, the two major findings have been obtained. First, the UHPFC seems to be a very promising material for repair and rehabilitation of concrete structures owing to the superior mechanical bond performance and the impermeability characteristics, probably leading to increasing of the service life of concrete structures. Secondly, among the five surface roughening methods, the sand blasting method provides the most superior mechanical bond, even higher than that of monolithically casted NC specimens.

2.4.2 Carbonell Muñoz et al. (2014)

Carbonell Muñoz et al. (2014) explored the bond characteristics between UHPC and NSC under varying stress configurations and environmental conditions by setting extensive test variables: 1) surface roughness, 2) age of bond, 3) exposure to freeze-thaw cycles and 4) wetting conditions of the concrete substrate. For roughening the surface, slightly brushed (Smooth, Sm), chipped (Ch), brushed (Br), sand blasted (Sb), grooved (Gr) and rough (aggregate exposure, R) methods were adopted. To evaluate the bond characteristics, splitting tensile, slant shear and pull-off tests were performed.

Based on the extensive test results, it was concluded that for all scenarios investigated aside from the initial scenarios where the concrete substrate had an ambient dry condition, the bond performance exceeded recommended requirements given by ACI 546-06. Furthermore, the bond performance between the UHPC and NSC can be considered successful, because the tensile strength of the bond and the overlay material are greater than that of the concrete substrate. However, it should be mentioned that the maximum stress of the concrete substrate were lower than expected values, which could be attributed to several factors, such as extreme shrinkage of the overlay material. To investigate such effects, further study should be conducted.

2.4.3 Lim and Hong (2016)

Lim and Hong (Lim and Hong, 2016) performed a set of slant shear test with 66 UHPC-NSC composite specimens to evaluate the interfacial shear strength of concrete strengthened with UHPFRC. The test variables were chosen as roughness of the interface (smooth, and roughened), concrete compressive strength of ordinary concrete ($f_{cd} = 24\text{MPa}$, and 60MPa), and fiber volume ratio in UHPFRC ($V_f = 0.5\%$, 1.0% , 1.5% , and 2.0%). The authors used Shot-blasting method to roughen the surfaces of the ordinary

concrete, by which the surfaces were roughened with 0.3mm depth.

According to the test results, as the compressive strength of the ordinary concrete increases, the interfacial shear strength also tends to increase. In addition, even without the shear friction reinforcement, the shear strength of the surface roughened specimens exceeded the upper limit of the shear strength between the different types of concrete presented in current code provisions. However, it should be also mentioned that the fiber volume ratio in UHPFRC and the interfacial shear strength were not correlated.

2.5 RC Members Retrofitted by Cement-Based overlay

2.5.1 Rocha (2012)

To analyze the behavior of strengthened beams and the performance of the interface, the author performed a set of flexural beam test with 9 beams that are strengthened by a RC overlay on the tension side. The materials used in the overlay have identical properties to the ones used in the substrate. In that region where the new concrete overlay would be placed, grooves were created at the interface, using pneumatic hammers. The test variables are the concrete strength and the amount of shear connectors: 1) no shear connectors, 2) uniformly distributed, and 3) concentrated only near the edges, expecting the elimination of a debonding failure mode in this region.

In the dissertation, the effects of adhesion and reinforcement crossing the interface are analyzed. According to the author, RC overlays can significantly improve flexural resistance in horizontal concrete elements such as beams or slabs, and further improvement can be achieved by installing the shear connector up to 39% for case 2) and 79% for case 3) in relation to specimens without shear connectors. These increases can be attributed to failure mode. A clean rupture along the interface was only obtained in case 1). Failure along the interface occurred shortly after a inclined shear crack was formed near the supports. However, for case 2) and 3), which are reinforced with shear connectors, ruptures began in the RC overlay and propagated to the existing midspan flexural crack. This indicates that although failure modes are related to resistance of the interface, interfacial failure was probably not the main reason why the composite structure failed. Therefore, it was concluded that the addition of steel crossing the interface is important, not only for the increase in shear strength, but also for the overall load bearing behavior.

2.5.2 Hable et al. (2006)

Hable et al. (2006) investigated the structural behavior of composite UHPFRC-concrete elements with an analytical cross-sectional model in a parametric study in order to define requirements on materials and on geometric structural parameters. **Fig 2-4** shows the description of configuration and the analytical model of UHPFRC-concrete elements. The authors generated, and validated the model considering configuration of the cross section, thickness of the UHPFRC layer, tensile properties of the UHPFRC and additional reinforcement in the UHPFRC layer. According to the authors, interaction of reinforcement and UHPFRC has to be optimized to prevent macrocracks localization, leading to strain softening behavior of UHPFRC layer. In addition, the authors proposed for configuration PR and R, a thickness of the UHPFRC layer of 5cm, considering additional reinforcement placed in it.

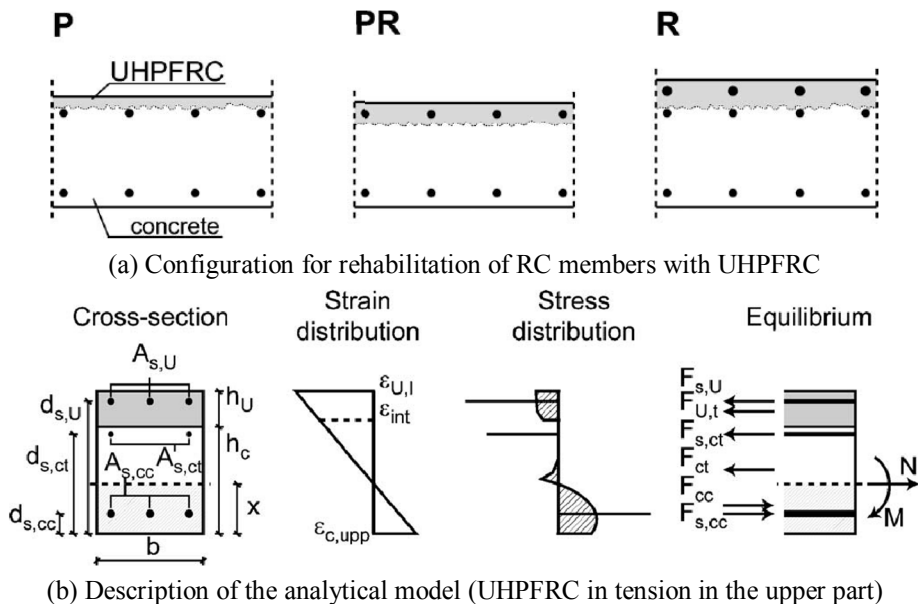


Fig 2-4. Description of configuration and the analytical model of UHPFRC-concrete elements (Hable et al., 2006)

2.5.3 Noshiravani and Brühwiler (2013, 2014)

Noshiravani and Brühwiler performed experimental study and theoretically analyzed the structural behavior of RU-RC composite beams with UHPFRC layer on the tension side. One critical finding is that although the ultimate resistance of RU-RC beams is much higher than their reference RC beams, their rotation at ultimate limit is between 90 and 100% of the latter, which is unmatched with conventional sense. This phenomenon was explained in the experimental study by adopting intermeidate crack-induced debonding (ICD) zone near the interface. The RU-RC composite beam behaves monolithically at uncracked and crack stage, while it behaves like two-layer beam with an interlayer slip at the onset of ICD at corresponding region.

To predict the structural behavior of the RU-RC beams based on the test results, the authors proposed Fictitious Composite Hinge (FCH) model as shown in **Fig 2-5**. The FCH model was developed to calculate the force-deflection response of RU-RC composite members both up to their maximum bending resistance and beyond yielding. Depending on the crack pattern, the model starts from coming up with assuming that the rotation is due to the opening of one flexural hinge or a flexure-shear hinge, which generally consist of the cumulative sum of the crack openings in a cracked region of a member.

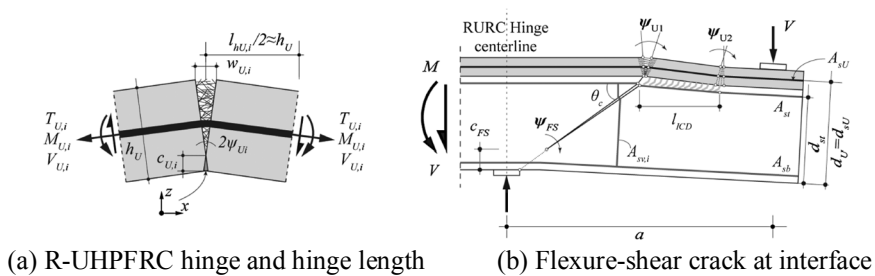


Fig 2-5. Fictitious Composite Hinge model (Noshiravani and Brühwiler, 2014)

2.5.4 Bastien-Masse (2015)

Bastien-Masse performed experimental study and theoretically analyzed the load-rotation behavior, cracking pattern and failure mode of UHPFRC-RC composite slab without column over the RC slab. The test variables are the thickness of the UHPFRC overlay and the yield strength of steel re-bars in it. According to the test result, the thin layer of UHPFRC with or without steel re-bars serves as a tensile reinforcement for the RC slab, creating a composite element, leading to significantly increasing the rigidity and the punching shear resistance of a RC unretrofitted slab. Especially for cracking patterns, it should be notified that the layer of UHPC could not be punched by the top of the concrete cone and the critical shear crack in the RC section had to rotate to become parallel to the interface. Based on the experimental observation, the author proposed a multilinear moment-curvature relation for the R-UHPFRC-RC composite section, which can then be combined with a newly proposed composite failure criterion based on CSCT to predict the punching shear resistance. From the author's viewpoint, the contribution mechanism of the UHPFRC overlay to the punching shear resistance was explained by tensile stresses perpendicularly induced to the interface with the concrete. The total punching shear resistance is expressed as the sum of the contributions of RC section and UHPFRC overlay.

$$V_R(\psi) = V_c(\psi) + V_U \quad (2-4)$$

Where,

$$\frac{V_c(\psi)}{b_0 d_{sc} \sqrt{f_c'}} = \frac{3/4}{1 + 15 \frac{\psi d_{sc}}{d_{g0} + d_g}} \quad (2-5)$$

$$V_U = 2\pi \cdot f_{ct} \cdot h_U \cdot \left(r_U + \frac{h_U}{2} \right) \quad (2-6)$$

Where,

- $V_R(\psi)$ = total punching shear force, N
- $V_c(\psi)$ = concrete contribution to punching shear resistance, N
- V_U = UHPFRC contribution to punching shear resistance, N
- b_0 = Critical perimeter for punching shear set at $d_{sc}/2$ from the column face, mm
- d_{sc} = flexural depth for tensile reinforcement in RC section, mm
- f'_c = concrete compressive strength, MPa
- f_{ct} = concrete tensile strength, MPa
- ψ = slab rotation
- d_{g0} = reference aggregate size set at 16mm
- d_g = Maximum diameter of aggregate, mm
- h_c = height of RC section, mm
- d_U = height of UHPFRC overlay, mm
- r_U = radius of inclined crack at the top of the slab located at $h_c + h_U$ from the column side, mm

The **Fig 2-6** shows the scheme of the proposed analytical model for the contribution of UHPFRC overlay to the total punching shear resistance. The model that Bastien-Masse proposed was developed based on observations made on composite slabs with thickness of the layer between 25mm and 50mm and thickness ratio (h_U / h_c) between 0.1 and 0.3. However, as also Bastien-Masse mentioned before in the previous research (Bastien-Masse and Brühwiler, 2016), for thickness ratios higher than 0.3, other shear carrying mechanism can activate, and additionally, the steel reinforcement ratio in the UHPFRC overlay would affect the contribution to total punching shear resistance of the composite members to a degree, which is directly relevant to the present study.

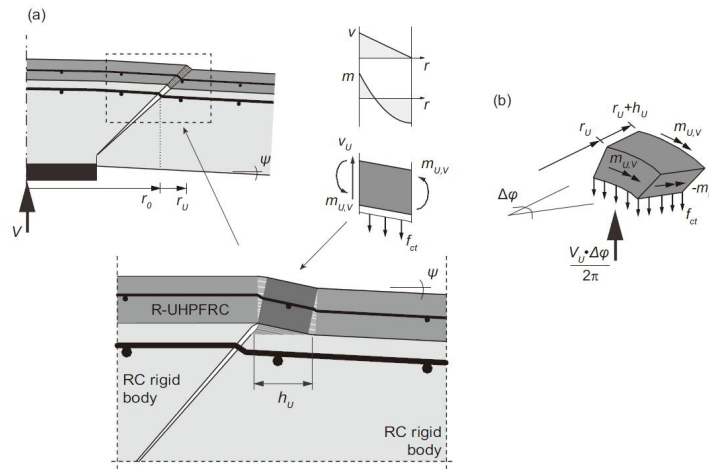


Fig 2-6. UHPFRC resisting mechanism (a) out-of-plane bending mechanism; (b) efforts in the UHPFRC sector element (Bastien-Masse, 2015)

Chapter 3. Current Code Provisions

3.1 ACI 318-11 (2011)

The design method of slab-column connections according to ACI 318-05 was developed in the 1960s and was primarily based on work by Moe (1961) and Joint ACI-ASCE Committee 326 (1988). No considerable changes have been made to the punching provisions since. The punching shear design specified in the ACI 318-11 code is generally based on empirical formulation, whereby the factored shear force should not be greater than the nominal shear strength ($V_u \leq \phi V_n$). However, the method of calculating the nominal shear strength of concrete contribution (V_c) is rather different according to the existence of shear reinforcement. In case of slabs without any transverse reinforcement, the shear strength is determined by the minimum value of the following equations.

$$V_c = 0.17 \left(1 + \frac{2}{\beta_c} \right) \lambda \sqrt{f'_c} b_0 d \quad (3-1)$$

$$V_c = 0.083 \left(\frac{\alpha_s d}{b_0} + 2 \right) \lambda \sqrt{f'_c} b_0 d \quad (3-2)$$

$$V_c = 0.33 \lambda \sqrt{f'_c} b_0 d \quad (3-3)$$

Where,

V_c = nominal shear strength provided by concrete, N

- λ = modification factor reflecting the reduced mechanical properties of lightweight concrete
 β_c = ratio of long to short sides of column, concentrated load or reaction area
 b_0 = critical perimeter, mm
 d = distance from extreme compression fiber to centroid of longitudinal tension reinforcement, mm
 α_s = Constant used to compute V_c in slabs and footings, take 40 for interior columns, 30 for edge columns, and 20 for corner columns

Note that for two-way action, the critical sections to be investigated shall be located so that its perimeter b_0 is a minimum but need not approach closer than $d/2$ to edges or corners of columns, concentrated loads, or reaction areas. Especially for square or rectangular columns, concentrated loads, or reaction areas, the critical sections with four straight sides shall be permitted as shown in **Fig 3-1**.

3.2 KCI 2012 (2012)

According to KCI 2012 code, design shear strength (ϕV_n) of a section where shear force is applied, is required to be greater than the factored shear force (V_u), which is same concept as ACI 318-11.

$$V_u \leq \phi V_n \quad (3-4)$$

$$V_n = V_c + V_s \quad (3-5)$$

The nominal shear strength is calculated by simple summation of shear strength contributions of concrete and shear reinforcement. The design of the

nominal shear strength of concrete contribution (V_c) of structures exhibiting two-way behavior such as a two-way slab or footing is particularly stated in KCI 2012 Section 7.12.2 by considering various factors. That is, unlike the previous design method, which was empirically formulated considering only the compressive strength of concrete, the present design method further takes into account the relationship between the reinforcement ratio, depth of compression zone and size effect and aspect ratio. Additionally, the Rankine's failure criterion, which assuming that the failure occurs when principal stress reaches the material strength, is applied to determine the nominal shear strength. The detailed information about calculating procedure is as followed.

$$V_c = v_c b_0 d \quad (3-6)$$

$$v_c = \lambda k_s k_{bo} f_{te} \cot \Psi (c_u / d) \quad (3-7)$$

Where,

$$k_s = (300 / d)^{0.25} \leq 1.0 \quad (3-8)$$

$$k_{bo} = 4 / \sqrt{\alpha_s (b_0 / d)} \leq 1.25 \quad (3-9)$$

$$f_{te} = 0.21 \sqrt{f_c'} \quad (3-10)$$

$$\cot \Psi = \sqrt{f_{te} (f_{te} + f_{cc})} / f_{te} \quad (3-11)$$

$$c_u = d \left[25 \sqrt{\rho / f_c'} - 300 (\rho / f_c') \right] \quad (3-12)$$

$$f_{cc} = (2/3) f_c' \quad (3-13)$$

Where,

- λ = modification factor reflecting the reduced mechanical properties of lightweight concrete
 v_c = nominal shear stress, MPa
 b_0 = critical perimeter, mm
 d = distance from extreme compression fiber to centroid of longitudinal tension reinforcement, mm
 k_s = size effect factor
 k_{bo} = aspect ratio factor
 f_{te} = effective tensile strength reduced by the transverse compressive stress, MPa
 Ψ = crack angle of slab in flexure zone
 c_u = depth of compression zone, neglecting compressive reinforcement
 f_{cc} = mean value of compressive stress applying to compression zone at critical section, MPa
 α_s = coefficient factor when deciding V_c in two-way slab or footing slab; take 1.0 for interior columns, 1.33 for edge columns, and 2.0 for corner columns
 ρ = the ratio of flexural tensile reinforcement

Note that ratio of flexural tensile reinforcement ρ is used when $\rho \leq 0.03$, and when $\rho \leq 0.005$, then 0.005 can be used. Furthermore, critical perimeter b_0 should be minimized, but it is not necessary to place it closer than $d/2$ from the boundaries of concentrated load, reaction zone, column and column head, etc. Especially for rectangular column, the critical perimeter b_0 can be defined as a straight line parallel to the four sides of the column as demonstrated in **Fig 3-1**.

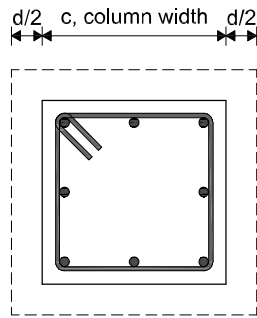


Fig 3-1. Critical section according to ACI 318-11 and KCI 2012

3.3 Eurocode 2 (2004)

Eurocode 2 defines the different concept about the important section from the ACI 318-11 and KCI 2012 design codes. Two control perimeters are defined in Eurocode2; at the column perimeter and at the distance of $2d$ from the column face. The design punching shear resistance is calculated based on the basic control perimeter u_1 . The basic control perimeter u_1 may normally be taken to be at a distance $2d$ from the loaded area, and should be constructed so as to minimize its length as shown in **Fig 3-2**.

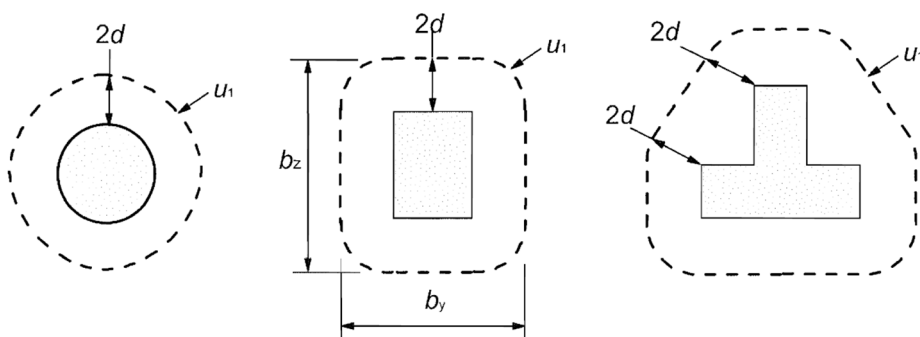


Fig 3-2. Typical basic control perimeters (EC2, 2004)

The design punching shear resistance of slabs and column bases without shear reinforcement can be calculated as follows. To investigate the real shear

resistance, and exclude the design purpose, which may lead to significantly conservative results, the partial factor for concrete γ_c is not considered.

$$v_{Rd,c} = 0.18k(100\rho_l f_{ck})^{1/3} + k_1\sigma_{cp} \geq v_{\min} \quad (3-14)$$

Where,

$$k = 1 + \sqrt{\frac{200}{d}} \leq 2.0 \quad (3-15)$$

$$\rho_l = \sqrt{\rho_{ly} \cdot \rho_{lz}} \leq 0.02 \quad (3-16)$$

$$v_{\min} = 0.035k^{3/2} f_{ck}^{1/2} \quad (3-17)$$

Where,

- $v_{Rd,c}$ = design value of the punching shear resistance of a slab without punching shear reinforcement along the control section considered, MPa
- f_{ck} = characteristic compressive cylinder strength of concrete at 28 days, MPa
- k = coefficient considering size effect
- k_1 = 0.1
- σ_{cp} = compressive stress in the concrete from axial load or prestressing, MPa
- ρ_l = reinforcement ratio for longitudinal reinforcement
- ρ_{ly}, ρ_{lz} = reinforcement ratio for longitudinal reinforcement in y- and z- directions respectively, within a slab width equal to the column width plus 3d each side
- d = effective depth of the cross section, mm

Note that the average reinforcement ratio is obtained by the geometric mean of the reinforcement ratio in y- and z- directions.

Along with the basic control perimeter, punching shear calculation at the

column perimeter also should be performed using Eq.(3-18), and the obtained value shall not be greater than the capacity of the concrete struts $v_{Rd,max}$, which is recommended to be $0.5v_{cd}$.

$$v_{Ed} = \frac{\beta V_{Ed}}{u_0 d} \leq v_{Rd,max} \quad (3-18)$$

$$v = 0.6 \left(1 - \frac{f_{ck}}{250} \right) \quad (3-19)$$

$$f_{cd} = \alpha_{cc} \eta f_{ck} / \gamma_c \quad (3-20)$$

Where,

- u_0 = length of column periphery, mm
- β = factor concerning eccentricity
- $v_{Rd,max}$ = capacity of concrete struts expressed as a stress, MPa
- v = Strength reduction factor for concrete cracked in shear, MPa
- f_{cd} = Design value of the concrete compressive strength in the direction of the longitudinal member axis, MPa
- α_{cc} = Coefficient taking into account long term effects of compressive (tensile) load and the way load is applied
- η = Factor defining effective strength

3.4 JSCE (2010)

Design provision for punching shear capacity is presented in Section 9.2.2.3 (Design punching shear capacity of planar members). According to JSCE, for members subjected to the local loads such as column-slab connections and footings, the possibility of punching shear failure shall be examined. The failure mode of punching shear shall be such that conical or

pyramidal shape of fractured slope is created. Eq.(3-21) for the shear capacity is derived on the assumption that the design cross-section is located $d/2$ from the loaded area as shown in Fig 3-3.

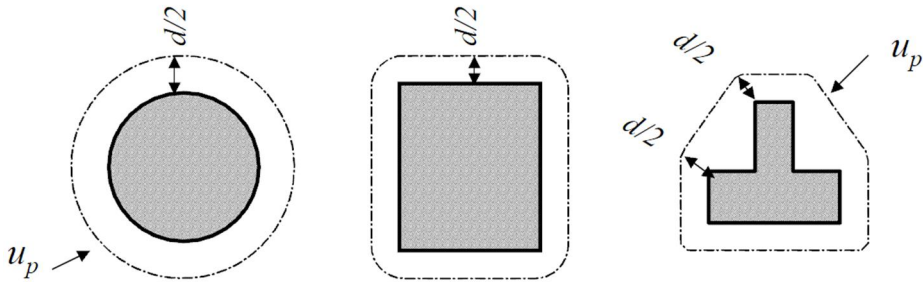


Fig 3-3. Typical design cross section (JSCE, 2010)

(1) When the loaded area is positioned far from free edges or openings and the eccentricity of the load is small, the design punching shear capacity V_{pcd} shall be determined using Eq.(3-21).

$$V_{pcd} = \beta_d \cdot \beta_p \cdot \beta_r \cdot f'_{pcd} \cdot u_p \cdot d / \gamma_b \quad (3-21)$$

Where,

$$f'_{pcd} = 0.2 \sqrt{f'_{cd}} \leq 1.2 \quad (3-22)$$

$$\beta_d = \sqrt[4]{1000/d} \leq 1.5 \quad (3-23)$$

$$\beta_p = \sqrt[3]{100p} \leq 1.5 \quad (3-24)$$

$$\beta_r = 1 + 1 / (1 + 0.25u/d) \quad (3-25)$$

Where,

f'_{pcd} = design compressive strength of concrete, MPa

- u = peripheral length of loaded area, mm
- u_p = peripheral length of the design cross section located at a distance $d/2$ from the loaded area, mm
- d = effective depth defined as the average values for the reinforcement in two directions, mm
- p = reinforcement ratio defined as the average values for the reinforcement in two directions
- γ_b = member factor, may generally be taken as 1.3

(2) When the loaded area is located in the vicinity of free edges or openings in members, the reduction of the punching shear capacity shall be appropriately taken into account.

(3) When the loads are applied eccentrically to the loaded area, the effects of flexure and torsion shall also be considered.

Chapter 4. Specimen Design and Test Set-up

4.1 Introduction

In order to evaluate the punching shear resistance mechanism of RC interior slab-column connections with UHPC overlay on the tension side of existing RC structures, a series of punching shear test were planned by setting the UHPC overlay thickness and the steel reinforcement ratio in the UHPC overlay as variables. For the design of the UHPC overlay, Habel et al. (Habel et al., 2006) suggested that the thickness be about 10~20% of height of the retrofitting target, and when considering additional steel reinforcement in the layer of UHPC, thickness of 5cm is proposed based on an analytical model to make sure efficient use of the UHPC overlay as retrofitting method. Thus, the UHPC overlay thickness was set to 0, 30 and 50mm. In addition, a small amount of small diameter steel re-bars placed in the UHPC overlay inhibits micro-cracks of the UHPC overlay from propagating to the macro-cracks and even promotes further distribution of the micro-cracks against external load. That is, it can ultimately increase bending and shear resistance, and improve strain-hardening behavior of the composite system. Therefore, to investigate the effect of additional steel re-bars in the UHPC overlay on the punching shear resistance, steel re-bar layouts of 0, D10@180mm and D10@90mm were planned.

4.2 Design Concept

Five square UHPC-RC interior slab-column connections without transverse reinforcement were planned and constructed. The retrofitting target

used in the present study are designed based on the below proto type of ordinary RC flat plate system. The proto type of the present study is an interior flat plate system having a 5m span as shown in **Fig 4-1**.

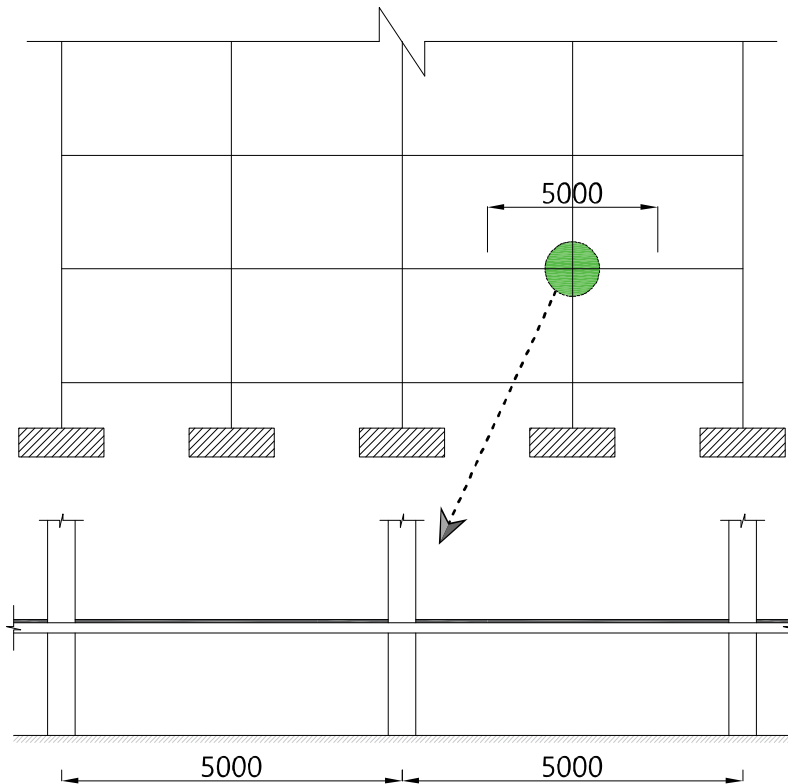
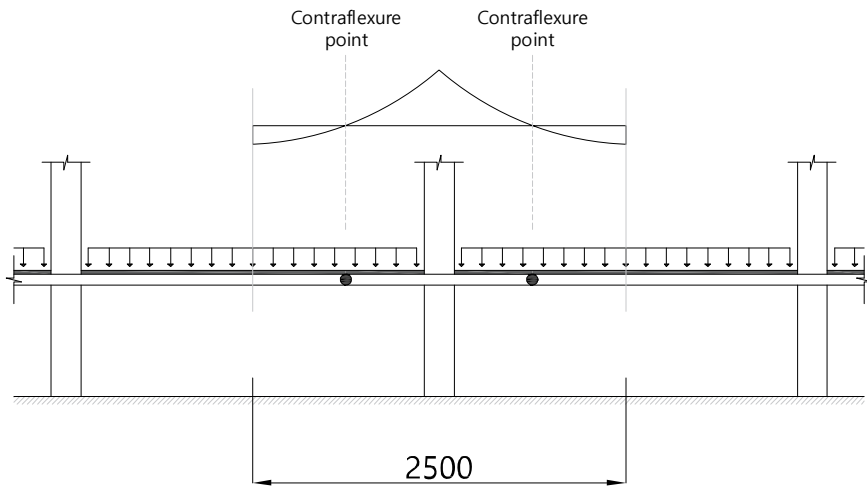
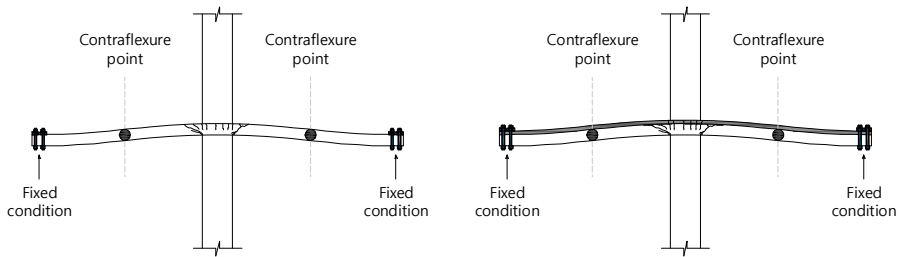


Fig 4-1. Proto type of the study

However due to limitation of laboratory size and actuator's capacity, the specimens are scaled at half as described in **Fig 4-2**. It should be also notified that in the present study, since the basic concept of the retrofitting method using the UHPC overlay is to retrofit existing RC structures rather than to design composite slabs consisting of such as pre-cast (PC) and cast-in-place (CIP) concrete structures, no dowel bars or shear connectors are considered. However, to confirm sufficient interface performance, sand blasting method for roughening the surface was adopted.



(a) Moment diagram in interior slab-column connection



(b) Scheme for retrofitting target

(c) Scheme for retrofitted target

Fig 4-2. Specimen modelling for test

4.3 Construction and Detail of Test Specimens

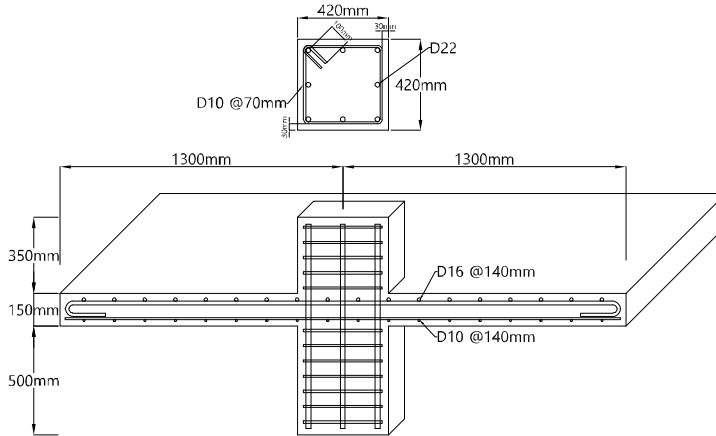


Fig 4-3. Specification of retrofitting target

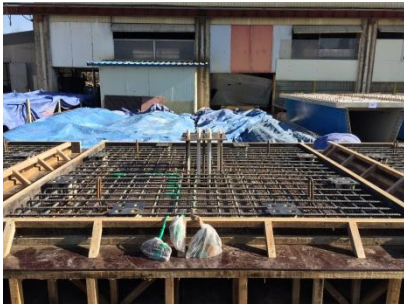
Five square UHPC-RC composite slabs without transverse reinforcement were constructed. The RC sections of the all specimens were fabricated with conventional normal strength concrete with a maximum aggregate size of 25mm. Each RC substrate has a column with a square cross section of 420mm by 420mm. The slab size is 2600mm by 2600mm with a total thickness of 150mm, but the distance from the center of the column to the each support was planned to be 1250mm as mentioned in the above subsection. Concrete cover was kept constant and equal to 20mm for all specimens. All presented specimens had same orthogonal reinforcement layout and a standard longitudinal reinforcement ratio in RC section equal to 1.24% for tension side reinforcement and 0.435% for compression side reinforcement using 16mm and 10mm diameter re-bars equally spaced at 140mm, respectively. The specification and some details of the retrofitting target are schematically illustrated in **Fig 4-3**, and the construction sequence of the RC specimens is described stepwise in **Fig 4-4**.



(a) Arrangement rebar



(b) Strain gage installation



(c) Formwork installation



(d) Concrete pouring



(e) Surface treatment



(f) Curing



(g) Specimens lifting

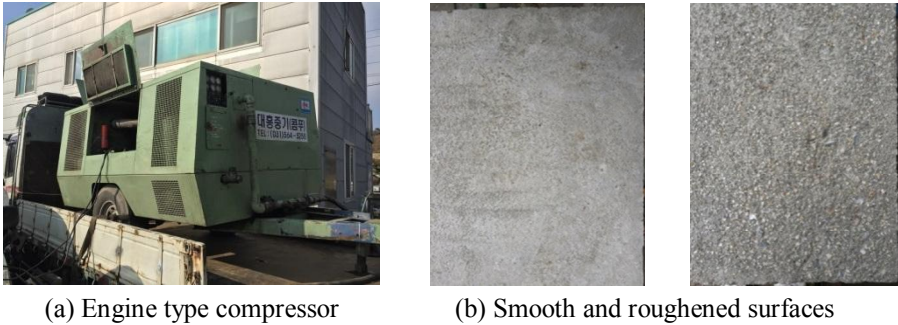


(h) Completed RC specimen

Fig 4-4. Casting sequence of RC specimen

For RC members with an UHPC overlay on the tension side, interface condition between the RC substrate and the UHPC overlay should be carefully taken into account. In order to retain recommendable interfacial bond condition at the interface between the different types of concrete, the surface roughening methods have to be conducted according to several previous research results. By roughening the interface, a certain degree of mechanical interlock between the concrete layers can be created. Among various surface roughening methods (left smooth, sand-blasting, shot-blasting, wire-brushing, hammer-chipping, hand-scrubbing, etc.) proposed in current desing codes, the sand-blasting method which exhibits superior bond strength can not only reduce external impact and the loss of existing members to a minimum, but also effectively forms a rough surface. In this experiment, thus, all the RC substrate's top surfaces were sand-blasted.

It is well known that when the substrate concrete surface is sand-blasted, the interface exhibits excellent adhesion performance. It is a mechanical treatment method, which makes the surface rough by spraying sufficiently dried sand particles on the targeted surface. In the present study, size of 1.2~1.5mm sand particles were sprayed using an engine type compressor with discharge pressure of about 0.88~0.98MPa. According to worker, the surfaces were cut by 0.2~1.0mm as shown in **Fig 4-5**. For efficient shear transfer at the interfaces, the sand-blasted surfaces were washed with water to prevent latency, and the UHPC was casted after removing residual dust on the surfaces by wind pressure. Since no reinforcement crosses the interface, shear transfer would rely soley on concrete-to-concrete adhesion performance.



(a) Engine type compressor

(b) Smooth and roughened surfaces

Fig 4-5. Machine and comparison of surfaces before and after sandblasting

When casting the layer of UHPC, in order to prevent the steel fiber balling, the UHPC was sufficiently mixed in a huge mixer and poured. After the pouring, no additional mechanical treatment such as vibrator was applied to prevent sinking of the steel fiber. It also has to be mentioned that especially for the specimens with additional steel re-bars in the UHPC overlay with thickness of 50mm, the UHPC overlay cover thickness was planned to be 15mm, which is smaller than that of ordinary RC slab structures. However, it is quite logical when considering the UHPC's homogeneous and tight material compositions.

Due to the different material compositions and properties from the normal concrete, UHPC must follow the curing conditions according to the guidelines to ensure a certain level of mechanical and chemical performances as already mentioned before. Therefore, after casting the UHPC overlay on the RC substrates, the specimens were cured at $20\pm 2^{\circ}\text{C}$ for 24 hours, and then cured at a high temperature of $90\pm 5^{\circ}\text{C}$ with $95\pm 5\%$ humidity for 48 hours. RC substrates with the UHPC overlay except for R specimen were also cured under the same conditions during the curing period.



(a) Interface sand-blasting



(b) Formwork installation



(c) Rebar, strain gage installation



(d) Providing humidity



(e) UHPC pouring



(f) Steam curing



(g) Completed specimen

Fig 4-6. Casting sequence of UHPC overlay

Table 4-1 below summarizes the retrofitting method, slab-column dimensions and reinforcement ratios of the specimens. In addition, the table specifically shows the design parameters of each specimen. All the specimen have same dimensions and reinforcement ratios for RC section, as already mentioned, and only U50S and U50L test specimens have additional steel re-bars placed in the UHPC overlay.

In **Table 4-2**, the nomenclature of the specimens is characterized by three parts. The first term indicates reference (R) or UHPC overlaid (U) slab-column connections, and the second term indicates the retrofitting thickness of UHPC overlay. Lastly, the third term is the amount of steel reinforcement placed in the UHPC overlay (S=D10@180mm, L=D10@90mm).

Table 4-1. Dimensions and reinforcement details of specimens

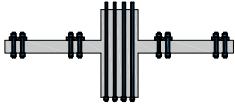
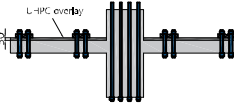
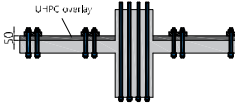
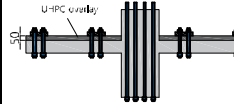
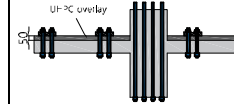
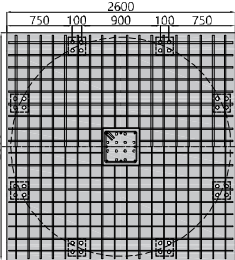
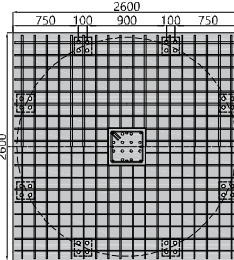
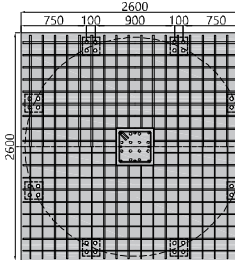
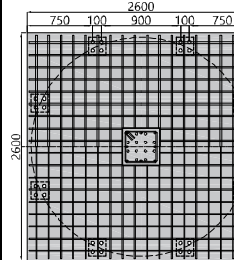
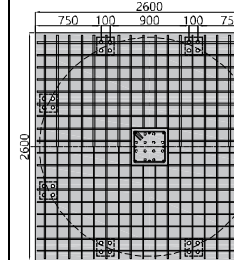
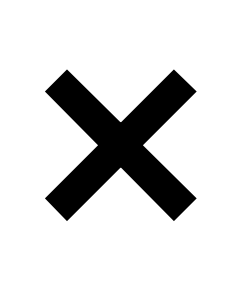
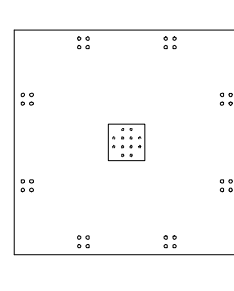
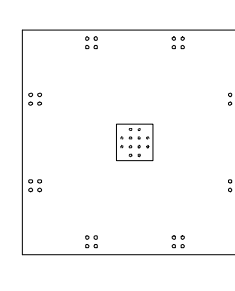
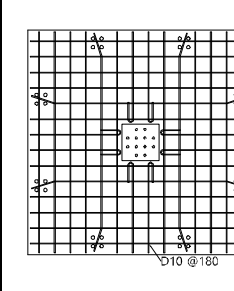
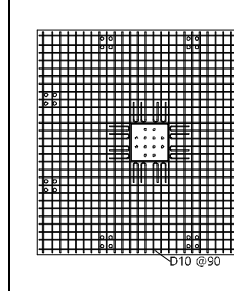
	R	U30	U50	U50S	U50L
Retrofit method	Reference	$h_U = 30\text{mm}$	$h_U = 50\text{mm}$	$h_U = 50\text{mm}$ Rebars=D10@180	$h_U = 50\text{mm}$ Rebars=D10@90
Section					
RC plan					
UHPC plan					

Table 4-2. Design parameters of test specimens

I.D.	Slab-column connection Dimension					Reinforcement								
						Steel in RC			Steel in UHPC			Steel fiber in UHPC		
	B (mm)	r_q (mm)	C (mm)	h_c (mm)	h_U (mm)	d_{sc} (mm)	Layout t (mm)	ρ_{sc} (%)	d_{sU} (mm)	Layout t (mm)	ρ_{sU} (%)	l_f (mm)	d_f (mm)	V_f (%)
R	2600	1250	420	150	0				-	-	-	-	-	-
U30	2600	1250	420	150	30				-	-	-	13	0.2	2
U50	2600	1250	420	150	50	114 / 30	D16 @140 / D10 @140	1.24 % / 0.437 %	-	-	-	13	0.2	2
U50S	2600	1250	420	150	50				175	D10 @180	0.226 %	13	0.2	2
U50L	2600	1250	420	150	50				175	D10 @90	0.452 %	13	0.2	2

Note) B = side length of slab specimen, r_q = radius of supports from force introduction, C = side length of column, h_c = thickness of RC section, h_U = thickness of UHPC overlay, d_{sc} = effective flexural depth from the extreme compression fiber to the centroid of tension steel rebars in RC section, d_{sU} = effective flexural depth from the extreme compression fiber to the centroid of steel rebars in UHPC overlay, l_f = length of steel fiber, d_f = diameter of steel fiber, V_f = volume fraction of steel fiber

4.4 Test Set-up

The **Fig 4-7** and **Fig 4-8** show the overall situation of the experiment and test set-up used for the present study. A total of 12 shear bolts in size of diameter of 24mm was installed at the bottom of an actuator with a capacity of 2000kN and penetrated through the column of the test specimens and fixed to the lower part of the column. The specimens were supported by fixed support condition by steel plates of size equal to 200mm x 200mm x 40mm at 8 points equally spaced around circumference with radius of 1250mm from the center of the column, so that the line of contraflexure points of radial bending moments can be assumed to be located at 625mm from the center. Each steel plate was fixed to the instrumented jig setting by tightening with four 24mm diameter shear bolts. Then, Linear Variable Displacement Transducers (LVDT) at top and bottom surfaces, PI-type crack gauges at the top surface and concrete strain gauges at the bottom surface were installed to manually measure the displacement, slab rotation and strains at determined points. The locations of LVDTs are shown in **Fig 4-8**, and that of other measurements are shown in **Fig 4-9** and **Fig 4-10**.

The experiments were performed by applying a concentrated monotonic load to the column base, pulling up the column to the upward direction using the actuator. The direct punching load was applied until the test specimen reached its peak load. The tests were processed by displacement control at constant rate, 2mm/min, and during tests, force, displacement at center and supports, crack openings at top surface, concrete and steel strains were automatically measured. For these test specimens, self-weight and weight of the test setup were deducted from the measured load.



(a) View of test set-up



(b) Steel plate anchored at supports



(c) Steel jig anchored at column

Fig 4-7. Photo of test set-up

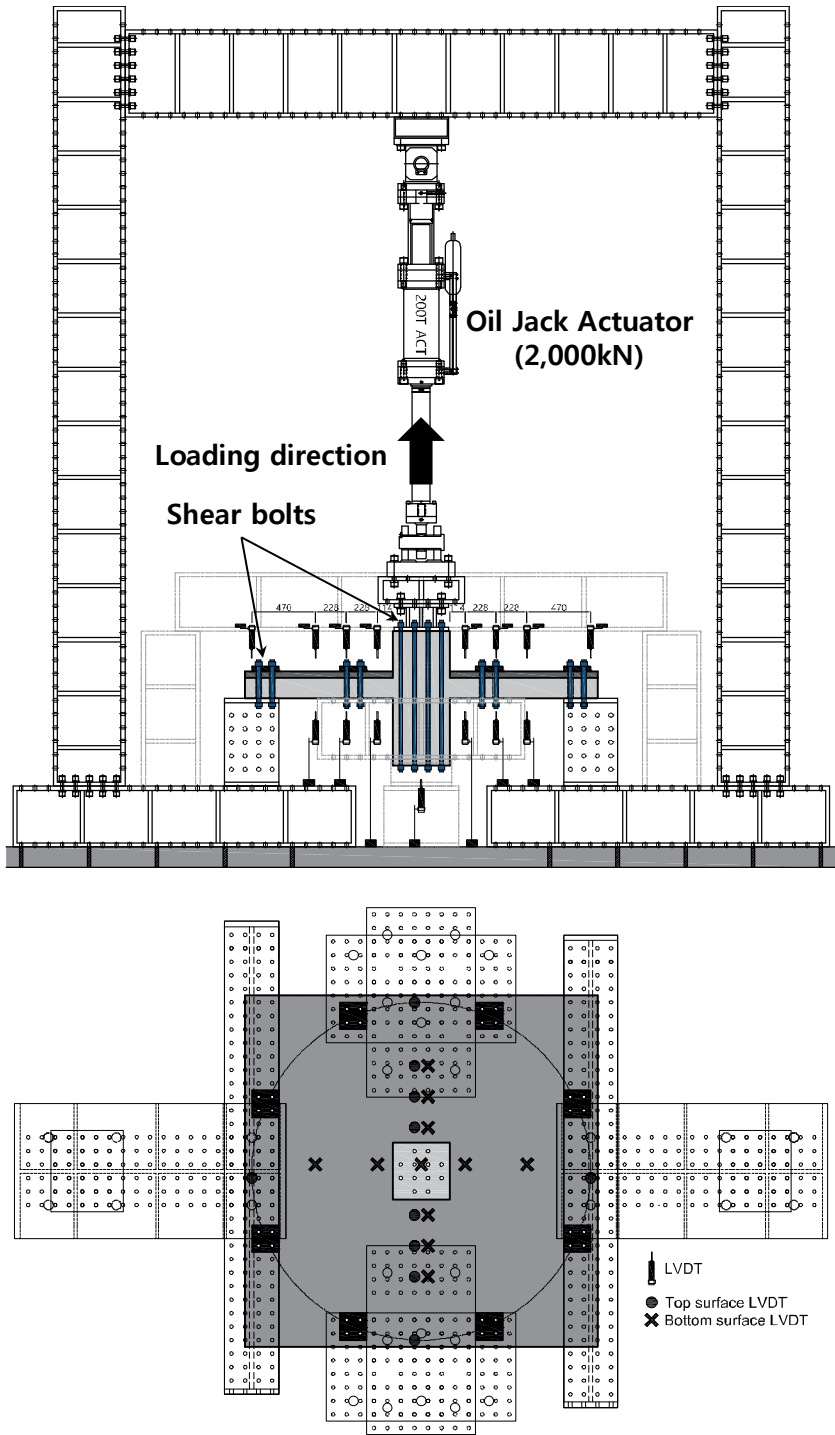


Fig 4-8. Test set-up and disposition of LVDTs

4.5 Materials

For the fabrication of the test specimens, the designed compressive strength of normal strength concrete was 30MPa. Two placements in total were made to construct specimens corresponding to R, U30, U50, U50S and U50L slab-column connection specimens. **Table 4-3** shows the material composition of NSC used in fabricating the RC slab-column connections. Since compressive strength and tensile strength were required in order to analyze structural performance, cylinder type concrete specimens of size of 100mm x 200mm were fabricated, and cured in the same conditions as that for the experimental specimens in accordance with KS F 2403.

Table 4-3. Material composition of NSC

Nominal strength (MPa)	W/C (%)	Unit weight (kg/m ³)				
		Water	Cement	Sand	Gravel	Admixture
30	43.1	169	392	825	952	2.74

Note) Maximum aggregate size = 25mm, Slump = 120mm

A compressive strength test was manually conducted as recommended in KS F 2405 after 28 days from the casting days and on the same day as the experiment date. The measured mean compressive strengths of NCS were, for each experimental specimen, based on the three concrete cylinder coupon tests in accordance with KS F 2405. Since it has been certified worldwide that the direct tensile test is generally not applicable for NSC due to high irregularities and coefficient of variations of measurement results, the tensile strengths were indirectly calculated using an equation provided in KCI 2012. **Table 4-4** summarizes the compressive and calculated tensile strengths of NSC.

Table 4-4. Material properties of NSC

	Name	Age at testing (day)	NSC (MPa)		
			f'_c	f_t	E_c
Actual strength (avg. value)	R	73	41.8	3.88	29500
	U30	75	38.9	3.74	28800
	U50	75			
	U50S	75			
	U50L	70	41.8	3.88	29510

Note) f'_c = compressive strength of NSC, f_t = tensile strength of NSC, E_c = Young's modulus of NSC, f_t are calculated by $f_t = 0.6\sqrt{f'_c}$ (MPa), and E_c are calculated by $E_c = 8500\sqrt[3]{f'_c}$ according to KCI 2012.

In this experiment, the designed compressive strength of UHPC is 180MPa. The UHPC two placements in total were made to construct a thin layer of UHPC on each RC slab-column connection specimen, one batch for U30, U50S and U50L specimens and the other batch for U50 specimen. **Table 4-5** shows the material composition of UHPC used in fabricating the rehabilitating layers over the RC substrates.

Table 4-5. Material composition of UHPC

Nominal strength (MPa)	W/C (%)	Unit weight (kg/m ³)				
		Water	Premix binder	Fine aggregate	Super plasticizer	AE
180	0.2	197.1	1269.5	867.4	18.1	0.5

Note) Premix binder = cement, Zr, Bs, filler, expansion agent, shrinkage reducing agent premix, Slump flow = 740mm, AE = Air-entraining agent

A compressive strength test and a tensile strength test were manually conducted as recommended in K-UHPC design guideline on the same day as experiment date using cylinder type specimens of size of 100mm x 200mm and notched dog-bone shaped specimens, respectively. **Fig 4-11** shows test set-ups for determining the compressive and tensile strengths of UHPC. The

measured mean compressive and tensile strengths of UHPC were based on the three UHPC coupon test. **Table 4-6** summarizes the compressive and tensile strengths of UHPC used in the present study.

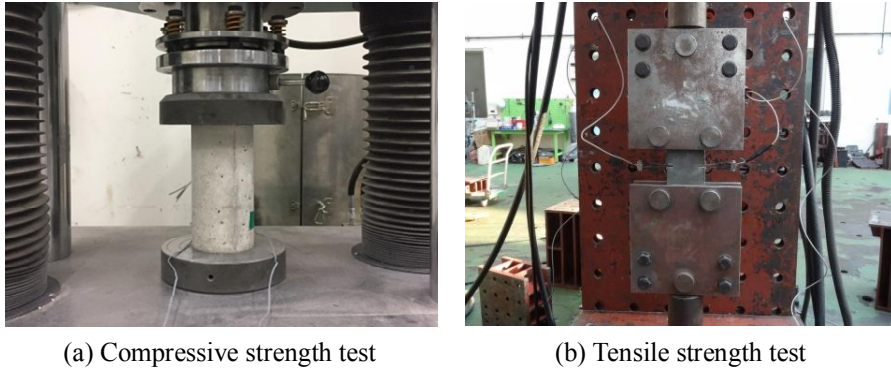


Fig 4-11. Test set-ups for compressive and tensile strength of UHPC

Table 4-6. Material properties of UHPC

	Name	Age at testing (day)	UHPC (MPa)			
			f_{cU}	f_{Ute}	f_{Utu}	E_U
Actual strength (avg. value)	R	-	-	-	-	-
	U30	55	196.5	7.0	14.3	51264
	U50	40	186.6	7.0	14.3	51264
	U50S	54	196.5	7.0	14.3	51264
	U50L	54	196.5	7.0	14.3	51264

Note) f_{cU} = UHPC compressive strength, f_{Ute} = maximum tensile elastic strength of UHPC, f_{Utu} = tensile strength of UHPC, E_U = Young's modulus of UHPC, calculated as specified in K-UHPC 2012

In this experiment, a total of 3 types of steel re-bars were used. D10 re-bars were used for bottom flexural reinforcement of RC slab, additional reinforcement in UHPC overlay and column tie stirrup. D16 re-bars were used for top flexural reinforcement of RC slab, and D22 re-bars were used for the column longitudinal reinforcement. To analyze the properties of the steel re-

bars, a tensile test was conducted in accordance with KS B 0801. **Fig 4-12** shows test set-up for determining tensile strength of steel re-bars. For each type of steel re-bars, three test coupons were chosen and tested. The averages of three test values were used for determining the yield strength and ultimate tensile strength and corresponding strains. The tensile test results of the steel re-bars used in the present study are shown in **Table 4-7**.

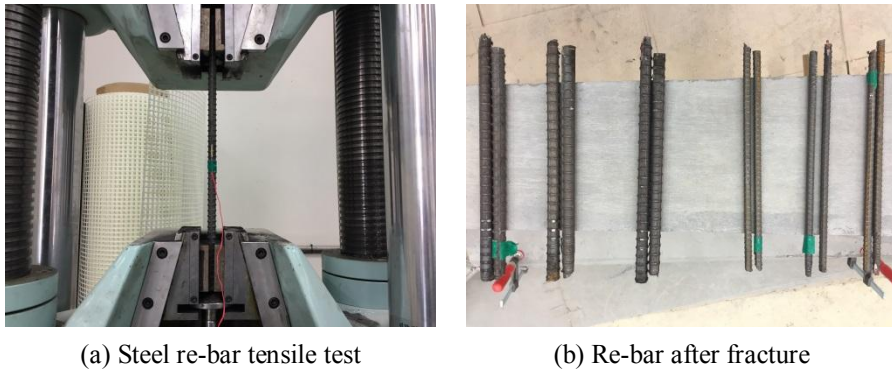


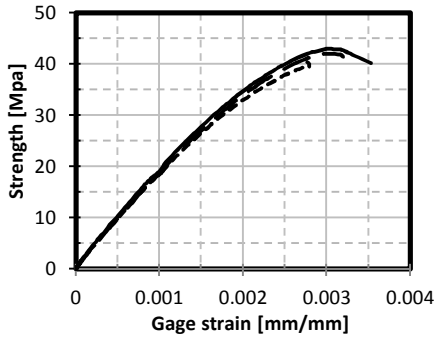
Fig 4-12. Test set-ups for tensile strength of steel re-bars

Table 4-7. Material properties of steel reinforcements

	Steel grade	\varnothing (mm)	f_{sy} (MPa)	ε_{sy}	f_{su} (MPa)	ε_{su}	E_s (GPa)
Actual strength (avg.value)	SD400	D10	454	0.00251	584	0.143	200
		D16	460	0.00233	578	0.248	200
		D22	544	0.00265	662	0.116	200

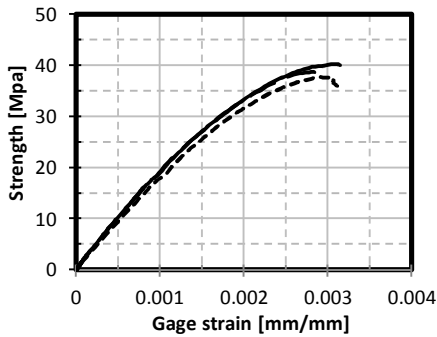
Note) f_{sy} = yield strength of steel reinforcement, f_{su} = ultimate tensile strength of steel reinforcement, E_s = young's modulus of steel reinforcement

Fig 4-13 to **Fig 4-15** shows in detail the total stress-strain relationship and measured strength of the coupon test results of NSC, UHPC and steel re-bars used in the present study.



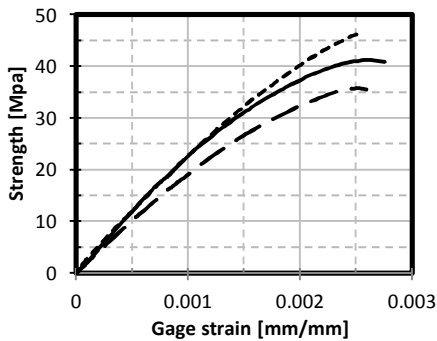
Test Number	f'_c [MPa]
1	43.035
2	42.017
3	40.362
Average	41.8

(a) Concrete compressive strength for R specimen



Test Number	f'_c [MPa]
1	40.234
2	38.706
3	37.688
Average	38.9

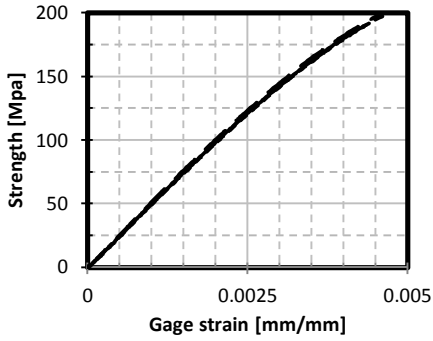
(b) Concrete compressive strength for U30, U50 and U50S specimens



Test Number	f'_c [MPa]
1	41.253
2	35.778
3	48.510
Average	41.8

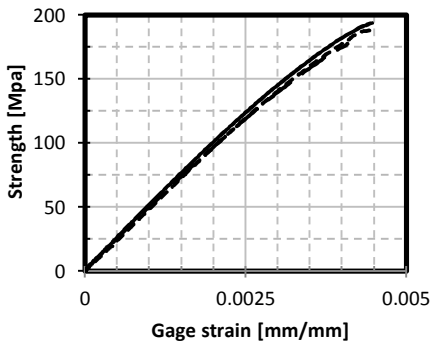
(c) Concrete compressive strength for U50L specimen

Fig 4-13. NSC compressive strength used in tests



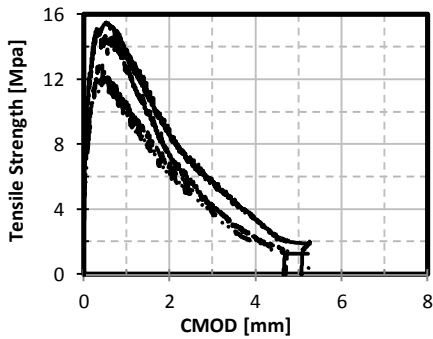
Test Number	f_{cU} [MPa]
1	190.35
2	199.77
3	199.26
Average	196.5

(a) UHPC compressive strength for U30, U50S and U50L specimens



Test Number	f_{cU} [MPa]
1	193.91
2	177.74
3	188.06
Average	186.5

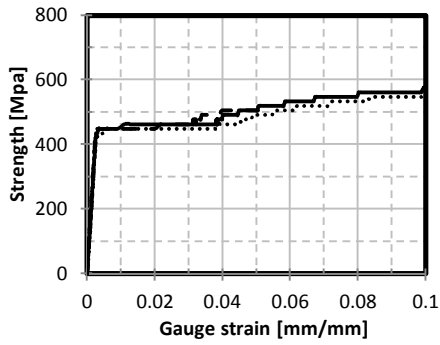
(b) UHPC compressive strength for U50 specimen



Test Number	f_{Ute} [MPa]	f_{Utu} [MPa]
1	6.9	14.5
2	9.0	15.5
3	5.1	12.9
Average	7.0	14.3

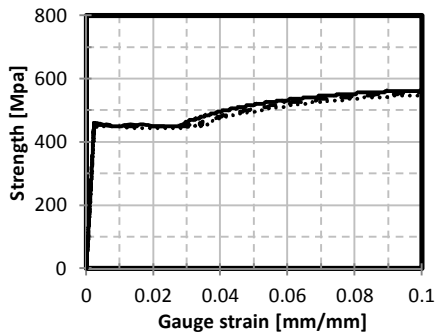
(c) UHPC tensile strength used for specimens

Fig 4-14. UHPC compressive and tensile strength used in tests



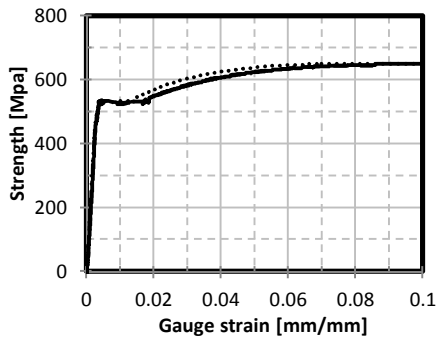
Test Number	f_{sy} [MPa]	f_{su} [MPa]
1	463	589
2	450	575
3	450	589
Average	454	584

(a) Yield and tensile strength of D10 rebar



Test Number	f_{sy} [MPa]	f_{su} [MPa]
1	465	578
2	460	578
3	455	578
Average	460	578

(b) Yield and tensile strength of D16 rebar



Test Number	f_{sy} [MPa]	f_{su} [MPa]
1	544	662
2	541	660
3	546	665
Average	544	662

(c) Yield and tensile strength of D22 rebar

Fig 4-15. Steel rebar yield and tensile strength used in tests

Chapter 5. Concentric Loading Test of UHPC-RC Composite Slab

5.1 Introduction

A series of 5 RC and UHPC-RC composite slab-column connections were submitted to a point force to evaluate the resistance contribution of UHPC overlay to total punching shear capacity. The behavior of specimens was observed and cracks were marked after fully conducting the experiment. Experimental data was collected using the installed concrete and steel strain gauges to measure the strain of the materials and the PI-type crack gauges to measure crack openings at tension side, and lastly, the LVDTs to measure the deflection and rotation of the test specimens. Test results are presented in the following subsections.

Overall, all the specimens showed significantly improved performance, and all failed in punching shear mode accompanying sudden drop of load bearing resistance after the maximum force is recorded. Final failure is triggered by the failure of the RC section. Once the RC section fails, the UHPC overlay cannot carry the entire shear force alone and the whole slab fails. Meanwhile, the specimens retrofitted by UHPC overlay with or without steel re-bars showed larger shear resistance capacity and deformation capacity at failure than the control specimen. This test results indicated that the UHPC overlay can improve the rotation capacity of a member as well as the punching shear capacity. Especially from an economical point of view, the maximum shear resistance versus increased self weight of the slab due to the UHPC overlay was found to be increased further, and this tendency appeared

to be correspondingly larger as the retrofitting ratio increased, as described in **Table 5-1**.

Table 5-1. Comparison of increasing ratios between strength and self weight

I.D.	Ultimate strength (kN)	Slab self weight (kg)	Strength ratios (Normalized by f'_c)	Self weight ratios	Strength versus Self weight
R	644.4	2370.1	1.000	1.000	1.000
U30	758.4	2863.9	1.220	1.208	1.010
U50	908.9	3193.0	1.462	1.347	1.085
U50S	984.5	3237.1	1.584	1.366	1.160
U50L	1170.7	3281.1	1.817	1.384	1.312

An overview of the main test results are summarized in **Table 5-2** for each slab-column connection specimens. The flexural strengths were calculated by using conventional yield line method. Additionally, it should be mentioned that, since the specimens were not pre-loaded or cracked before applying the thin layer of UHPC, the results of the present study are applicable in practice to existing slab-column connections that did not experience extensive structural flexural cracking or damage resulting from an excessive gravity load or lateral load.

Concentric Loading Test of UHPC-RC Composite Slab

Table 5-2. Experimental test results

I.D.	Failure mode	Flexural strength (kN)	Inclined shear crack angle (°)			Load stage(mm, kN)						Strength ratio
						Cracking stage		Ultimate stage		Failure stage		
			V_{flex}	α_N	α_S	α	Δ_{cr}	V_{cr}	Δ_u	V_u	$\Delta_{failure}$	
R	FS	676.0	27.4	31.7	29.6	0.785	126.1	21.64	644.4	21.98	636.1	0.95
U30	S/DB	973.8	24.9	28	26.5	0.867	200.7	13.63	758.4	14.18	707.7	0.78
U50	S/DB	1203.0	23	22.1	22.6	0.713	235.4	15.57	908.9	16.53	855.1	0.76
U50S	S/DB	1455.7	22.6	26.2	24.4	0.638	259.4	13.7	984.5	14.53	879.1	0.68
U50L	S/DB	1718.4	27.1	23.8	25.5	0.675	278.2	14.86	1170.6	15.21	1157	0.70

Note) FS=Flexural shear failure, S=Shear failure, DB=Debonding at the tip of the diagonal shear crack

5.2 Test Results

5.2.1 Load vs displacement relationships

Since the initial cracks are so microscopic that they can not be observed with the naked eye, the point at which the linear relationship ends in the load-displacement relationship is determined as the initial cracking stage. The load and displacement corresponding to this step was defined as the initial cracking load (V_{cr}), and the initial cracking displacement (Δ_{cr}), respectively. Furthermore, the initial stiffness was determined through the slope in this section.

Fig 5-1 shows the load-displacement relationship and the deformed shapes measured from the top and bottom surface of the control specimen. For the control specimen, stiffness deterioration was observed at around 126 kN due to the initial longitudinal flexural crack, and an almost proportional relation between displacement and axial load was then maintained before it reached its maximum load. At around 500 kN, one of the longitudinal steel reinforcement in the RC section located at d_{sc} from the column face has reached the yield strain ε_{scsy} , but without big difference in the load-displacement behavior. After reaching its maximum load at around 644 kN, the conical shaped concrete cover at the top surface was spalled out by punching shear, causing subsequent substantial strength deterioration. Thus, as the peak strength did not reach the predicted flexural capacity, while coinciding with the yielding of steel re-bars in the vicinity of the column, the measured maximum load V_u was determined by flexure-shear failure.

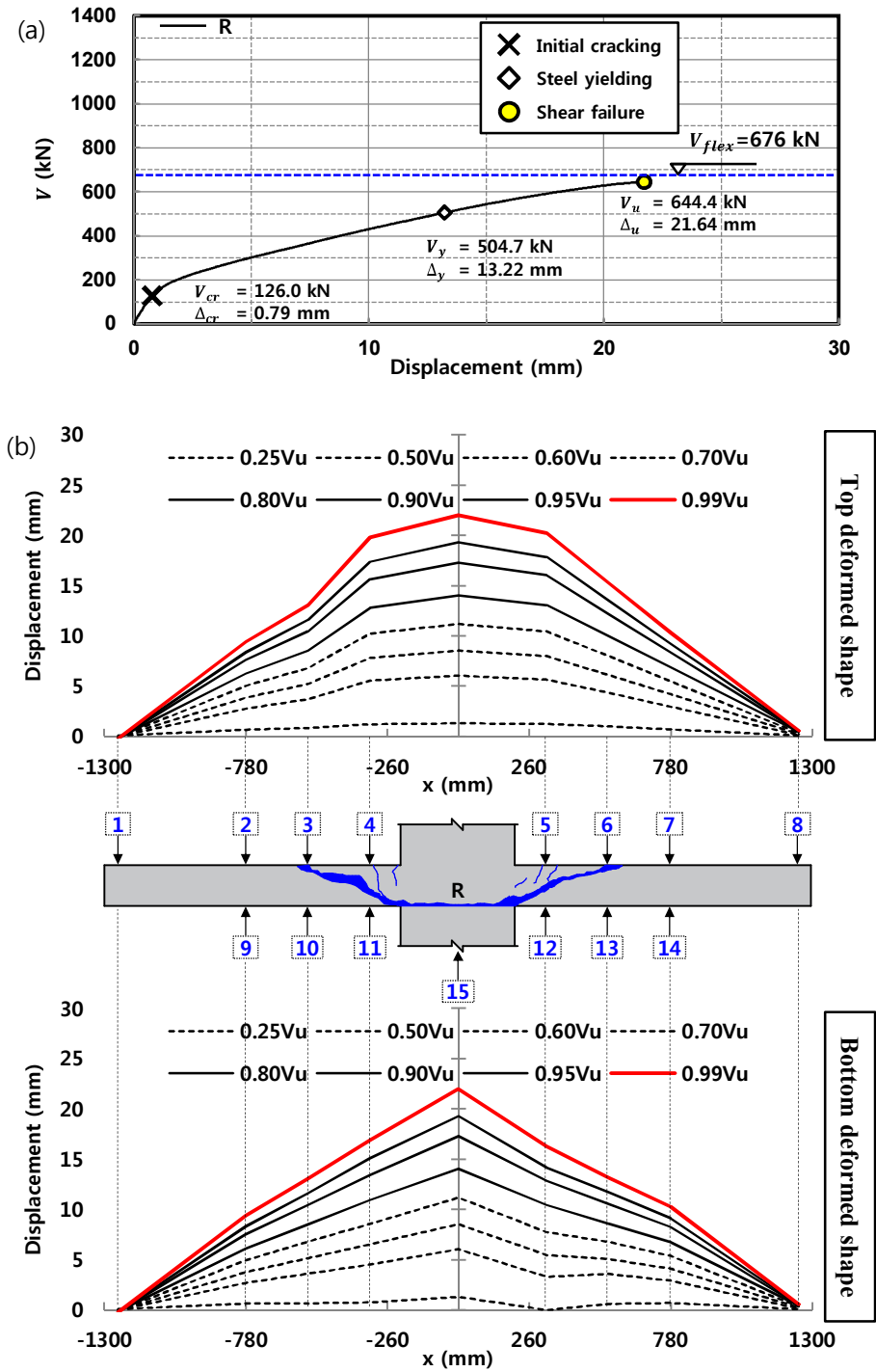


Fig 5-1. Load-displacement relationship (a) and deformed shapes (b) of R

For all the retrofitted specimens, consistently, stiffness deterioration was observed at around 200~270 kN due to the initial longitudinal flexural crack, and an almost proportional relation between displacement and axial load was then maintained before it reached its maximum load. In addition, no re-bars experienced yielding for all retrofitted specimens, which indicates that the measured maximum loads V_u are determined by punching shear failure, causing subsequent substantial strength deterioration. After reaching maximum loads, in contrast to the control specimen, the bridging effect of the steel fibers embedded in the UHPC overlay prevented the concrete cover from being spalled out, which can be featured as an another advantage of the UHPC overlay.

In U30 (**Fig 5-2**) with 30mm UHPC overlay, the failure occurred at displacement $\Delta_u=13.6$ mm. Due to the 30mm UHPC overlay, the maximum shear resistance was increased to 758.4 kN, which was on average 18% and 22% greater than that of R for the case of maximum load V_u and normalized maximum load $V_{u,norm}$, respectively.

In U50 (**Fig 5-3**) with 50mm UHPC overlay, the peak load occurred at slightly larger displacement $\Delta_u=15.6$ mm. the maximum shear resistance was increased to 908.9 kN, which was on average 41% and 46% greater than that of R for V_u and $V_{u,norm}$, respectively. During the test, the pressure level of the actuator was suddenly dropped so that after restoring the pressure, the test was resumed.

In U50S (**Fig 5-4**) with 50mm UHPC overlay plus D10@180mm steel re-bars in it, the failure occurred at displacement $\Delta_u=13.7$ mm. the maximum shear resistance was increased to 984.5 kN, which was on average 53% and

58% greater than that of R for V_u and $V_{u,norm}$, respectively.

In U50L (**Fig 5-5**) with 50mm UHPC overlay plus D10@90mm steel re-bars in it, at slightly larger displacement $\Delta_u=14.9$ mm the failure occurred. The maximum shear resistance was increased to 1,170.6 kN, which was on average 82% greater than that of R for V_u and $V_{u,norm}$.

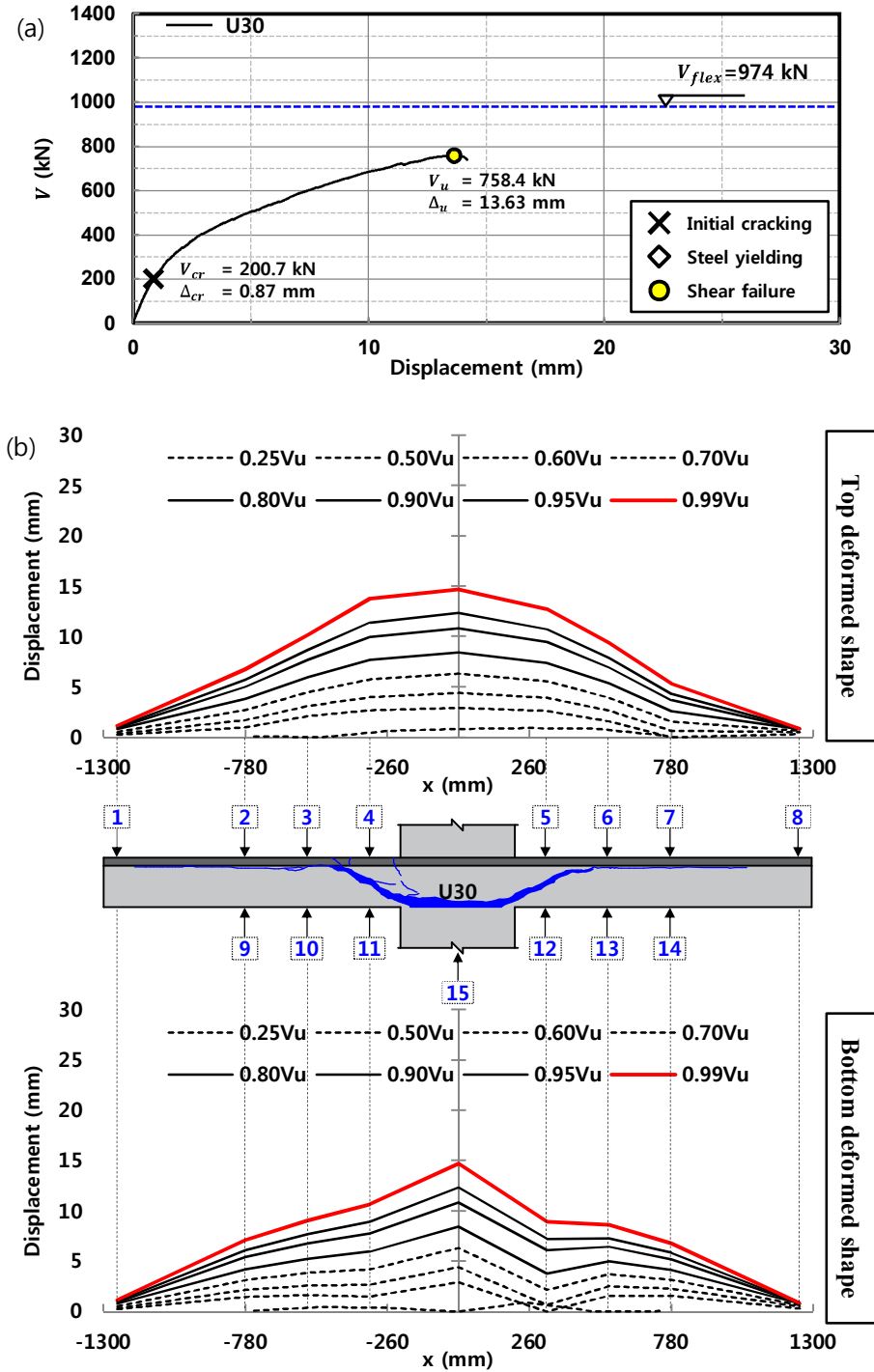


Fig 5-2. Load-displacement relationship (a) and deformed shapes (b) of U30

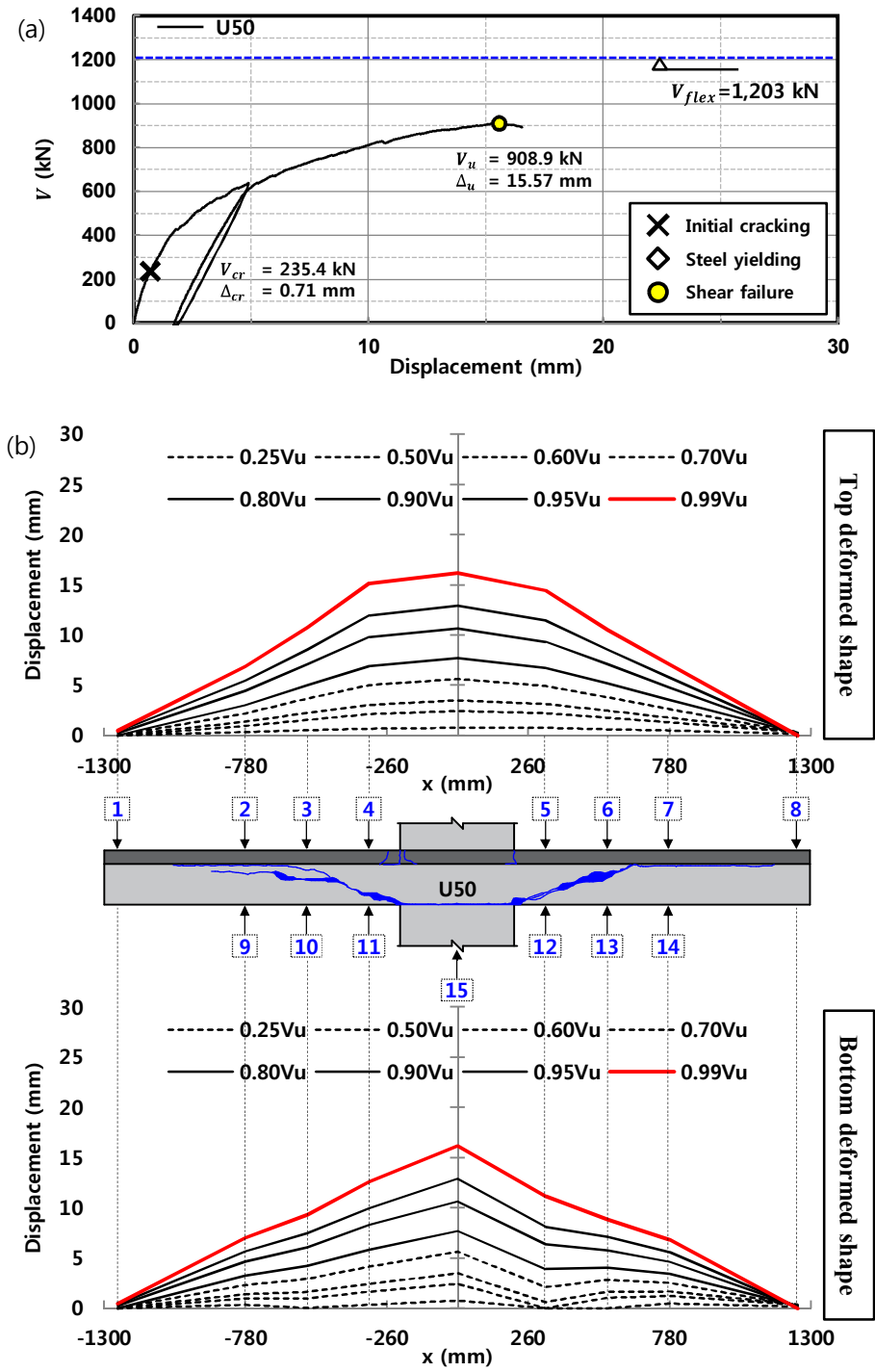


Fig 5-3. Load-displacement relationship (a) and deformed shapes (b) of U50

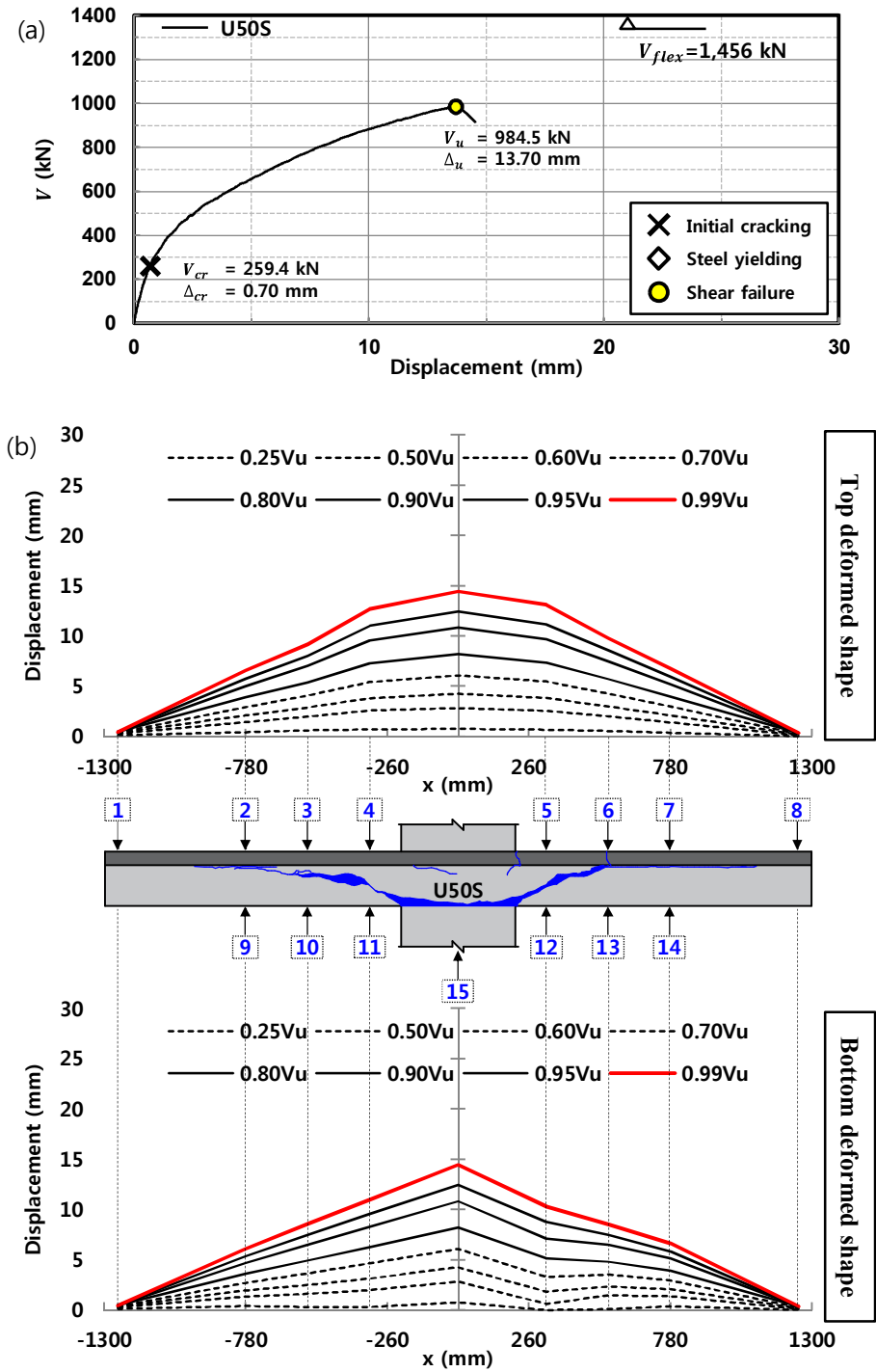


Fig 5-4. Load-displacement relationship (a) and deformed shapes (b) of U50S

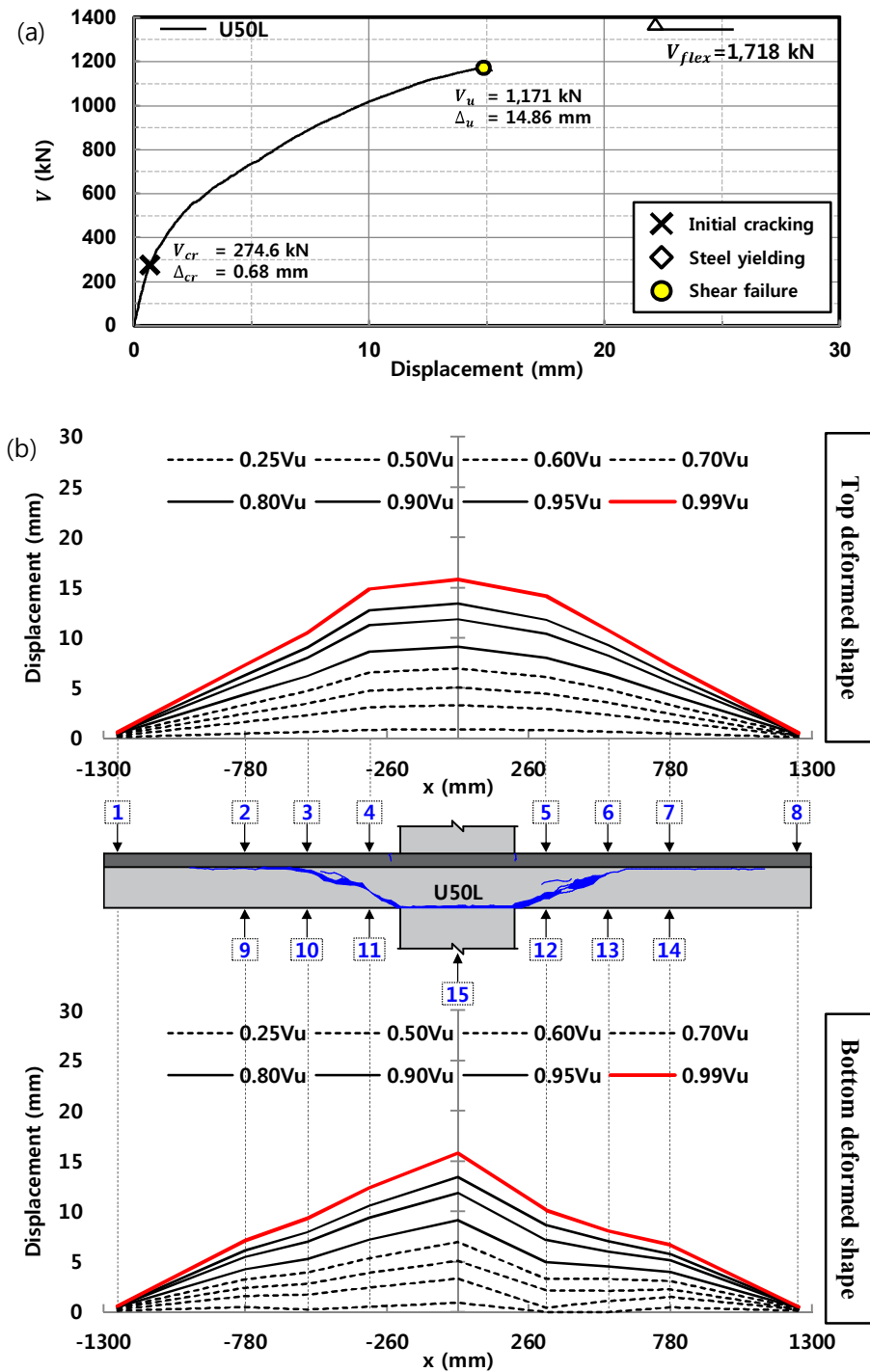
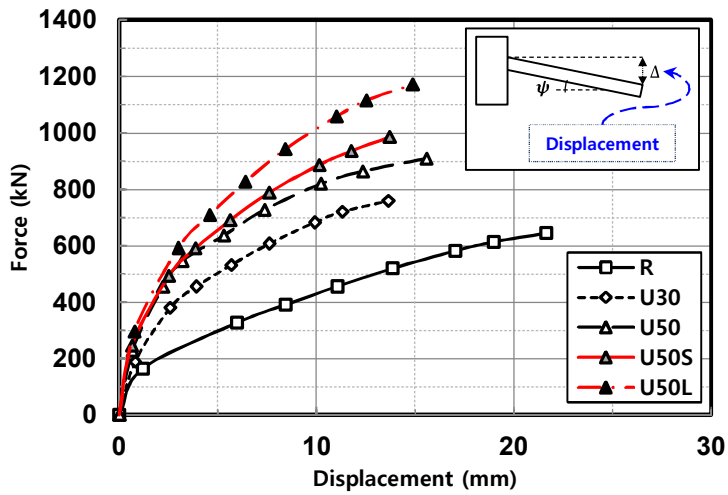
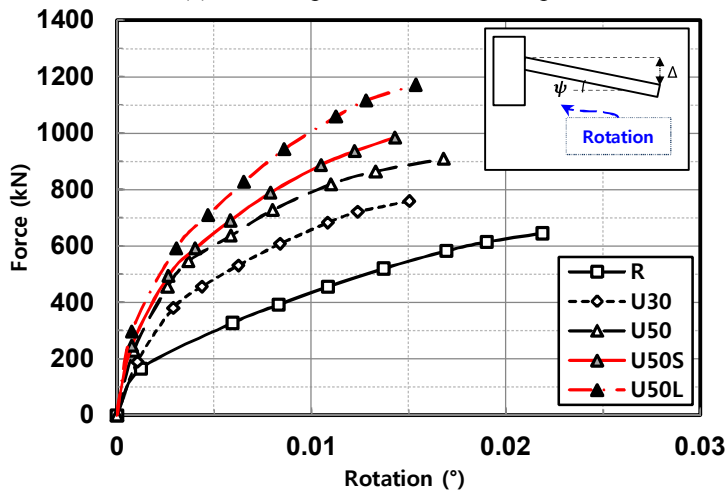


Fig 5-5. Load-displacement relationship (a) and deformed shapes (b) of U50L

Fig 5-6 shows altogether the load-deformation behavior of the specimens. Two parameters regarding to the deformation capacity are introduced in Fig 5-6; 1) Δ =displacement (mm) and 2) ψ =rotation ($^{\circ}$). The slab rotation, based on the assumption of the sector model proposed by Kinnunen and Nylander, was estimated from the displacement differences measured at the north and south sides of bottom surface of a slab.



(a) Load-displacement relationship



(b) Load-rotation relationship

Fig 5-6. Load-deformation relationships of specimens

On the basis of comparison of the load-deformation behaviors, it can be easily concluded that the layer of UHPC significantly increased the rigidity of the slab and provided additional shear resistance to the RC slab-column connections. Furthermore, the following important experimental results can be found by deep consideration.

Firstly, when comparing the test results of U50, U50S and U50L, the use of steel re-bars in the UHPC overlay has a significant influence on the resistance and deformation of the composite slab, which is different outcome from that of previous research performed by Bastien-Masse (2015), where the use of steel re-bars in the UHPC overlay did not have an important influence on the resistance or deformation of the composite slab. This experimental result directly implies that the load transfer mechanism of the UHPC-RC composite slab should be reconsidered from a slightly different point of view from the previous study.

Next, regarding to the deformability, the deformation capacity of the retrofitted specimens turned out to be maintained above a certain level even though the retrofitting level increased, which is unmatched with the conventional sense. To identify this trend of the structural behavior of the UHPC-RC composite slab, cracking patterns, strains and thickness variations should be investigated altogether.

5.2.2 Cracking patterns

The cracking patterns at the top tensile surface and the cut section of the specimens were carefully observed. Based on the observation, it was found that by adding a thin layer of UHPC overlay, a larger number of radial cracks are visible which means that the UHPC overlay mainly contributes to the punching shear resistance by a tangential bending mechanism. The specimens were cut off acrossing the North-South axis adjacent to the column face after the tests were ended and the internal shear and flexural cracking patterns were observed on the cut sections. **Fig 5-7** to **Fig 5-11** illustrate the fully developed cracking patterns of the top tensile face and the cut section for each specimen.

All punching cones observed on the cut sections, including the RC slab and UHPC-RC composite slabs, have a similar shear cracking patterns with an angle α between 20° and 30° with respect to the horizontal line for the RC slab and UHPC-RC composite slabs, respectively. The decreased inclination of the critical shear crack in the lower part of the concrete might be attributed to the increased effective flexural depth due to the additional UHPC overlay, although it does not appear to be significant. The inclined critical shear crack cannot propagate through the UHPC overlay. In the composite slabs, as also observed in the previous test results (Bastien-Masse, 2015), the diagonal shear crack rotates just below the interface between the UHPC overlay and the RC substrate at the level of the top steel re-bar layout in the concrete.

It is also worth noting that no significant vertical flexural bending crack is observed near the column in the RC sections of the composite slabs contrary to R specimen. However, some vertical cracks are visible in the UHPC overlay, developing radially, directly implying that the UHPC overlay mainly carries the bending efforts in the tangential direction. Near the column, at the distance of 140mm from the column face, these longitudinal cracks

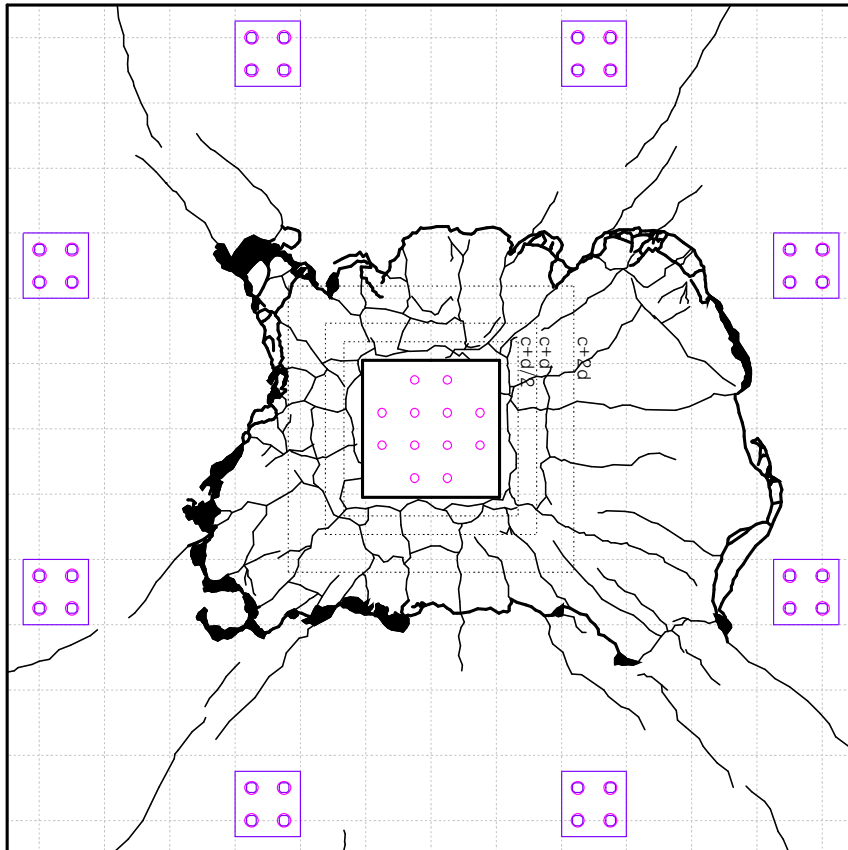
have a typical crack mouth opening larger than 0.3mm for composite slabs (see **Chapter 5.2.4**), which means the direct participation of the UHPC overlay in global shear resistance.

For R, after flexural cracks were slightly developed, a conical shaped punching cone at the top surface was formed at the same time as the load-carrying capacity was suddenly decreased. Near the punching shear cracks, spalling of the concrete cover was observed, and further flexural and shear cracks did not develop.

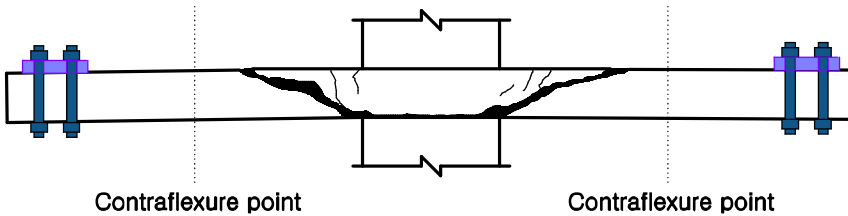
In case of U30, after the initial flexural cracking, the flexural cracks progressed in the longitudinal direction as the load increased, and until the load increased to the maximum resistance, many flexural cracks occurred. The conical shaped punching cone at the top surface occurred slightly after the sudden drop in load resistance. In addition, macro cracks in the UHPC overlay were observed at the corner of the column where the tensile stress concentrated.

In case of U50, U50S and U50L, after the initial flexural cracking at slightly higher load level than that of R and U30, many flexural cracks progressed in the longitudinal direction as the load increased. The flexural cracks become more prevalent with increasing retrofitting ratio, which can be attributed to the improved crack controlling effect of the UHPC reinforced with steel re-bars. Thus, as the retrofitting ratio increased, the maximum crack opening correspondingly decreased as can be seen in **Chapter 5.2.4**. The conical shaped punching cone at the top surface also occurred, however, it was too small to distinguish with naked eyes.

Cracking patterns of R



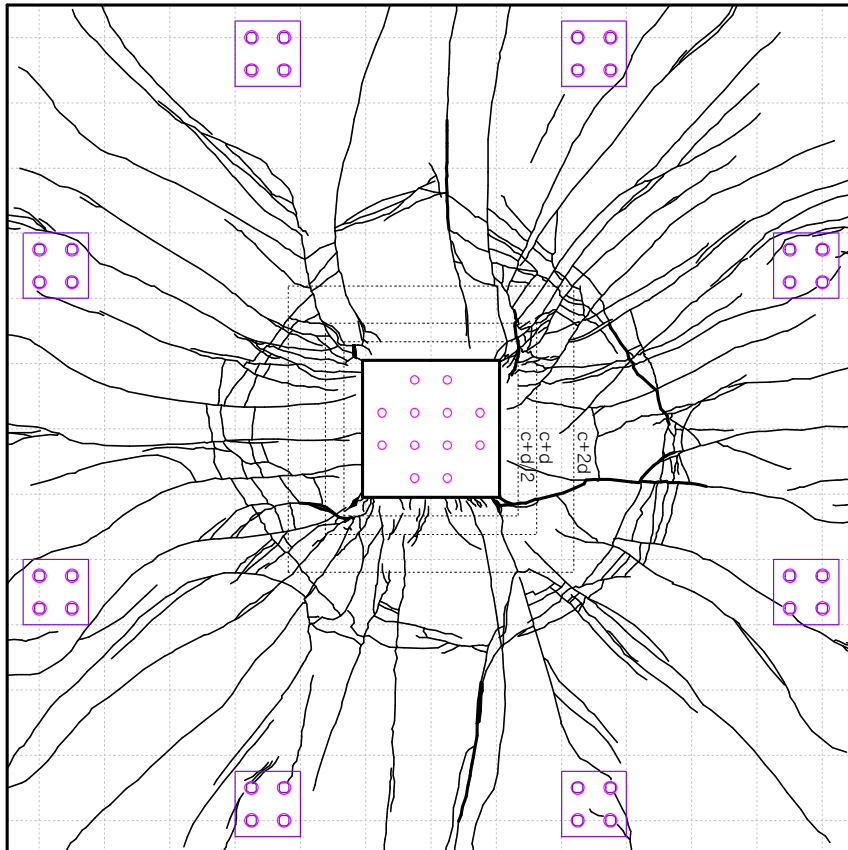
(a) Fully developed cracking pattern of the top tensile face



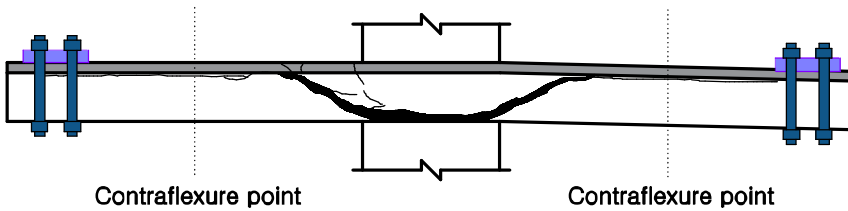
(b) Fully developed cracking pattern on cut section

Fig 5-7. Fully developed cracking patterns of R specimen

Cracking patterns of U30



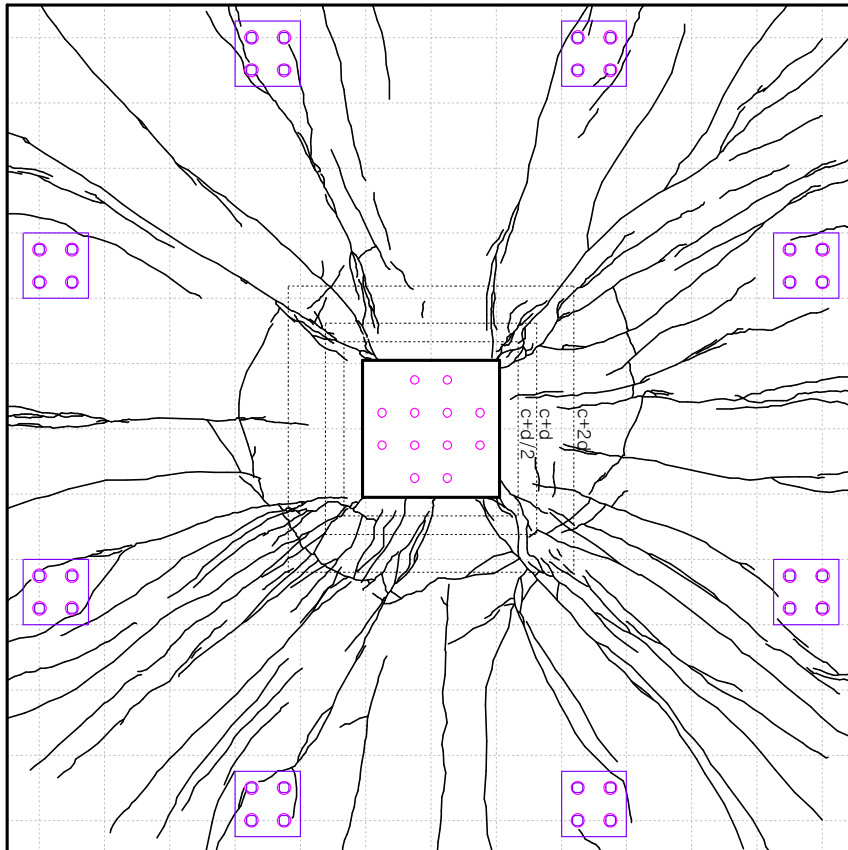
(a) Fully developed cracking pattern of the top tensile face



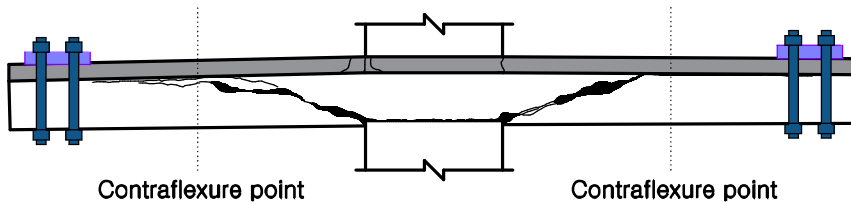
(b) Fully developed cracking pattern on cut section

Fig 5-8. Fully developed cracking patterns of U30 specimen

Cracking patterns of U50



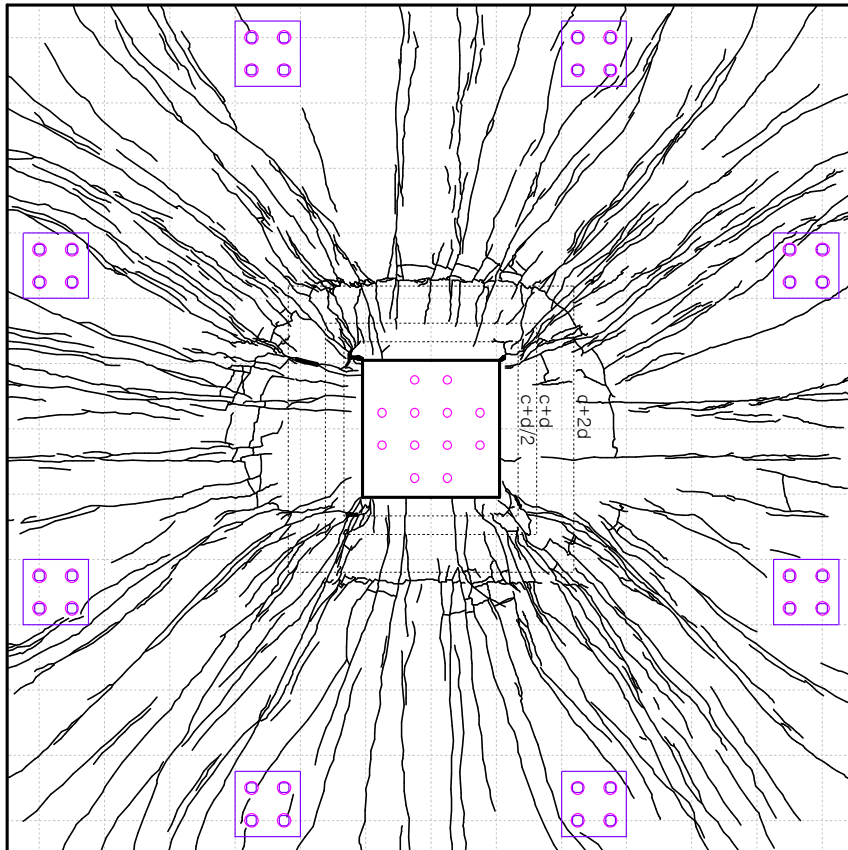
(a) Fully developed cracking pattern of the top tensile face



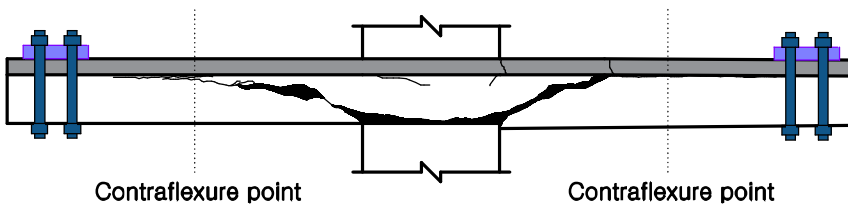
(b) Fully developed cracking pattern on cut section

Fig 5-9. Fully developed cracking patterns of U50 specimen

Cracking patterns of U50S



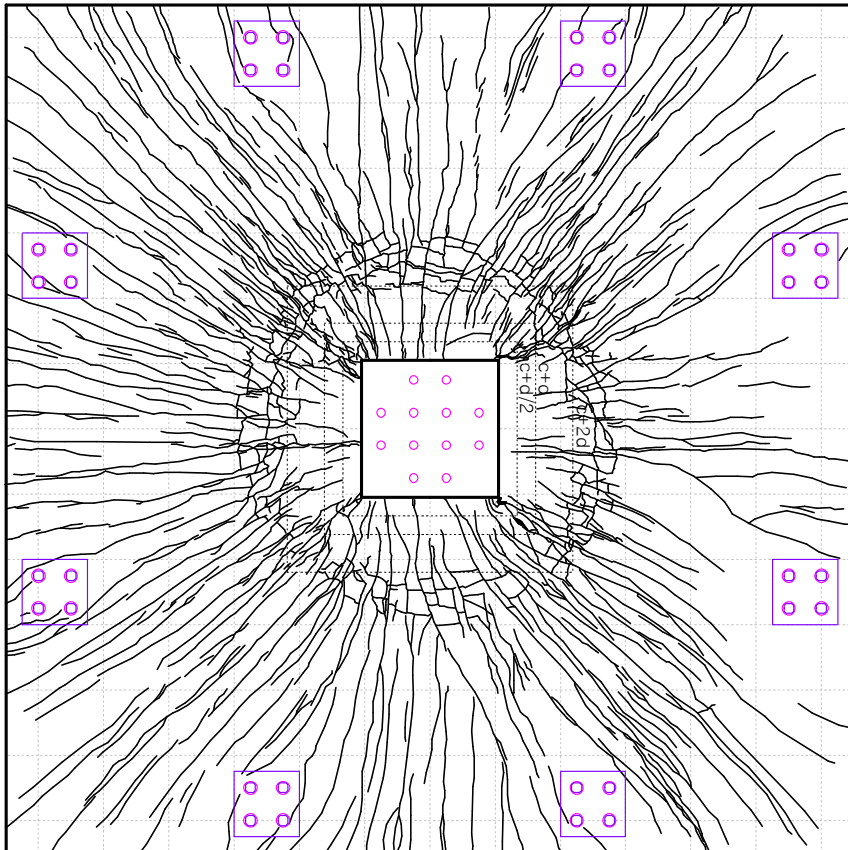
(a) Fully developed cracking pattern of the top tensile face



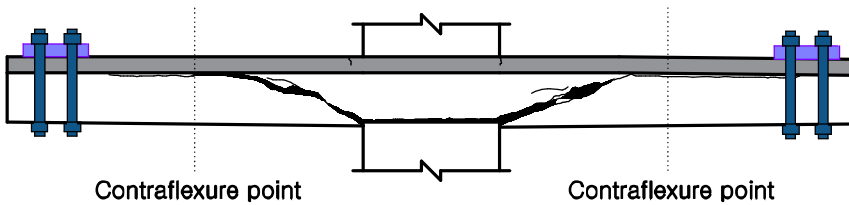
(b) Fully developed cracking pattern on cut section

Fig 5-10. Fully developed cracking patterns of U50S specimen

Cracking patterns of U50L



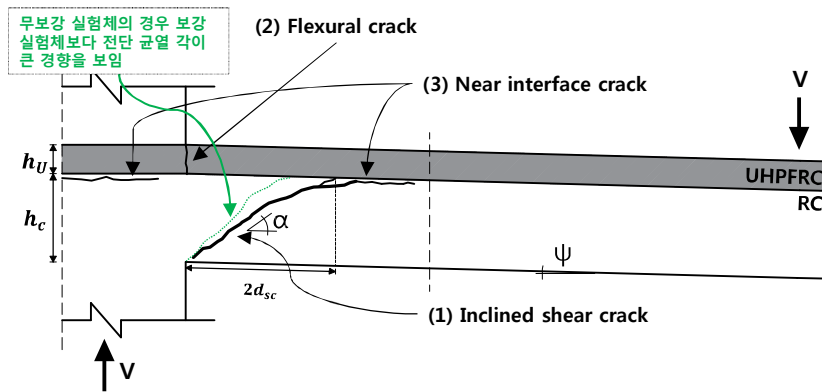
(a) Fully developed cracking pattern of the top tensile face



(b) Fully developed cracking pattern on cut section

Fig 5-11. Fully developed cracking patterns of U50L specimen

The overall cracking patterns show that the inclined shear cracks generated in the RC section cannot be propagated into the UHPC overlay, which is based on very dense material composition and high tensile strength. Rather, the cracks propagate by rotating horizontally to the longitudinal direction of the slab at the interface, leading to formation of Near Interface Cracking (NIC). This means that the thin layer of UHPC contributes to the improvement of the punching shear capacity of the UHPC-RC composite slabs by providing additional load-bearing resistance by means of changing the load transfer mechanism at the interface from shear to interface shear, or out of plane bending due to the prying action resisted by the UHPC overlay. Therefore, punching shear cracks in tangential direction at the RC section did not occur prominently at the top surface. Typical cracking patterns observed in the cut section are distinguished by three patterns as shown in Fig 5-12.



(a) Typical cracking patterns



(b) Inclined shear, flexural and near interface crack in specimens

Fig 5-12. Typical failure cracks developed in UHPC-RC composite slabs

5.2.3 Thickness variation

The thickness variation measurements give indications on how the inclined shear cracking developed inside the slab. The **Fig 5-13** shows the thickness variation due to the inclined shear crack corresponding to various loading steps and the measurement positions, where the thickness variation was measured through difference between displacements measured at top and bottom surfaces of the same cross section. Two measurements were taken located at 114mm from the column on the south and north.

The test results show similar trends to those of the previous study performed by Bastien-Masse (2015). In the case of the retrofitted slabs, the thickness variations turned out to be larger than those of the reference slab. In addition, the inclined shear cracks began to occur between about 50% and 70% of the peak strength for the retrofitted specimens.

Concentric Loading Test of UHPC-RC Composite Slab

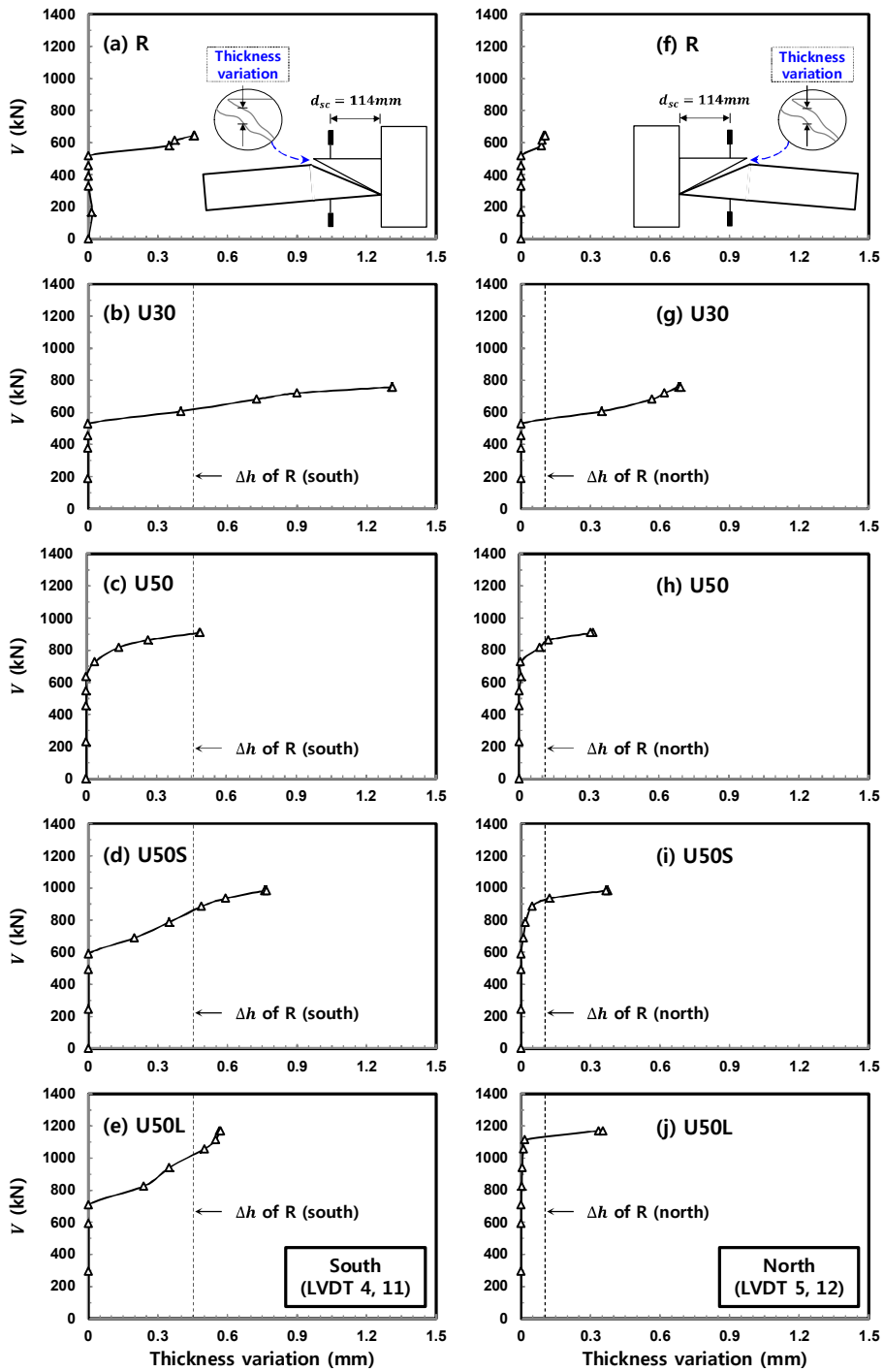


Fig 5-13. Change of thickness in two locations (south and north)

5.2.4 Crack opening in tension surface

Crack openings in radial and tangential directions were measured by using PI-5-250 type and PI-5-100 crack gauges, respectively. The **Fig 5-14** shows the crack openings in radial and tangential directions. According to the measured data, the crack mouth opening displacement (CMOD) at maximum resistance is larger than 0.3mm, as measured by the crack gauges. Thus, the UHPC overlay is in strain-softening phase in this location, meaning that the measured crack openings are higher than the crack opening at ultimate tensile strength as defined in K-UHPC structural design guideline ($w_u=0.3\text{mm}$). One noticeable thing is that the crack opening propagation in tangential direction in the UHPC overlay was significantly suppressed by additional steel re-bars in the UHPC overlay.

Concentric Loading Test of UHPC-RC Composite Slab

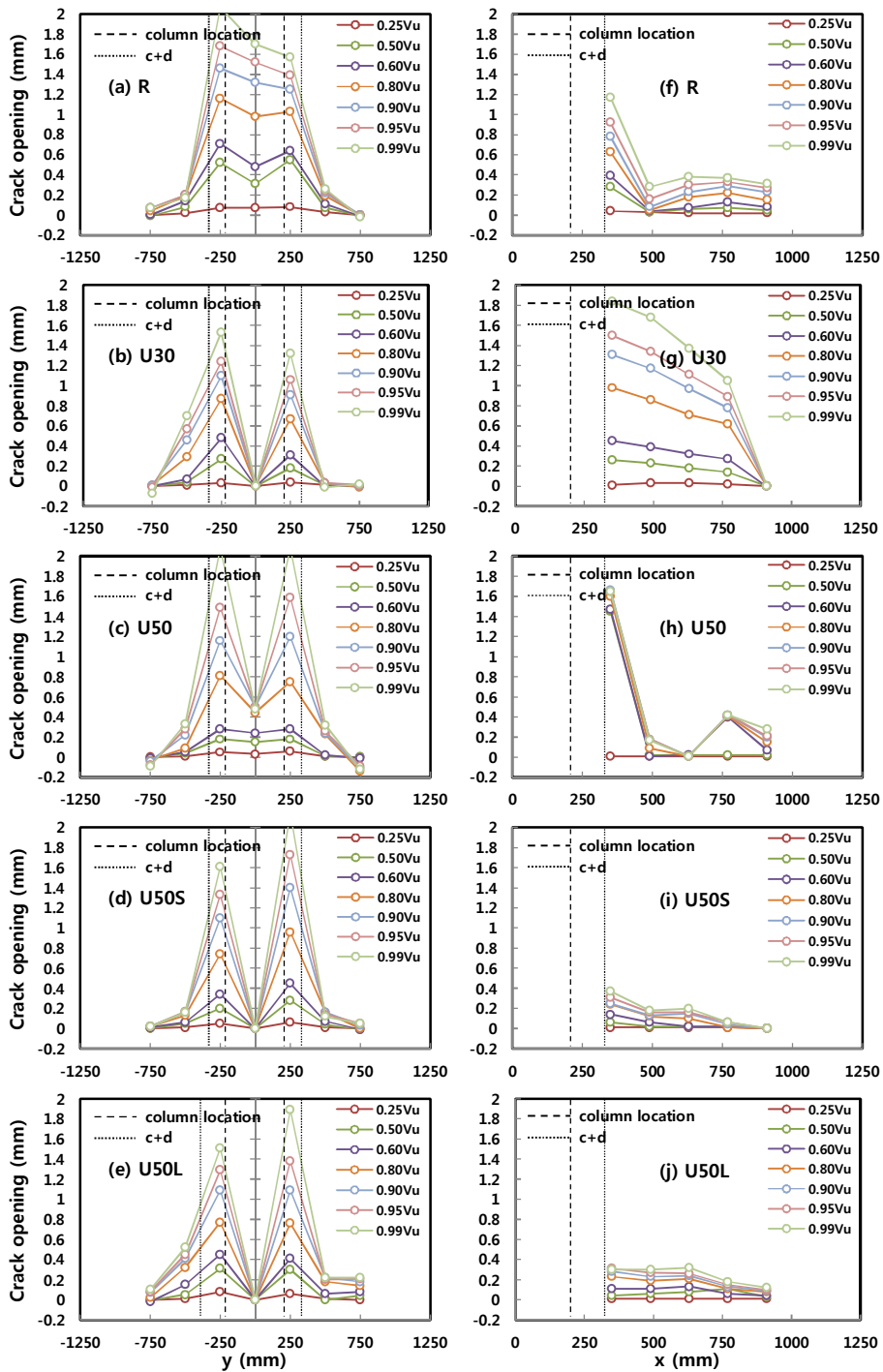


Fig 5-14. Crack opening in radial (left) and tangential (right) directions

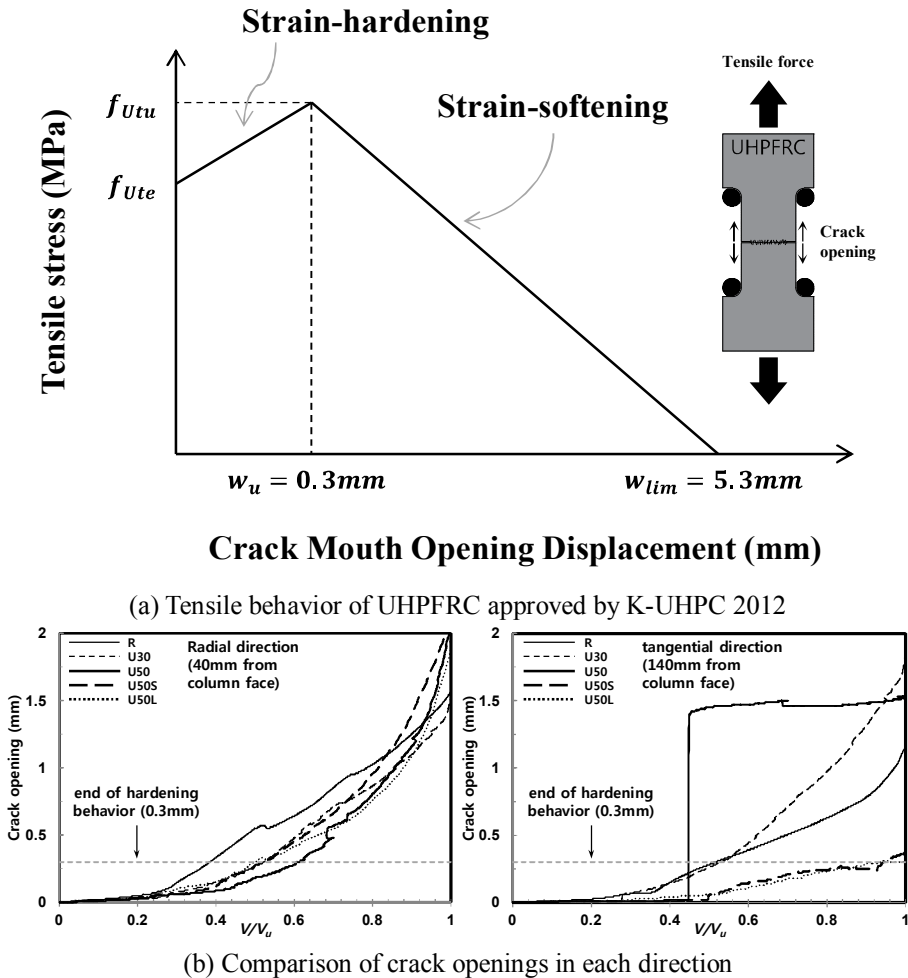


Fig 5-15. Relationship between tensile behavior of UHPFRC and crack openings

The point where the strain-hardening behavior is transformed to the strain-softening behavior is defined equal to 0.3mm in K-UHPC structural design guideline. Actually, it was experimentally observed that the strain-hardening behavior ends when the CMOD of the notched UHPC tensile specimens reaches 0.3mm. Thus, it indicates that the UHPC overlay directly contributed to the load bearing resistance of the composite slabs.

5.2.5 Strain in steel re-bars

The obtained strain gauge data show that none of the main tensile reinforcement reached yield strain except for the case of control specimen (R), providing evidence that the drastic strength degradation occurred due to concrete fracture. Meanwhile, none of the bottom reinforcement for all the specimens experienced yielding. As indicated, **Fig 5-16** to **Fig 5-20** show the strains in the flexural tensile reinforcements placed in orthogonal direction, which are placed at the distance of d_{sc} (=114mm) and 140mm for longitudinal direction and tangential direction strain, respectively. The strains in the flexural reinforcement remained in the elastic region during testing.

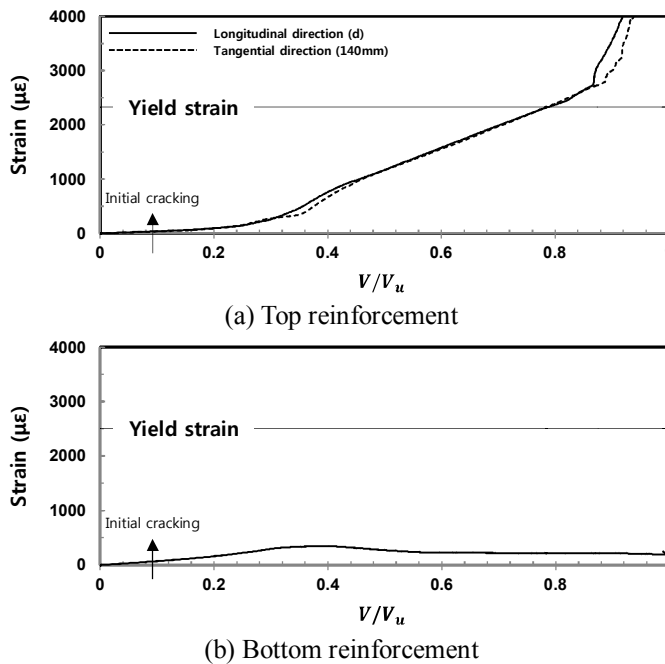
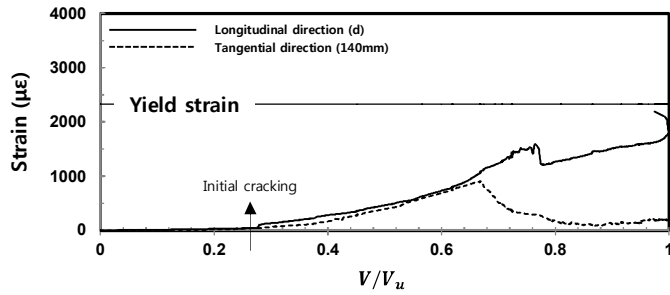
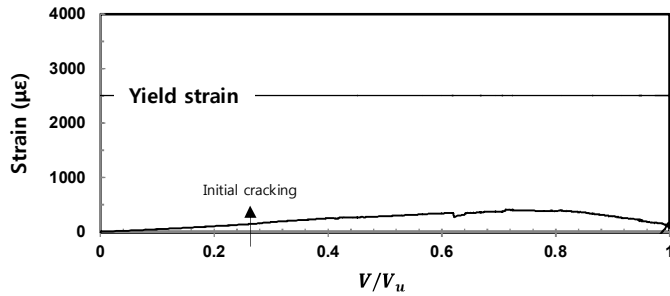


Fig 5-16. Measured strains of re-bars in RC section of R

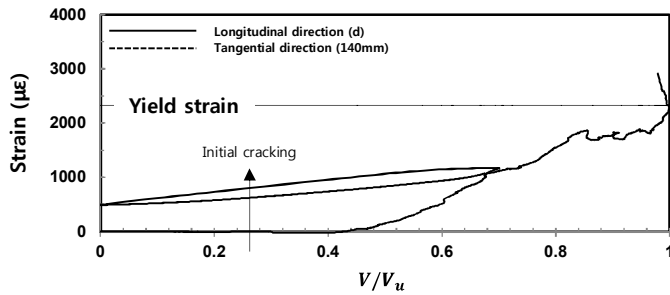


(a) Top reinforcement

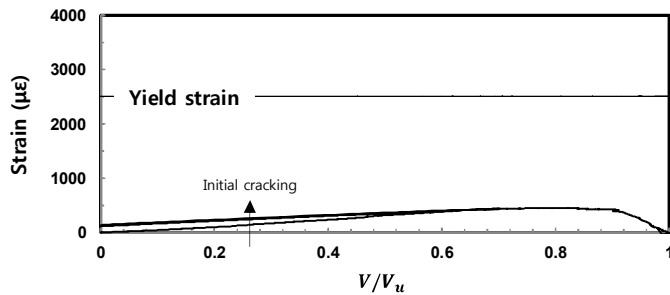


(b) Bottom reinforcement

Fig 5-17. Measured strains of re-bars in RC section of U30

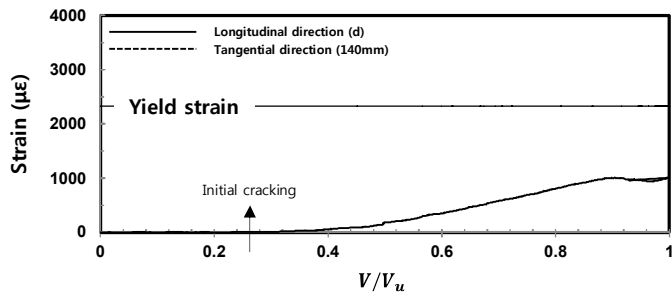


(a) Top reinforcement

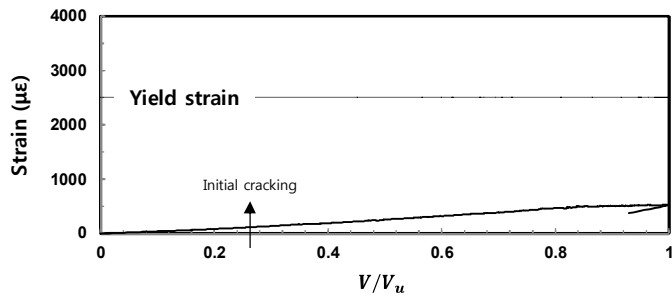


(b) Bottom reinforcement

Fig 5-18. Measured strains of re-bars in RC section of U50

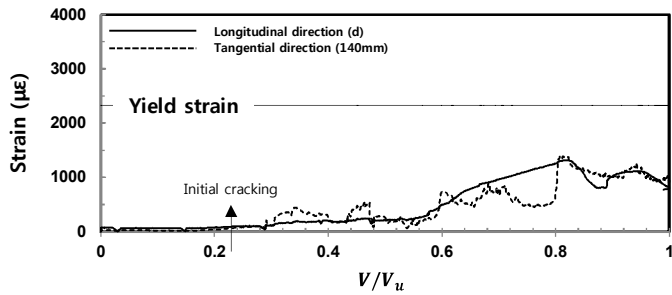


(a) Top reinforcement

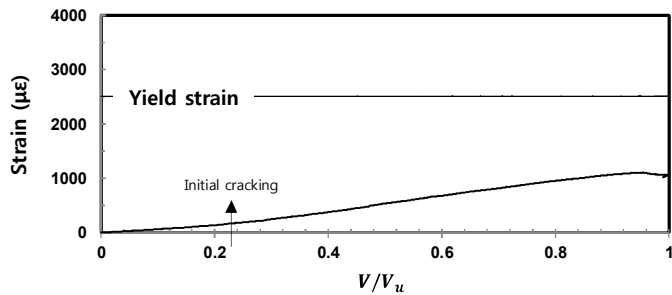


(b) Bottom reinforcement

Fig 5-19. Measured strains of re-bars in RC section of U50S



(a) Top reinforcement



(b) Bottom reinforcement

Fig 5-20. Measured strains of re-bars in RC section of U50L

It is worth notifying that except for the control specimen R, all the other specimens retrofitted by the UHPC overlay do not experience yielding at the tension reinforcements. The comparison of longitudinal tension steel reinforcement strains of each specimen located at the distance of d_{sc} (=114mm) from the column face is shown in **Fig 5-21**. For compressive strains at the bottom steel re-bars, the compressive strains slightly increased by adding a layer of UHPC. However, no noticeable difference was captured.

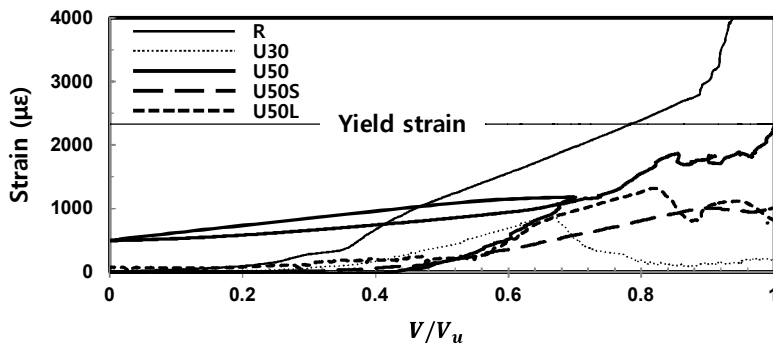


Fig 5-21. Comparison of measured strain of top re-bars in RC section

5.2.6 Strain in concrete compressive surface

Fig 5-22 to **Fig 5-26** show the compressive strains at the bottom surface of each specimen. The compressive strains were measured in longitudinal and tangential directions on the east and south sides of the specimens and the mean values of the measured strains were used. The graphs, which are arranged on the left side, describe the longitudinal and tangential direction compressive strains in which the 40mm, 114mm and 342mm mean the distance from the column face. Meanwhile, the graphs arranged on the right side describe the average compressive strains at each point located at the distance of 40mm, 114mm and 342mm from the column face during load steps. It should be mentioned that overall, the longitudinal compressive strains are significantly bigger than that of the tangential direction.

Additionally, Kinnunen and Nylander (1960) concluded that, based on observation of several test results, the slab-column connections subjected to the monotonic gravity load failed in punching shear failure mode when the longitudinal compressive strain $\alpha\varepsilon_0$ at the bottom of the slab-column connections reached 0.00196. This empirical perspective is also well matched with the present test results.

Meanwhile, according to the test results performed by Bastien-Masse (Bastien-Masse, 2015) with a total of 4 UHPFRC-RC composite slabs, the compressive strains at the bottom surface reached about 0.004 strain, which is nearly twice that of conventional RC slab specimens. However, as a result of the present study, the above phenomenon was not observed, and rather, the compressive strains at the bottom surface tend to be slightly decreased when applying the UHPC overlay.

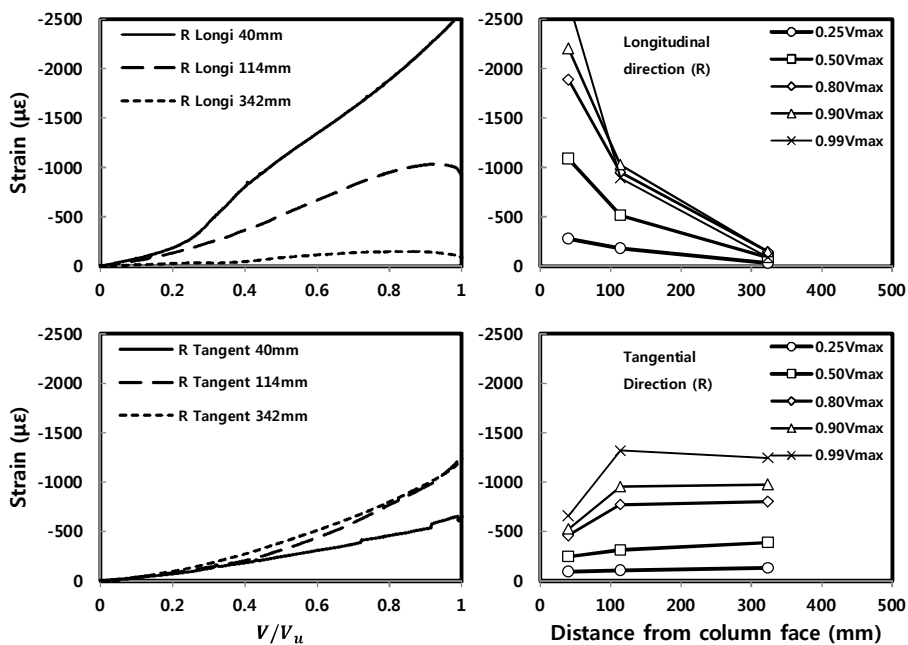


Fig 5-22. Measured compressive strain in R

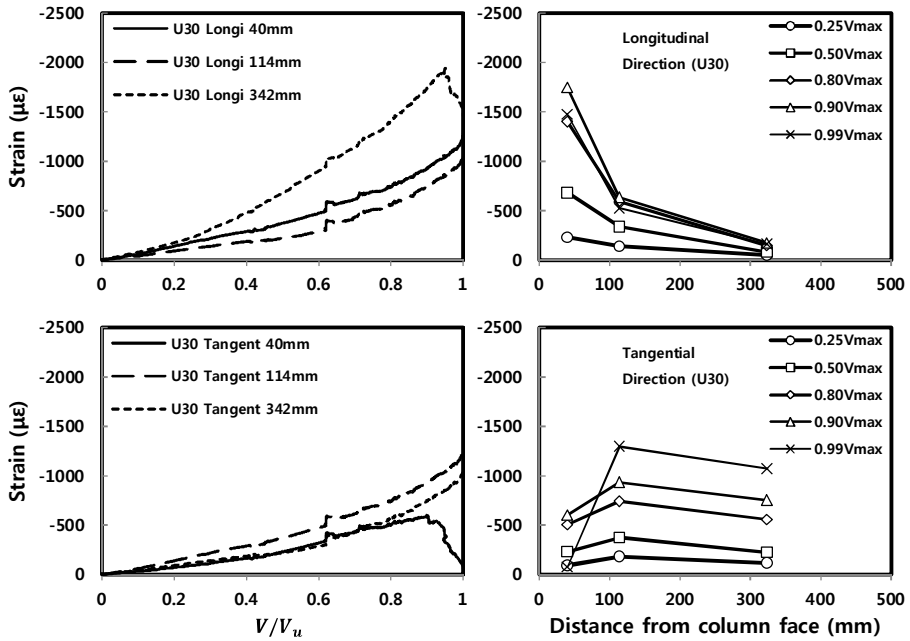


Fig 5-23. Measured compressive strain in U30

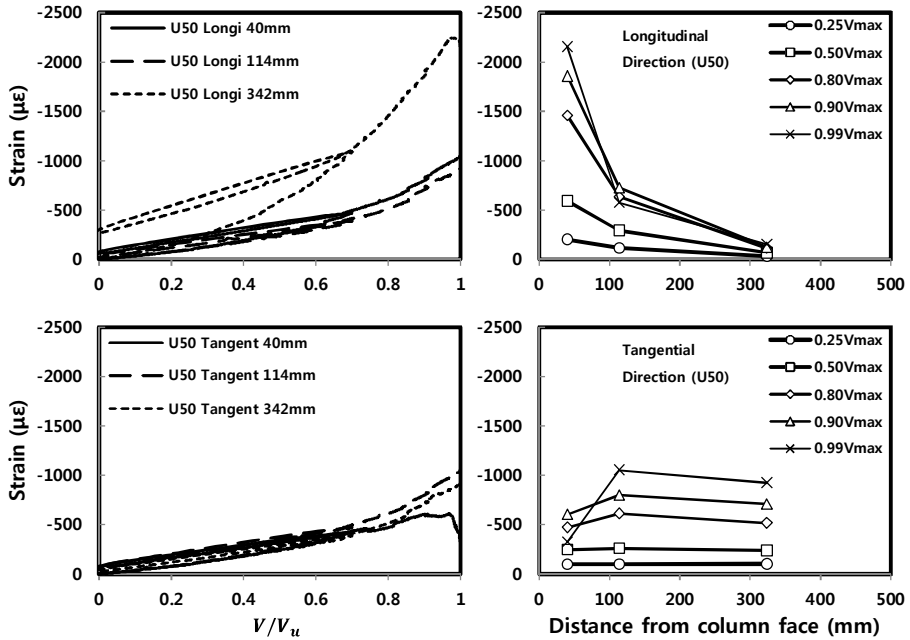


Fig 5-24. Measured compressive strain in U50

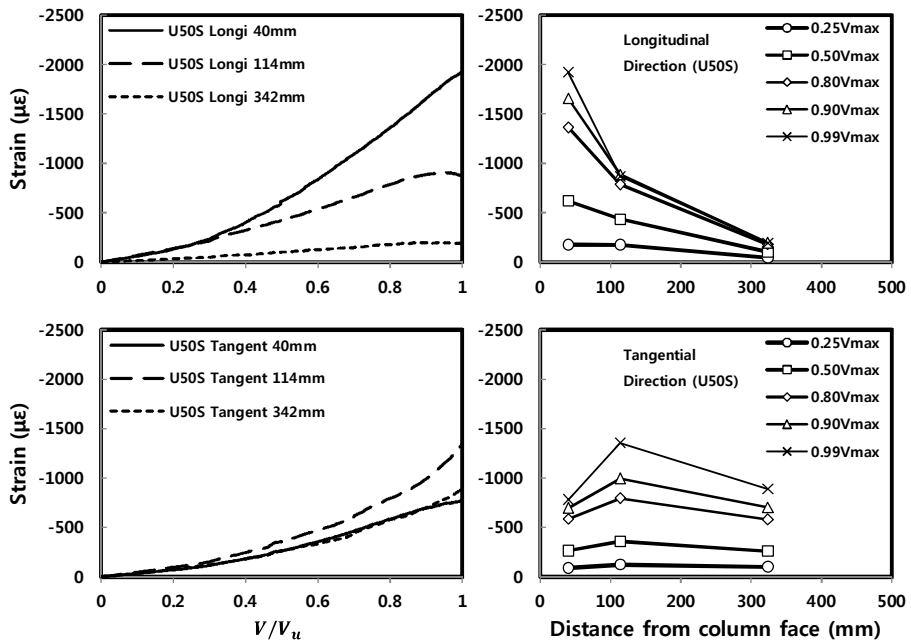


Fig 5-25. Measured compressive strain in U50S

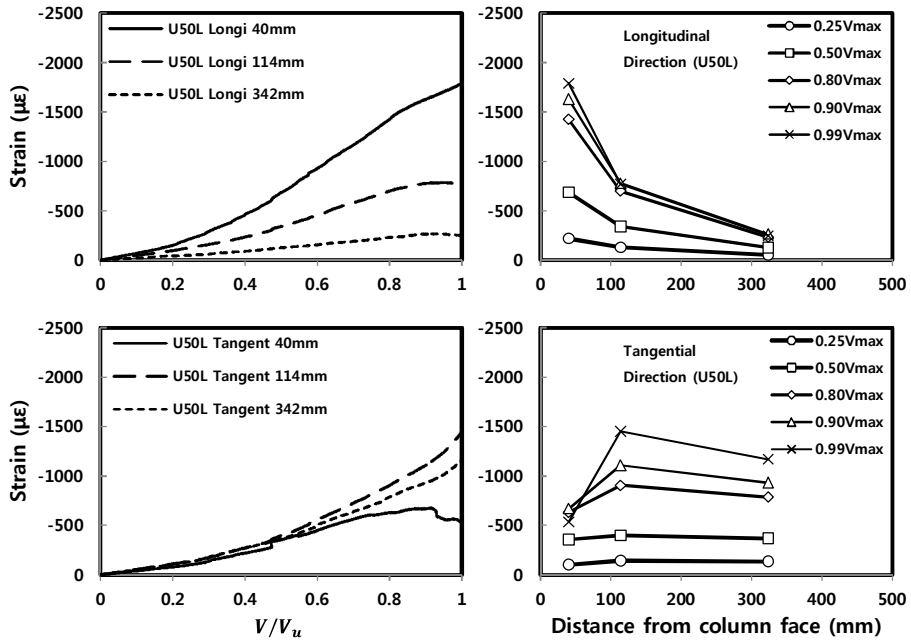


Fig 5-26. Measured compressive strain in U50L

5.3 Punching Shear Strength Predictions

There exist several provisions to evaluate the punching shear capacity of RC slab. In this study, the design expressions provided by ACI 318-11, KCI 2012, EC2 and JSCE are selected to evaluate the prediction of the punching shear resistance. Since these design expressions do not have any terms about the UHPC overlay, they cannot be directly used for the UHPC-RC composite slab. However, this study tried to apply these design expressions to the whole test results for verifying applicability to the UHPC-RC composite slab by two strategies: 1) reflecting the retrofitting effect in the form of effective flexural depth and effective reinforcement ratio, and 2) directly calculating the sum of the punching shear strength of RC section and the UHPC overlay. That is, refined design expressions by the two strategies as expressed in **Fig 5-27** were adopted. Ultimately, the main purpose of this section is to precisely comprehend the shear transfer mechanism of the UHPC overlay

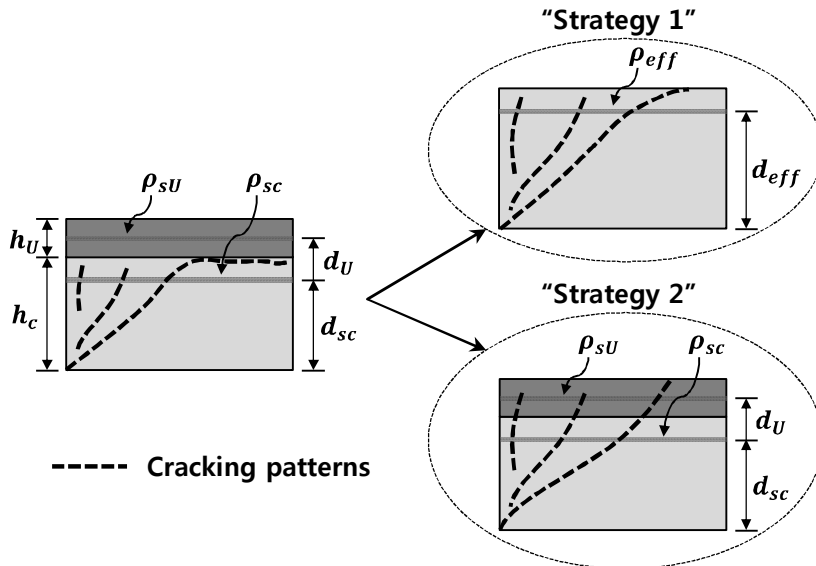


Fig 5-27. Two strategies for application of code design expressions

1) Strategy 1 : reflecting the retrofitting effect in the form of effective flexural depth and effective reinforcement ratio

To take into account the contribution of UHPC overlay, the effective flexural depth and the effective flexural reinforcement ratio were directly used, because the current design codes give no terms regarding to the contribution of the UHPC overlay, obviously leading to conservative results. Especially for KCI 2012, Eurocode2 and JSCE code provisions, as the design expressions for punching shear capacity take the reinforcement ratio ρ as a critical parameter, modified form of the reinforcement ratio was taken into account normalized by the yield strength of the top reinforcement in RC section. Thus, the modified effective flexural depth can be calculated by the Eq.(5-1), and the modified effective reinforcement ratio can be calculated by the Eq.(5-2) as follows.

$$d_{eff} = \frac{\sum d_i A_i f_i}{\sum A_i f_i} \quad (5-1)$$

$$\rho_{eff} = \frac{\rho_{sc} d_{sc} + \rho_U d_U \frac{f_{Uu}}{f_{sc,sy}} + \rho_{sU} d_{sU} \frac{f_{sU,sy}}{f_{sc,sy}}}{d_{eff}} \quad (5-2)$$

The calculation results of effective flexural depth and reinforcement ratio are summarized in **Table 5-3**. It should be notified that by taking the contribution of UHPC overlay into account, flexural depth and reinforcement ratio become significantly increased. These results directly imply that by adding the thin layer of UHPC, the contribution of RC section to the global punching shear capacity would increase, attributed to increased depth of compression zone in RC section, which is the main shear carrying mechanism according to the KCI 2012 code provision. Then, the refined code provisions

by strategy 1 can be computed by substituting d_{sc} and ρ_{sc} to d_{eff} and ρ_{eff} , respectively.

Table 5-3. Effective flexural depth and reinforcement ratio of specimens

Specimen	d_{sc} (mm)	ρ_{sc} (%)	d_{eff} (mm)	ρ_{eff} (%)
R			114	1.240
U30			126.65	1.484
U50	114	1.240	135.64	1.615
U50S			141.60	1.823
U50L			145.99	2.036

2) Strategy 2 : directly calculating the sum of the punching shear strength of RC section and the UHPC overlay

Concerning the diagonal shear cracks to propagate into the UHPC overly as illustrated in , the total punching shear strength would be calculated as the sum of the punching shear strength of each section. To calculate the contribution of the UHPC overlay, the term defined in K-UHPC design code about the punching shear strength of UHPC slab was used. The term is obtained by multiplying design average tensile strength by effective depth, circumferential length and member reduction factor as expressed in Eq.(5-3).

$$V_{pcd} = \phi_b f_{vd} u_p d \quad (5-3)$$

$$f_{vd} = \frac{1}{w_v} \int_0^{w_v} \phi_c \sigma_k(w) dw \quad (5-4)$$

Where,

V_{pcd} = Design punching shear strength of UHPC slab, N

ϕ_b = Member reduction factor, generally 0.77

- f_{vd} = Design average tensile strength in the direction perpendicular to the diagonal tensile crack of UHPC
- w_v = Max (w_u , 0.3mm)
- ϕ_c = Material reduction factor considering the orientation of the steel fibers, 0.8
- $\sigma_k(w)$ = Tension-softening curve of UHPC as defined in K-UHPC
- u_p = Circumferential length of design cross section, computed at the position located at a distance $d/2$ from the loaded face
- d = Effective depth, which can be assumed to be 80% of the thickness of the deck

In this study, the orientation effect is already considered at material level, material reduction factor ϕ_c is assumed to be 1.0. Then the refined code provisions by strategy 2 can be computed by the following equation.

$$V_{d, strategy2} = V_d + V_{pcd} \quad (5-5)$$

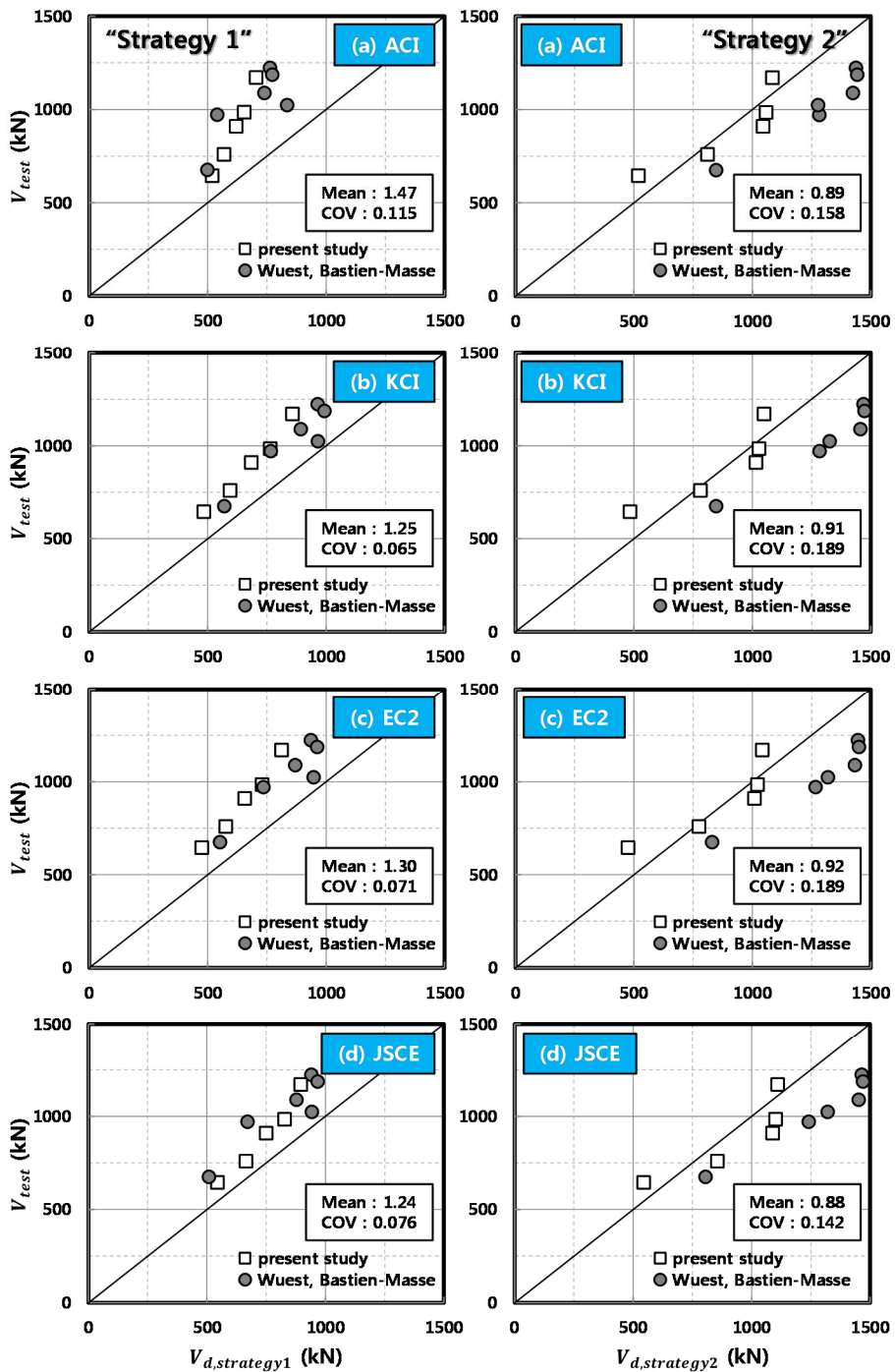
In order to verify the test results of the UHPC-RC composite slab test and to validate the possibility of application of the design expressions, the experimental test results conducted by Wuest (2007) and Bastien-Masse (2015) on similar subject of the present study were also considered. **Table 5-4** shows the calculated effective flexural depth and effective reinforcement ratio of test specimens of Wuest (2007) and Bastien-Masse (2015) also based on the Eq.(5-1) and Eq.(5-2), respectively. **Fig 5-28** presents measured shear strength versus calculated shear strength by original design expressions and refined design expressions of several code provisions. As expected, the original design expression's predictions are significantly conservative, on the other hand, the refined design expressions give more favorable results. **Table 5-5** and **Table 5-6** summarizes the comparison of the punching shear capacities provided by the refined ACI 318-11, KCI 2012, Eurocode2 and JSCE code provisions by two strategies with the test results of the present

study and the results of Wuest (2007) and Bastien-Masse (2015) together.

Table 5-4. Effective flexural depth and effective reinforcement ratio of specimens of previous studies

No.	Specimen	d_{sc} (mm)	ρ_{sc} (%)	d_{eff} (mm)	ρ_{eff} (%)
1	SAMD1	136	0.74	161.7	1.81
2	SAMD2	136	0.74	153.0	1.02
3	PBM1	180	0.73	200.7	1.05
4	PBM2	180	0.73	205.3	1.19
5	PBM3	180	0.73	207.0	1.25
6	PBM4	210	0.75	218.5	0.94

Note) 1-2 : tested by Wuest (2007), 3-6: tested by Bastien-Masse (2015)



(a) predictions by Strategy 1

(b) predictions by Strategy 2

Fig 5-28. Comparisons of test results with strengths provided by design expressions

Table 5-5. Comparison of strength ratios of specimens predicted by refined code provisions (strategy 1)

No.	I.D.	Failure mode	Test results	Predicted strength (kN)					Ratio of test strengths to predictions			
			V_{test}	V_{ACI}	V_{KCI}	V_{EC2}	V_{JSCE}	$\frac{V_{test}}{V_{ACI}}$	$\frac{V_{test}}{V_{KCI}}$	$\frac{V_{test}}{V_{EC2}}$	$\frac{V_{test}}{V_{JSCE}}$	
1	R	FS	644.4	519.5	484.2	476.3	545.2	1.24	1.33	1.35	1.18	
2	U30	S/DB	758.4	570.0	595.4	576.5	665.5	1.33	1.27	1.32	1.14	
3	U50	S/DB	908.9	620.5	684.8	657.0	750.6	1.46	1.33	1.38	1.21	
4	U50S	S/DB	984.5	654.7	764.4	729.9	828.4	1.50	1.29	1.35	1.19	
5	U50L	S/DB	1170.6	705.2	857.8	812.5	896.0	1.66	1.36	1.44	1.31	
6	SAMD1	S/DB	971	540.5	766.6	735.9	672.1	1.80	1.27	1.32	1.44	
7	SAMD2	S/DB	675	499.3	570.6	552.5	509.0	1.35	1.18	1.22	1.33	
8	PBM1	S/DB	1089	739.4	893.0	869.8	878.3	1.47	1.22	1.25	1.24	
9	PBM2	S/DB	1223	763.8	964.1	935.7	941.5	1.60	1.27	1.31	1.30	
10	PBM3	S/DB	1186	772.8	993.3	962.9	967.6	1.53	1.19	1.23	1.23	
11	PBM4	S/DB	1023	835.9	965.4	947.0	943.4	1.22	1.06	1.08	1.08	
Average								1.47	1.25	1.30	1.24	
St.Dev								0.17	0.08	0.09	0.09	
COV(%)								11.45	6.51	7.13	7.63	
Min								1.22	1.06	1.08	1.08	
Max								1.80	1.36	1.44	1.44	

Note) 6-7 = Test results by Wuest, 8-11 = Test results by Bastien Masse

Note) Since there was no information on the yielding, all references in the literatures failed in punching shear were classified as shear failure (S) without distinction of flexure-shear failure (FS) and shear failure (S)

Concentric Loading Test of UHPC-RC Composite Slab

Table 5-6. Comparison of strength ratios of specimens predicted by refined code provisions (strategy 2)

No.	I.D.	Failure mode	Test results	Predicted strength (kN)					Ratio of test strengths to predictions			
			V_{test}	V_{ACI}	V_{KCI}	V_{EC2}	V_{JSCE}	$\frac{V_{test}}{V_{ACI}}$	$\frac{V_{test}}{V_{KCI}}$	$\frac{V_{test}}{V_{EC2}}$	$\frac{V_{test}}{V_{JSCE}}$	
1	R	FS	644.4	519.5	484.2	476.3	545.2	1.24	1.33	1.35	1.18	
2	U30	S/DB	758.4	811.7	782.0	775.5	855.8	0.93	0.97	0.98	0.89	
3	U50	S/DB	908.9	1045.5	1015.8	1009.3	1089.6	0.87	0.89	0.90	0.83	
4	U50S	S/DB	984.5	1057.8	1028.0	1021.6	1101.9	0.93	0.96	0.96	0.89	
5	U50L	S/DB	1170.6	1085.2	1049.9	1042.0	1110.9	1.08	1.12	1.12	1.05	
6	SAMD1	S/DB	971	1283.1	1283.7	1266.6	1241.8	0.76	0.76	0.77	0.78	
7	SAMD2	S/DB	675	847.2	847.8	830.7	805.9	0.80	0.80	0.81	0.84	
8	PBM1	S/DB	1089	1424.9	1456.4	1432.7	1452.4	0.76	0.75	0.76	0.75	
9	PBM2	S/DB	1223	1437.6	1469.1	1445.4	1465.2	0.85	0.83	0.85	0.83	
10	PBM3	S/DB	1186	1442.3	1473.8	1450.1	1469.9	0.82	0.80	0.82	0.81	
11	PBM4	S/DB	1023	1277.5	1326.1	1319.3	1321.4	0.80	0.77	0.78	0.77	
Average								0.89	0.91	0.92	0.88	
St.Dev								0.14	0.17	0.17	0.12	
COV(%)								15.75	18.93	18.92	14.21	
Min								0.76	0.75	0.76	0.75	
Max								1.24	1.33	1.35	1.18	

Note) 6-7 = Test results by Wuest, 8-11 = Test results by Bastien Masse

Note) Since there was no information on the yielding, all references in the literatures failed in punching shear were classified as shear failure (S) without distinction of flexure-shear failure (FS) and shear failure (S)

As a whole, the punching shear resistances are relatively underestimated when predicted by Strategy 1, on the other hand, overestimated when predicted by Strategy 2. This clearly confirms that the failure modes assumed in Strategy 1 and Strategy 2 do not accurately reflect the exact failure mode of the composite slabs, even though it is considered that the code design expressions basically underestimate the shear strength. It can also be inferred from the cracking patterns of the test specimens.

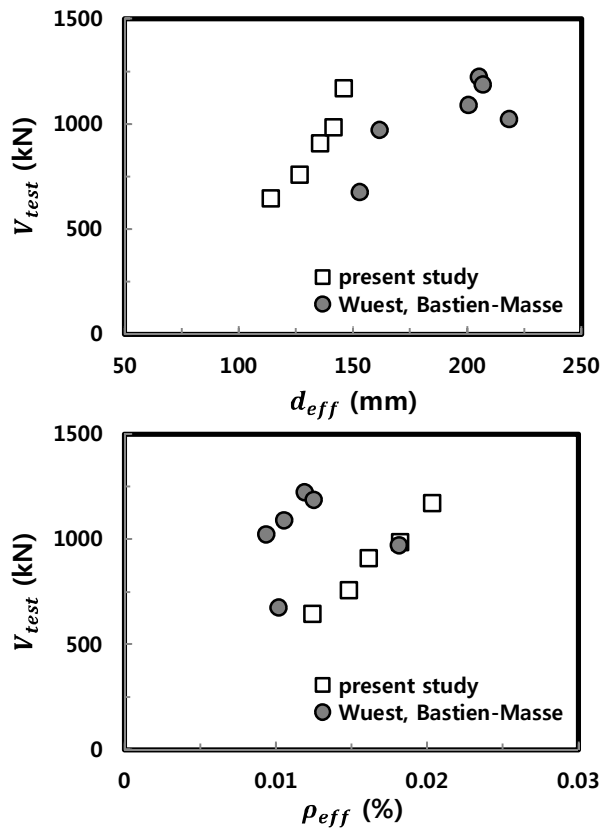


Fig 5-29. Experimental values dependent on critical parameters

The effects of some critical test parameters are verified as can be seen in Fig 5-29. The punching shear resistance is relatively proportional to the estimated effective flexural depth and effective reinforcement ratio. This

implies that the UHPC overlay acts as a two-dimensional tensile reinforcement, participating in shear carrying mechanism of the composite section.

The **Fig 5-30** to **Fig 5-33** show the relationship between the strength ratios for refined design expressions provided by each code provisions and the critical test parameters. The graphs shown on the left and the right represent the predictions by Strategy 1 and Strategy 2, respectively. Some informative values are given in the graphs. In terms of prediction by Strategy 1, it should be notified that when test parameters become bigger, the strength ratios become slightly increased, describing necessity for additional contribution term of the UHPC overlay to global punching shear capacity. This clearly means that due to the thin layer of UHPC overlay, not only the punching shear capacity corresponding to the improved flexural capacity is increased, but also the additional shear resistance can be obtained through the additional load transfer mechanism at the interface between RC section and UHPC overlay.

As a result of comparing the punching shear capacity derived by each of the refined design expressions with the test results, it was found that the refined design expressions quite well predict the punching shear strengths of the UHPC-RC composite slab. However, it is still underestimated (Strategy 1) or overestimated (Strategy 2), thus, an additional term regarding to the contribution of the UHPC overlay should be reevaluated. Therefore, in **Chapter 6**, this study suggested a new analytical approach for evaluating punching shear resistance of UHPC-RC composite slab with considering these additional contributions based on the load-deformation relationship, observed cracking pattern and failure mode of test specimens.

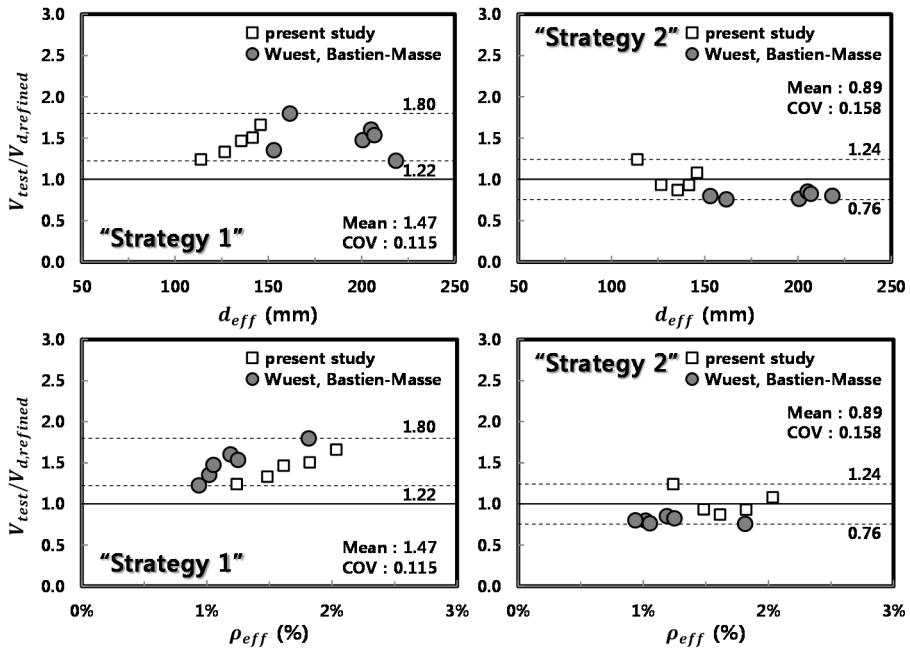


Fig 5-30. Strength ratios of specimens predicted by refined ACI 318-11

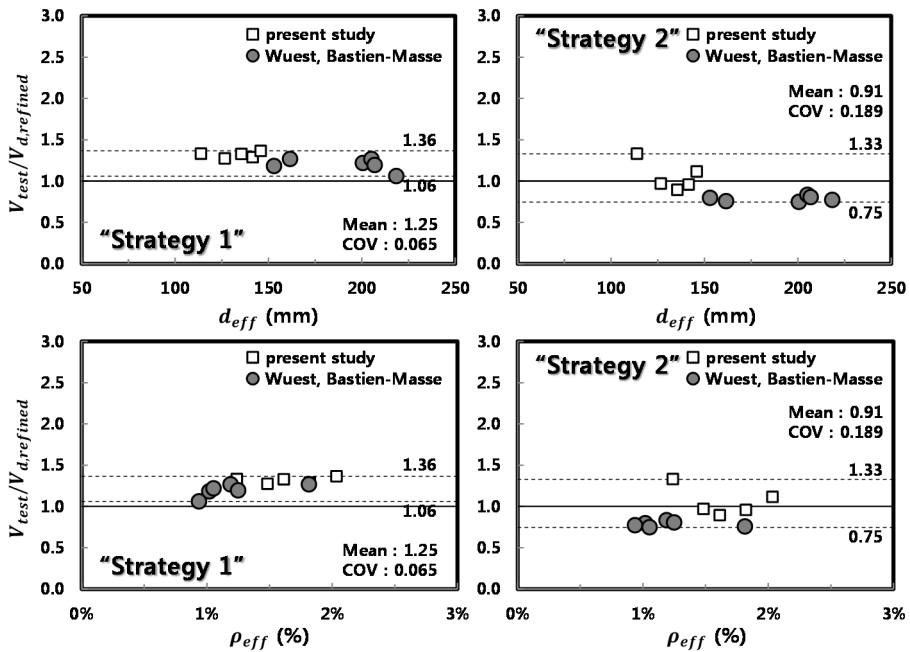


Fig 5-31. Strength ratios of specimens predicted by refined KCI 2012

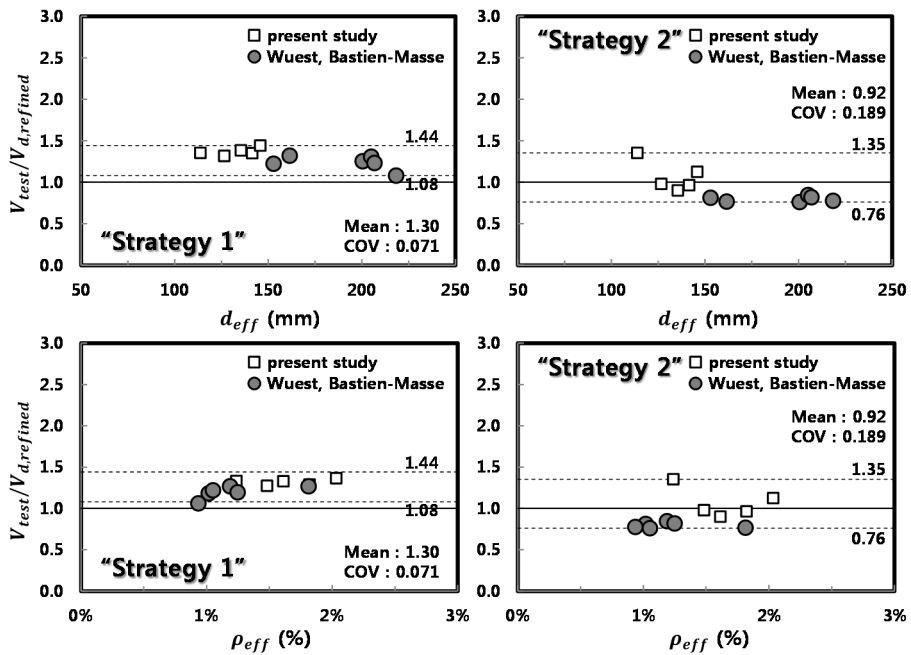


Fig 5-32. Strength ratios of specimens predicted by refined Eurocode2

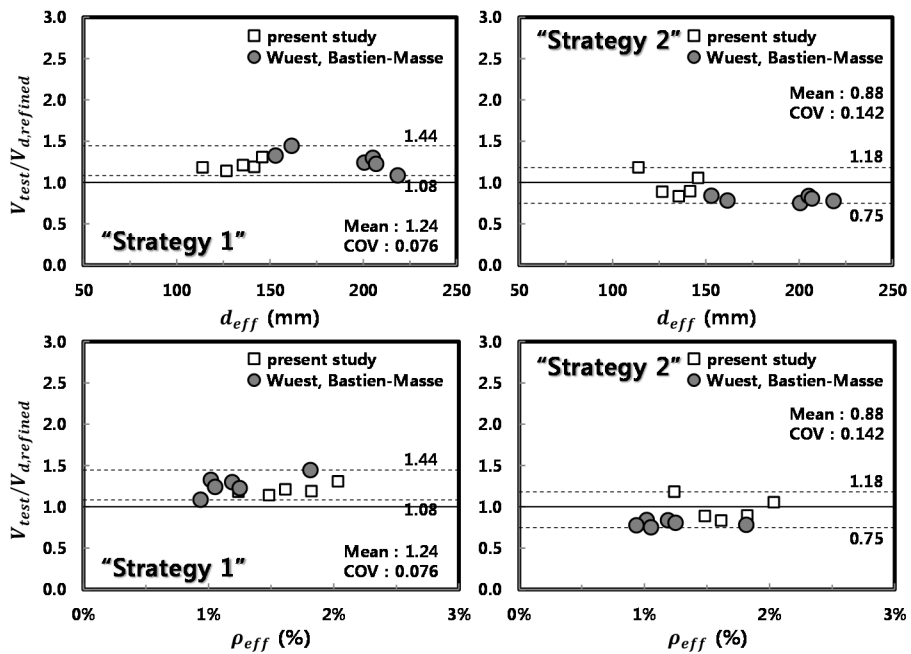


Fig 5-33. Strength ratios of specimens predicted by refined JSCE

5.4 Discussion

To verify the contribution of the UHPC overlay to global punching shear resistance of the UHPC-RC composite slab, five slab-column connections with varying UHPC thickness with or without steel re-bars in it were tested under displacement controlled concentric loading. All specimens were designed to be failed in punching shear mode by planning the flexural capacity intentionally higher than the predicted shear capacity. The test was terminated with a sudden drop in load carrying capacity, after which two major cracking patterns at cut section were observed; 1) diagonal shear crack in RC section and 2) debonding at the interface between the UHPC and concrete. Observed behavior and test results confirmed that the UHPC overlay significantly improves load-carrying capacity and shear resistance of a slab. Additionally, the test results have similar tendency with that of the previous experimental results reported by Noshiravani et al. (2013, 2014) and Bastien-Masse (2015) in terms of failure mode. The major findings of this chapter are summarized as follows.

- 1) By adding a thin layer of UHPC, the normalized punching shear resistance increases at least 22% for 30mm UHPC overlay and up to 82 % for 50mm UHPC overlay with steel in it. This confirms that the UHPC overlay acts as a two-dimensional reinforcement.
- 2) The use of steel re-bars in the UHPC overlay has a significant influence on the resistance and deformation of the composite slab, which is different outcome from that of previous research performed by Bastien-Masse (2015). This experimental result directly implies that the load transfer mechanism of the UHPC-RC composite slab should be reconsidered from a slightly different point of view from

the previous study.

- 3) Due to bending efforts, many microcracks are generated in the UHPC overlay, which tend to be more predominant as the reinforcement ratio in the UHPC overlay becomes increased. In addition, the inclined shear cracks generated in the RC section cannot penetrate the UHPC overlay during the test, but rather rotate at the interface and developed to NIC. Therefore, the punching cone shaped cracks on the surface of the UHPC overlay can hardly be distinguished with naked eyes.
- 4) At cut sections, two governing failure modes were observed; (1) diagonal shear failure due to inclined shear cracks in the RC section, and (2) debonding failure at the interface due to NIC. These two failure modes were thoroughly investigated in the theoretical analysis stage, being recognized as major failure mechanisms of the composite slabs.
- 5) At cut sections, angle of the diagonal shear cracks tend to be smaller when retrofitted by the UHPC overlay in comparison with that of the reference slab. In other words, the tip of the diagonal shear cracks get farther away as retrofitted by the UHPC overaly. Thus, in the present study, the length from the column face to the tip of the cracks was estimated to be equal to twice the effective depth based on the cracking patterns.
- 6) Regarding to the deformability, the deformation capacity of the retrofitted specimens turned out to be maintained above a certain level even though the retrofitting level increased, which is unmatched with the conventional sense. Considering the cracking

pattern, the out-of-plane bending in the UHPC overlay probably allows the RC section to deform further, leading to comparatively larger deformation and crack opening of the RC section. This implies the additional contribution of the UHPC overlay to shear resistance.

- 7) Near the column, the UHPC layer deflects slightly upward by the force acting at the tip of the inclined shear crack propagated from the RC section, leaving limited horizontal cracking at tension side of RC section near the column due to geometrical compatibility. As this phenomenon was not observed for the control specimen, which even experienced yielding of steel re-bar, this also explicitly means that the layer of UHPC provides additional shear resistance to the cracked RC section.

- 8) A design procedure using several current design code expressions is presented to account for the retrofitting effect of the UHPC overlay on the maximum resistance of a slab by two strategies. As a result, the predictions from ACI, KCI, EC2 and JSCE design expressions do not correctly estimate the punching shear capacity of the UHPC-RC composite slab, but with comparatively high correlation. This clearly means that due to the thin layer of UHPC overlay, not only the punching shear capacity corresponding to the improved flexural capacity is increased, but also the additional shear resistance can be obtained through the additional load transfer mechanism at the interface between RC section and UHPC overlay.

Chapter 6. Theoretical Analysis

The contribution of the UHPC overlay to the punching shear resistance of the member has not yet been clearly clarified, despite the efforts of the previous research dedicated from Bastien-Masse (2015). There is a need for an analytical model to predict more accurately the contribution of the UHPC overlay to the shear resistance and deformation capacity of UHPC-RC composite slabs. In this chapter, mechanical analysis about the behavior of the UHPC-RC composite slab-column connections will be conducted using physically sound model, CSCT (Critical Shear Crack Theory) proposed by Muttoni (Muttoni, 2008) and slightly modifying the CSCT to account for the contribution of the UHPC overlay to the global punching shear capacity and deformation capacity of the UHPC-RC composite slabs.

6.1 Failure Mechanism

In order to verify the contribution mechanism of the UHPC overlay to the global punching shear resistance, failure mechanism of the composite slab should be understood and mechanically explained. During the test, as described in **Chapter 5.2.2**, the typical failure modes were found to be 1) inclined shear cracks at RC section and 2) debonding failure at interface between the UHPC overlay and RC substrate as described in **Fig 6-1**. It should be noted that these two failure modes occurred coincidentally for all the retrofitted specimens irrespective of retrofitting type. Thus, the total punching shear capacity of the UHPC-RC composite slab is not determined

by one failure mode, but rather by a combination of these two failure modes, potentially meaning the possibility of two capacity curves.

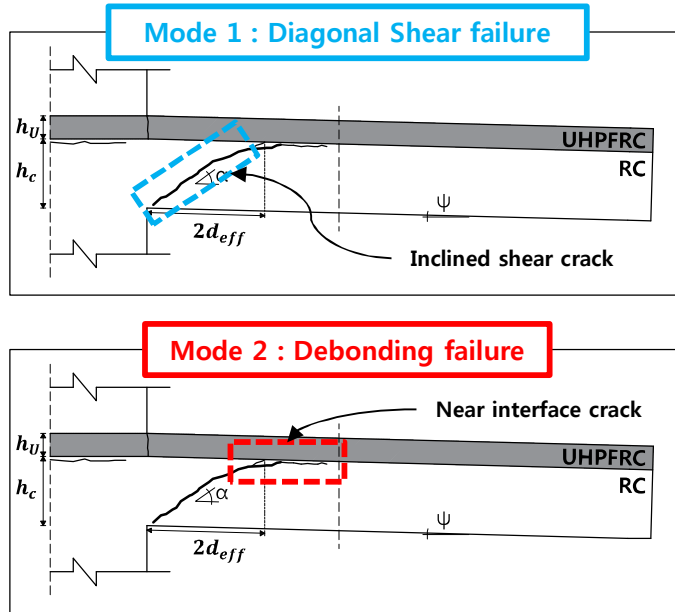


Fig 6-1. Two governing failure modes

Table 6-1. Collapse mechanisms

Failure	Properties	Crack angle	Yield
Flexural failure (F)	Pure rotational mechanism Rupture of rebar or crush of concrete at compression zone is observed	60°- 90°	O
Shear failure (S)	Due to crushing of concrete weakened by the diagonal shear crack or the yielding of any vertical reinforcement crossing the crack Occur in the presence of large concentrated forces close to supports	20°- 60°	X
Flexural-shear failure (FS)	Beginning as a rotational mechanism, nevertheless, the collapse of the member is a translational movement due to the crushing of concrete downstream from the crack tip	20°- 60°	O
Debonding failure (DB)	Due to near interface cracking (NIC), the substrate and the overlay debonded	0°- 10°	-

6.2 Proposed Analytical Method

6.2.1 Overview

Punching shear is usually the most widely reported governing failure mode of slab-column connections coinciding with a sudden drop of shear resistance, which ultimately can trigger a collapse of a whole structural system. Even though extensive researches about punching shear have been conducted for about half a century, most design approaches are still based on empirical formulations. In addition, none of some physically sound theories like the MCFT (Modified Compression Field Theory) and FASTM (Fixed Angle Softened Truss Model) for beams and one-way slabs have yet successfully been applied to the problem of punching shear, because these models were designed to predict the shear response of transversely reinforced members. Whereas, the CSCT was developed concerning members subjected to shear like beam or one-and two-way slab without transverse reinforcement, which is considered to be the most suitable model for the analysis of such a retrofitted UHPC-RC composite slab .

However, since validity of the CSCT was verified only for general type of slab-column connection, the UHPC-RC composite slab-column connection cannot be analyzed directly by using this model. As roughly described in **Fig 6-2**, failure criterion as well as the structural behavior of the two slabs will be considerably different. There does not also exist any terms related to the additional layer of UHPC in the model. Thus, the employed model should be slightly modified in order to be applicable and compatible with the present conditions of the UHPC-RC composite slab designed to be failed in punching shear mode.

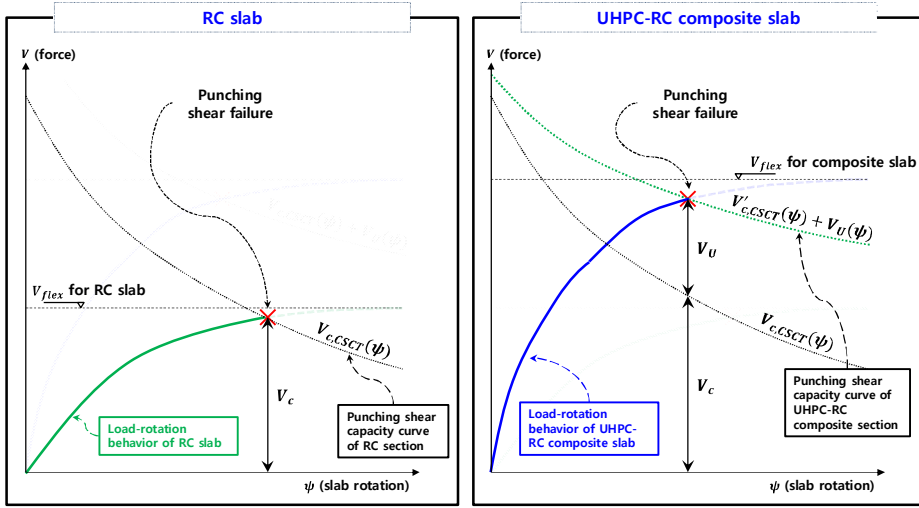


Fig 6-2. Typical demand and capacity curves for RC and UHPC-RC composite slabs

Basetien-Masse (2015) proposed an analytical design method to predict the punching shear capacity of a UHPC-RC composite slab, also based on the CSCT with slight modification as graphically shown in **Fig 6-3**. According to the method, the maximum contribution of the UHPC overlay to the global punching shear resistance depends on the thickness of the UHPC overlay and the tensile strength of the RC substrate f_{ct} . Thus, the total punching shear resistance is expressed as the sum of the contributions of RC section and UHPFRC overlay as already mentioned in **Chapter 2.5.4**.

$$V_R(\psi) = V_c(\psi) + V_U \quad (2-4)$$

Where,

$$\frac{V_c(\psi)}{b_0 d_{sc} \sqrt{f_c}} = \frac{3/4}{1 + 15 \frac{\psi d_{sc}}{d_{g0} + d_g}} \quad (2-5)$$

$$V_U = 2\pi \cdot f_{ct} \cdot h_U \cdot \left(r_U + \frac{h_U}{2} \right) \quad (2-6)$$

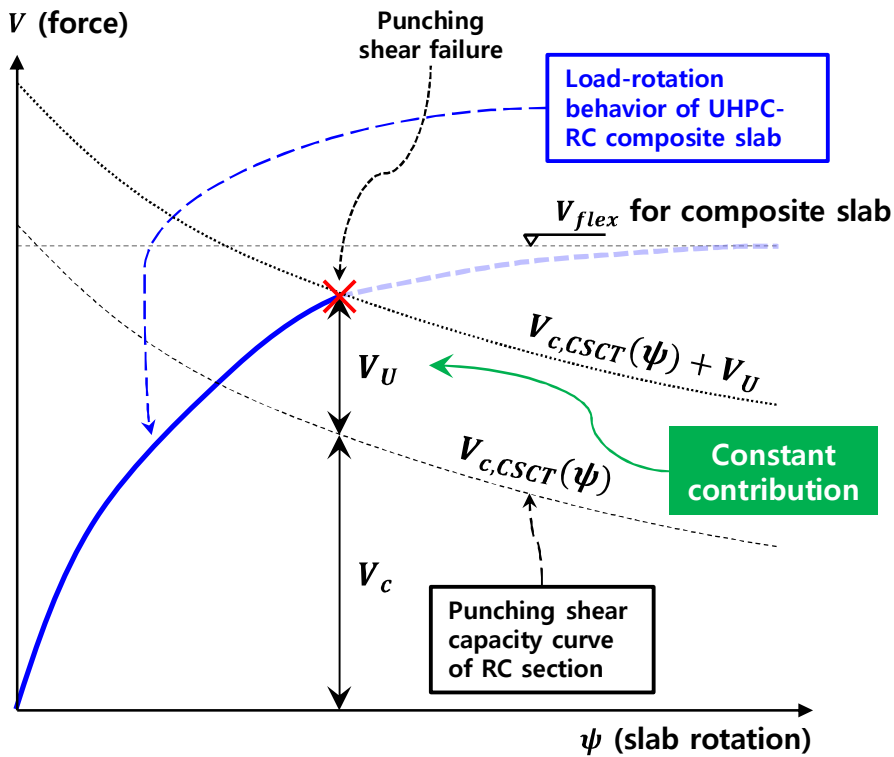


Fig 6-3. Proposed method by Bastien-Masse (2015)

Despite high accuracy with the test results performed by the author, however, the predictions of the present test results by the proposed method in the previous study become more inaccurate with increasing retrofitting ratio as shown in Fig 6-4, especially for U50L specimen with large amount of steel re-bars in the UHPC overlay. Because the UHPC-RC composite slabs have complex behavior induced by a combination of flexure, shear and interface shear, the contribution of the UHPC overlay to the global shear resistance cannot be simply expressed as a function only dependent on the thickness of the layer of UHPC and the tensile strength of the concrete. Rather, all of the parameters regarding to the UHPC overlay should be considered to accurately predict the contribution of the UHPC overlay.

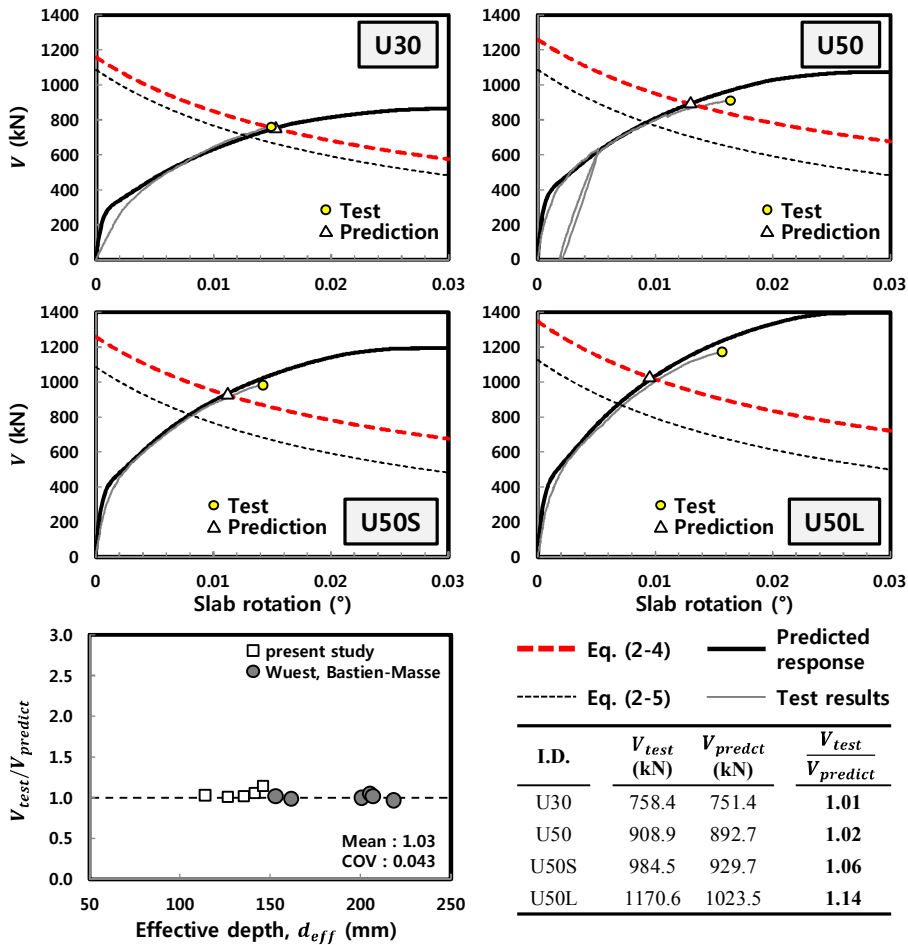


Fig 6-4. Strength ratios of test strength to prediction by proposed method by Bastien-Masse (2015)

In the present study, to overcome the limitations of the model proposed in the previous study, and to investigate more clearly the contribution of the UHPC overlay to the global punching shear resistance, a modified CSCT was proposed. The flow of the calculation process is not much different from that of the original CSCT and proposed method by Bastien-Masse, while, two sets of free body diagram formulated in a slab portion were newly proposed to estimate the additional contribution of the UHPC overlay to the shear resistance. By this method, each contribution can be calculated and referring

to the two failure modes observed in the experiment, two capacity curves corresponding to each failure mode were proposed, which is expressed as a function of each contribution. For the mode 1 failure (diagonal shear failure), the capacity curve is obtained as the sum of the contribution of the UHPC overlay and maximum load-carrying capacity of the concrete. For the mode 2 failure (debonding failure at the interface), the capacity curve is obtained as the sum of the contribution of the concrete and maximum load-carrying capacity of the UHPC overlay, which is delimited by the performance level of the interface.

Then, the performance point and corresponding failure mode can be determined by the intersection point where the demand curve meets one of the capacity curves occurring at smaller slab rotation. If the demand curve does not intersect any capacity curves, a slab will be eventually failed in flexural mode.

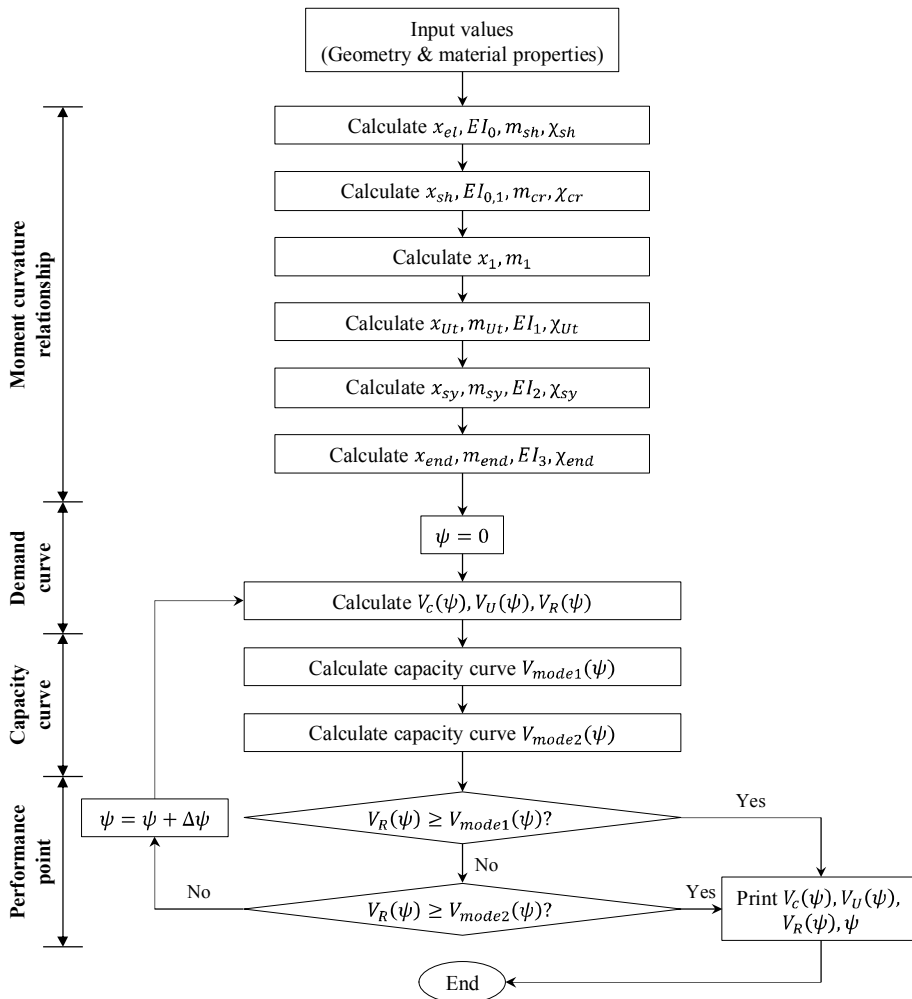


Fig 6-5. Proposed flow chart to analyze UHPC-RC composite slab

The **Fig 6-5** summarizes the flow of computing process of the proposed method. The actual load-rotation behaviors and failure modes of the test specimens in the present study were compared for validation with those predicted by the proposed method based on CSCT with slight modification.

6.2.2 Moment-curvature relationship of UHPC-RC composite section

Bastien-Masse (2015) already developed the multilinear moment-curvature relationship of the UHPC-RC composite section using similar methodology used in the CSCT. In the present study, the method proposed by Bastien-Masse was adopted, however, it was slightly modified to reflect the material stress-strain relationship obtained from the material test results and direct calculation of the flexural rigidity of the composite section.

Prior to the analysis, the following assumptions are made for the derivation of the multilinear moment curvature relationship of retrofitted structures.

- 1) The strains in the steel re-bars, concrete and UHPC are directly proportional to the distance from the neutral axis. That is, a plane section before loading remains plane after loading
- 2) There is no slip between the concrete surface and UHPC surface prior to intermediate crack-induced debonding (ICD), that is, the section is assumed monolithic.
- 3) There is no relative slip between steel re-bars and cement-based materials (concrete, UHPC)
- 4) In cracked section, the tensile strength of the concrete is neglected
- 5) Initial substrate strains of RC section due to self-weight and shrinkage effects of added UHPC overlay are assumed negligible.

Structural behavior of UHPC reinforced with additional steel re-bars subjected to tension is quite different from the behavior of UHPC without steel re-bars. According to an existing study performed by Jungwirth and Muttoni (Jungwirth & Muttoni, 2004), it was corroborated that the point at which the strain hardening behavior of R-UHPC ends is determined by the greater of the strain corresponding to the maximum strength of UHPC and the yield strain of steel re-bars. That is, the strain of R-UHPC at which the strain hardening behavior ends can be determined by the following equation. In the Eq.(6-1), the crack width at which the ultimate tensile strength f_{Utu} is reached is assumed to be 0.3mm. Furthermore, as defined in AFGC-SETRA, the tensile strain of UHPC can be calculated by dividing the crack width by 2/3 times the total thickness of the member.

$$\varepsilon_{Utu}^{RU} = \max \left(\varepsilon_{Utu} = \frac{0.3}{\frac{2}{3}(h_c + h_U)}, \varepsilon_{sU, sy} = \frac{f_{sU, sy}}{E_{sU}} \right) \quad (6-1)$$

As the strain corresponding to the maximum strength is redefined, the young's modulus of UHPC in region of strain hardening phase and strain softening phase should be also recalculated as follows. It is presumed that during elastic region, no additional consideration would be needed.

$$E_U^{RU} = E_U = \frac{f_{Ute}}{\varepsilon_{Ute}} \quad (6-2)$$

$$E_{Ush}^{RU} = \frac{f_{Utu} - f_{Ute}}{\varepsilon_{Utu}^{RU} - \varepsilon_{Ute}} \quad (6-3)$$

$$E_{Uss}^{RU} = -\frac{f_{Utu}}{(w_{Ulim} - w_{Utu}^{RU})} \cdot \frac{2}{3}(h_c + h_U) \quad (6-4)$$

Where, $w_{Ulim} = l_f / 2$, $\epsilon_{Ulim} = \frac{w_{Ulim}}{\frac{2}{3}(h_c + h_U)}$ and $w_{Utu}^{RU} = \epsilon_{Utu}^{RU} \cdot \frac{2}{3}(h_c + h_U)$, l_f

=length of steel fiber (mm)

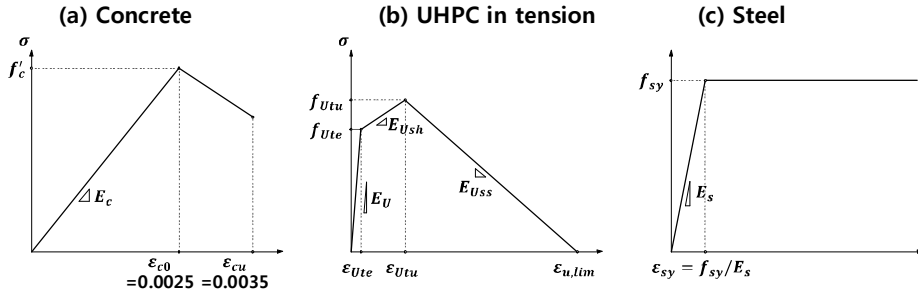


Fig 6-6. Modelling of material constitutive laws

Based on the above assumptions and preceding calculation, the moment-curvature relationship of the UHPC-RC composite section can be derived by using conventional cracked sectional analysis. The material properties were also modelled as described in **Fig 6-6**, based on the performed material tests.

1) $m - \chi$ relationship for elastic region ($\chi \leq \chi_{sh}$)

In the elastic region, all materials are in elastic state. Thus, the depth of compression zone x_{el} and the flexural rigidity EI_0 can be obtained as follows. The elastic phase ends when the UHPC overlay reaches its elastic tensile limit f_{Ute} , in other words, at strain-hardening curvature χ_{sh} .

$$x_{el} = \frac{\sum E_i A_i d_i}{\sum E_i A_i} \tag{6-5}$$

$$EI_0 = \frac{E_c h_c^3}{12} + \frac{E_U h_U^3}{12} + E_c h_c \left(\frac{h_c}{2} - x_{el} \right)^2 + E_U h_U (d_U - x_{el})^2 \tag{6-6}$$

$$\begin{aligned}\chi_{sh} &= -\frac{\varepsilon_{Ute}}{h_c + h_U - x_{el}} \\ &= -\frac{f_{Ute} / E_U}{h_c + h_U - x_{el}}\end{aligned}\quad (6-7)$$

$$m_{sh} = -EI_0 \chi_{sh} \quad (6-8)$$

2) $m - \chi$ relationship for strain-hardening region ($\chi_{sh} < \chi \leq \chi_{cr}$)

In this region, the UHPC overlay is in strain-hardening state, but the concrete have not reached cracking moment. Thus, the depth of compression zone x_{sh} and the flexural rigidity $EI_{0,1}$ can be obtained as follows, using the strain hardening rigidity of UHPC E_{Ush}^{RU} .

$$x_{sh} = \frac{\sum E_i A_i d_i}{\sum E_i A_i} \quad \text{for } E_U = E_{Ush}^{RU} \quad (6-9)$$

$$EI_{0,1} = EI_0 \quad \text{for } E_U = E_{Ush}^{RU} \quad (6-10)$$

$$\chi_{cr} = -\frac{f_{ct}}{E_c (h_c - x_{sh})} \quad (6-11)$$

$$m_{cr} = -EI_{0,1} (\chi_{cr} - \chi_{sh}) + m_{sh} \quad (6-12)$$

3) $m - \chi$ relationship for tension stiffening region ($\chi_{cr} < \chi \leq \chi_1$)

This region is attributed to the tension stiffening effect at RC section, which leads to decrease in curvature by χ_{ts} with no variation of moment. Eq.(6-13) is directly referred from the previous researches (Muttoni, 2008, Bastien-Masse, 2015).

$$\chi_{ts} = -\frac{f_{ct}}{\rho_{sc}\beta E_s} \cdot \frac{1}{6h_c} \quad (6-13)$$

$$\chi_1 = \frac{\chi_{sh}}{\beta} + \chi_{ts} \quad (6-14)$$

$$m_1 = m_{cr} \quad (6-15)$$

4-1) $m-\chi$ relationship for cracked-hardening region ($\chi_1 < \chi \leq \chi_{Ut}$), case (1) : UHPC's maximum tensile strength strain is smaller than yield strain of steel in UHPC ; $\varepsilon_{Utu} < \varepsilon_{sU, sy}$, $\varepsilon_{Utu}^{RU} = \varepsilon_{sU, sy}$

In first case, for simulate the cracked section properly, it was assumed that UHPC has reached the maximum tensile strength f_{Utu} , while no steel in both RC and UHPC reach the specified yield strengths. Then, some calculation processes can be preceded beginning with calculation of the compression zone depth x_{Ut} of the cracked section.

$$\sum F_x = F_U + F_{sU} + F_{sc} - F_{cc} = 0 \quad (6-16)$$

$$f(x_{Ut}) = -\frac{1}{2} \frac{f'_c}{\varepsilon_{co}} \varepsilon_{Utu} x_{Ut}^2 + \quad (6-17)$$

$$f_{Utu} h_U (d_{sU} - x_{Ut}) + \varepsilon_{Utu} \beta E_{sU} d_{sU} (d_{sU} - x_{Ut}) + \varepsilon_{Utu} (d_{sc} - x_{Ut}) \beta E_{sc} \rho_{sc} d_{sc} = 0$$

By solving the above force equilibrium equation, the compression zone depth x_{Ut} for craked section can be obtained.

$$m_{Ut} = F_{sc} \left(d_{sc} - \frac{x_{Ut}}{3} \right) + (F_U + F_{sU}) \left(d_U - \frac{x_{Ut}}{3} \right) \quad (6-18)$$

$$\begin{aligned}
 EI_1 &= -\frac{dm}{d\chi} & (6-19) \\
 &= \beta E_{sc} \rho_{sc} d_{sc}^3 \left(1 - \frac{x_{Ut}}{3d_{sc}}\right) \left(1 - \frac{x_{Ut}}{d_{sc}}\right) + \\
 &\quad \beta E_{sU} \rho_{sU} d_{sU}^3 \left(1 - \frac{x_{Ut}}{3d_{sU}}\right) \left(1 - \frac{x_{Ut}}{d_{sU}}\right) + \\
 &\quad E_{Ush}^{RU} h_U d_{sU}^2 \left(1 - \frac{x_{Ut}}{3d_{sU}}\right) \left(1 - \frac{x_{Ut}}{d_{sU}}\right)
 \end{aligned}$$

$$\chi_{Ut} = -\frac{m_{Ut} - m_{sh}}{EI_1} + \chi_{sh} - \chi_{ts} \quad (6-20)$$

4-2) $m-\chi$ relationship for cracked-hardening region ($\chi_1 < \chi \leq \chi_{Ut}$), case (2) : UHPC's maximum tensile strength strain is larger than yield strain of steel in UHPC ; $\varepsilon_{Utu} > \varepsilon_{sU, sy}$, $\varepsilon_{Utu}^{RU} = \varepsilon_{Utu}$

In second case, for simulate the cracked section properly, it was assumed that steel re-bars in UHPC has reached the yield strength $f_{sU, sy}$, while UHPC and steel in RC do not reach the maximum tensile strength and the yield strength, respectively. Then, some calculation processes can be preceded beginning with calculation of the compression zone depth x_{Ut} of the cracked section.

$$\sum F_x = F_{U2} + F_{sU2} + F_{sc2} - F_{cc2} = 0 \quad (6-21)$$

$$\begin{aligned}
 f(x_{Ut}) &= -\frac{1}{2} \frac{f'_c}{\varepsilon_{co}} \varepsilon_{sU, sy} x_{Ut}^2 + & (6-22) \\
 &\quad h_U \left(E_{Ush}^{RU} \varepsilon_{sU, sy} + f_{Ute} \right) (d_{sU} - x_{Ut}) + \\
 &\quad \beta f'_{sU, sy} \rho_{sU} d_{sU} (d_{sU} - x_{Ut}) + \\
 &\quad \varepsilon_{sU, sy} (d_{sc} - x_{Ut}) \beta E_{sc} \rho_{sc} d_{sc} = 0
 \end{aligned}$$

By solving the above force equilibrium equation, the compression zone depth x_{Ut} for cracked section can be obtained.

$$m_{Ut} = F_{sc2} \left(d_{sc} - \frac{x_{Ut}}{3} \right) + (F_{U2} + F_{sU2}) \left(d_U - \frac{x_{Ut}}{3} \right) \quad (6-23)$$

$$\begin{aligned} EI_1 &= -\frac{dm}{d\chi} \quad (6-24) \\ &= \beta E_{sc} \rho_{sc} d_{sc}^3 \left(1 - \frac{x_{Ut}}{3d_{sc}} \right) \left(1 - \frac{x_{Ut}}{d_{sc}} \right) + \\ &\quad \beta E_{sU} \rho_{sU} d_{sU}^3 \left(1 - \frac{x_{Ut}}{3d_{sU}} \right) \left(1 - \frac{x_{Ut}}{d_{sU}} \right) + \\ &\quad E_{Ush}^{RU} h_U d_{sU}^2 \left(1 - \frac{x_{Ut}}{3d_U} \right) \left(1 - \frac{x_{Ut}}{d_U} \right) \end{aligned}$$

$$\chi_{Ut} = -\frac{m_{Ut} - m_{sh}}{EI_1} + \chi_{sh} - \chi_{ts} \quad (6-25)$$

5) $m - \chi$ relationship for cracked-hardening 2 region ($\chi_{Ut} < \chi \leq \chi_{sy}$)

In this region, UHPC and steel in it already has passed through the strain hardening phase, and only steel in RC section is approaching the yield strength. Normally in this region, the compressive strain at the tip of the compression fiber is considerably greater due to the deeper compression zone depth attributed to the higher strength and stiffness of UHPC casting at the tension side, leading to nonlinear compressive stress-strain relationship of the compression zone. Thus, it would be reasonable to consider Whitney's rectangular stress block for compression zone from this region.

$$\sum F_x = F_{U3} + F_{sU3} + F_{sc3} - F_{cc3} = 0 \quad (6-26)$$

$$f(x_{sy}) = -0.85 f'_c \cdot 0.85 (d_{sc} - x_{sy}) x_{sy} + \quad (6-27)$$

$$\begin{aligned}
 & h_U E_{Uss}^{RU} \left[(d_U - x_{sy}) \varepsilon_{sc,sy} - (d_{sc} - x_{sy}) \varepsilon_{Ulim} \right] + \\
 & \beta f_{sU,sy} \rho_{sU} d_{sU} (d_{sc} - x_{sy}) + \\
 & \beta f_{sc,sy} \rho_{sc} d_{sc} (d_{sc} - x_{sy}) = 0
 \end{aligned}$$

$$m_{sy} = F_{sc3} \left(d_{sc} - \frac{0.85}{2} x_{sy} \right) + (F_{U3} + F_{sU3}) \left(d_U - \frac{0.85}{2} x_{sy} \right) \quad (6-28)$$

In this region, as the steel re-bars in the UHPC overlay have already been in yielding state, the UHPC is in strain-softening state, and the steel re-bars in the RC section is before yielding, only UHPC and re-bars in the RC section contribute to the flexural rigidity of the composite section, thus,

$$\begin{aligned}
 EI_2 &= -\frac{dm}{d\chi} \quad (6-29) \\
 &= \beta E_{sc} \rho_{sc} d_{sc}^3 \left(1 - \frac{0.85}{2} \frac{x_{sy}}{d_{sc}} \right) \left(1 - \frac{x_{sy}}{d_{sc}} \right) + \\
 & E_{Uss}^{RU} h_U d_U^2 \left(1 - \frac{0.85}{2} \frac{x_{sy}}{d_U} \right) \left(1 - \frac{x_{sy}}{d_U} \right)
 \end{aligned}$$

$$\chi_{sy} = -\frac{m_{sy} - m_{Ut}}{EI_2} + \chi_{Ut} \quad (6-30)$$

6) $m - \chi$ relationship for softening-yielding region ($\chi_{sy} < \chi \leq \chi_{end}$)

In this region, all steel in RC and UHPC section has reached the yield strain, and UHPC is already in strain softening phase. As discussed in the previous phase, it would be reasonable to consider Whitney's rectangular stress block for compression zone from this region. In order to estimate the compression zone depth of this phase, it is assumed that zero force in the UHPC at the end of this phase valid throughout the whole softening-yielding region.

$$\sum F_x = F_{sU4} + F_{sc4} - F_{cc4} = 0 \quad (6-31)$$

$$f(x_{end}) = -0.85f'_c \cdot 0.85x_{end} + \beta f_{sU, sy} \rho_{sU} d_{sU} + \beta f_{sc, sy} \rho_{sc} d_{sc} = 0 \quad (6-32)$$

$$m_{end} = F_{sc4} \left(d_{sc} - \frac{0.85}{2} x_{end} \right) + F_{sU4} \left(d_U - \frac{0.85}{2} x_{end} \right) \quad (6-33)$$

In this region, only the UHPC contributes to the flexural rigidity of the section, thus,

$$EI_3 = -\frac{dm}{d\chi} \quad (6-34)$$

$$= E_{Uss}^{RU} h_U d_U^2 \left(1 - \frac{0.85}{2} \frac{x_{end}}{d_U} \right) \left(1 - \frac{x_{end}}{d_U} \right)$$

$$\chi_{end} = -\frac{m_{end} - m_{sy}}{EI_3} + \chi_{sy} \quad (6-35)$$

At the end of the strain-softening behavior of the UHPC, only the yield strength of the steel re-bars act as tensile forces on the section. Thus, plastic behavior would occur from the curvature χ_{end} without any variation of the moment at the section.

Then the moment-curvature relationship can be summarized as a multilinear relationship as shown in **Fig 6-7** and expressed as a function of the curvature in Eq.(6-36). It can be confirmed that the estimated moment-curvature relationship of the UHPC-RC composite section is apparently larger than that of the RC section. Based on the results, the same assumptions as the original CSCT were applied about the longitudinal and tangential curvatures depending on the radius from the center of the slab.

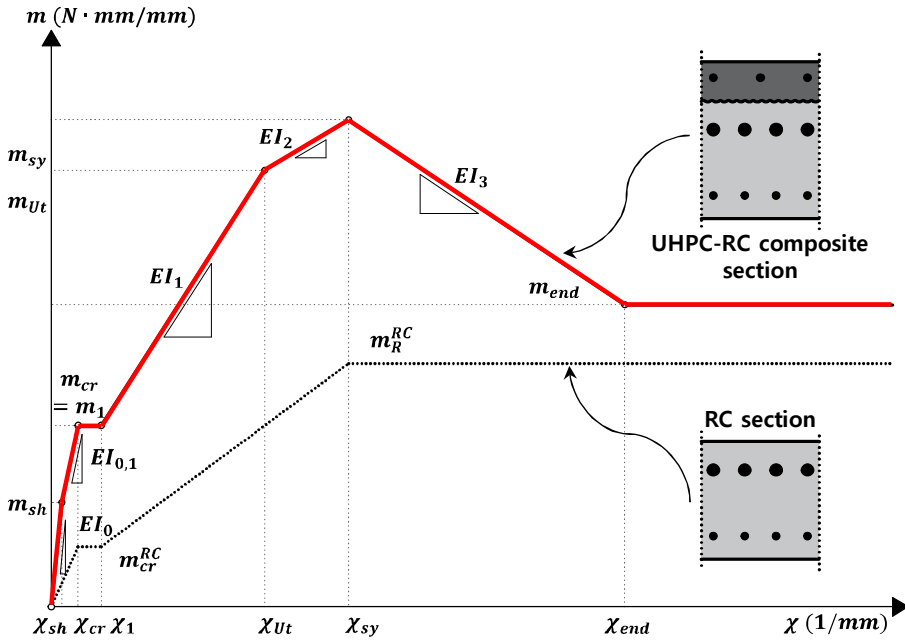


Fig 6-7. Moment-curvature relationship of UHPC-RC composite section

In comparison of the two moment-curvature relationships, as the composite section is formed, performance of the cross section is significantly increased. Moreover, the relationship for RC section can be formulated as simple quadrilinear function, on the other hand, that for UHPC-RC composite section is formulated as multilinear function, which can be attributed to structural behavior of UHPC under tensile loading.

$$\begin{aligned}
 -m(\chi) &= EI_0 \cdot (\chi) & (\chi \leq \chi_{sh}) & \quad (6-36) \\
 &= EI_{0,1} \cdot (\chi - \chi_{sh}) + m_{sh} & (\chi_{sh} < \chi \leq \chi_{cr}) & \\
 &= m_1 = m_{cr} & (\chi_{cr} < \chi \leq \chi_1) & \\
 &= EI_1 \cdot (\chi - \chi_1) + m_1 & (\chi_1 < \chi \leq \chi_{ut}) & \\
 &= EI_2 \cdot (\chi - \chi_{ut}) + m_{ut} & (\chi_{ut} < \chi \leq \chi_{sy}) & \\
 &= EI_3 \cdot (\chi - \chi_{sy}) + m_{sy} & (\chi_{sy} < \chi \leq \chi_{end}) & \\
 &= m_{end} & (\chi_{end} < \chi) &
 \end{aligned}$$

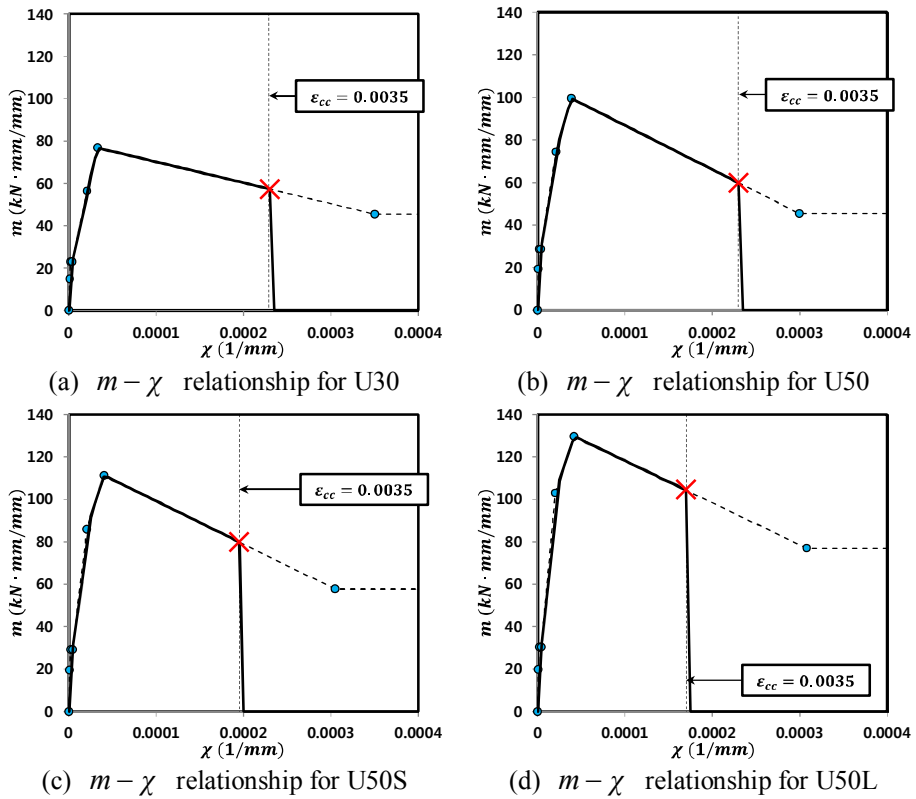


Fig 6-8. Calculated moment-curvature relationship of retrofitted specimens

Fig 6-8 shows the calculation results of moment-curvature relationship of the retrofitted specimens. The multilinear relationship was modelled assuming that when the maximum compressive strain at the tip of the compression fiber reaches 0.0035, the section fails. The relationship of the control specimen was simply calculated based on the quadrilinear moment-curvature relationship proposed by the CSCT.

6.2.3 Load-rotation behavior of UHPC-RC composite slab

Prior to formulate equilibrium equations to obtain the load-rotation behavior of the composite slabs, some important assumptions made during the analysis procedures should be recognized. As the slabs in the present study were supported by fixed condition, idealized form of slab under simply supported condition around the contraflexure line has to be assumed to apply the CSCT, since the model was proposed based on the form of a simply supported circular slab with a circular column located at center. **Fig 6-9** shows the idealized slab with simply supported condition, where r_s is radius of circular isolated slab element, r_q is radius of force introduction at the perimeter and r_c is radius of a circular column, which is calculated as the radius of a circular column having the same area as the square column.

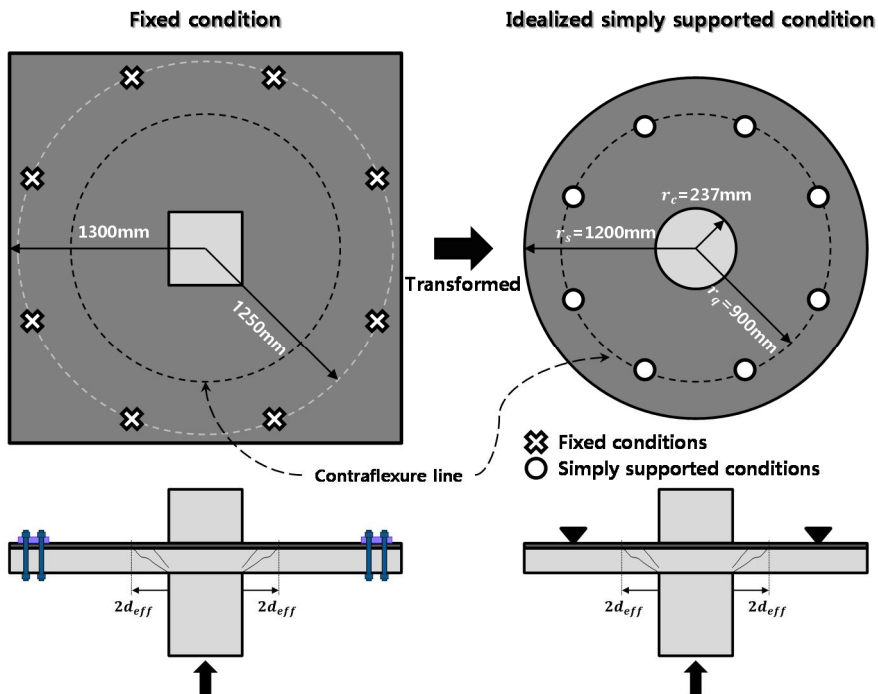


Fig 6-9. Idealized slab under simply supported conditions

Therefore, it is important to assume the appropriate values of r_s and r_q before proceeding the analysis as it is difficult to obtain the position of the contraflexure line theoretically due to the fixed supports being lifted up with increasing load. In this study, the values of r_s and r_q were assumed based on the test results of control specimen (R), and directly applied to all the retrofitted specimens. When the radius r_s and r_q are assumed to be 1200mm and 900mm, respectively, the load-rotation relationship predicted by CSCT appears to quite well simulate the actual test result of control specimen as described in **Fig 6-10**.

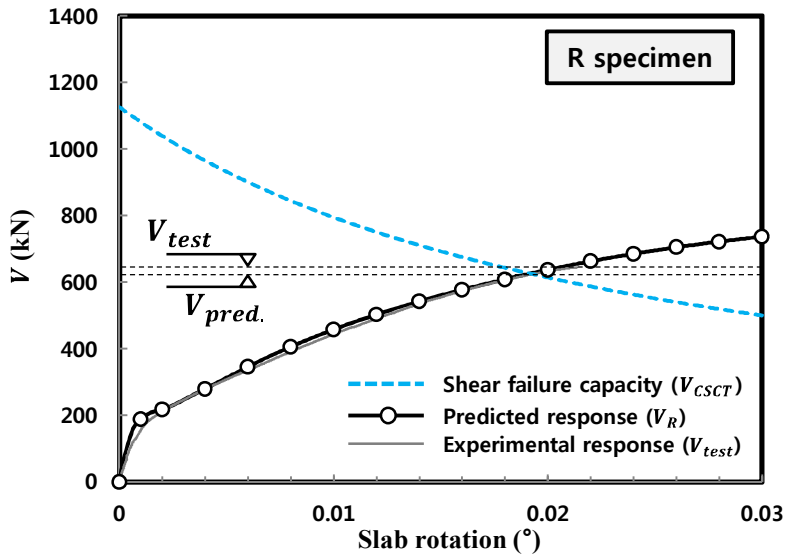


Fig 6-10. Prediction of load-rotation behavior of R through assumed r_s and r_q

Based on these assumptions and assumed values, derivation of the load-rotation behavior of the UHPC-RC composite slab with idealized simply supported condition was performed.

Based on the calculated multilinear moment-curvature relationship of the UHPC-RC composite section and the above assumptions, the load-rotation behavior can be derived by solving simple differential equilibrium equations formulated from a slab portion. In the CSCT, the load-rotation behavior is derived for a slab portion located outside the critical shear crack, which is assumed as a rigid body deforming like a conical shape with a constant slab rotation due to the tangential cracks and the radial curvature are concentrated in the proximity of the column (Muttoni, 2008). This rational approach can be applied to the case of the UHPC-RC composite slab as shown in Fig 6-11.

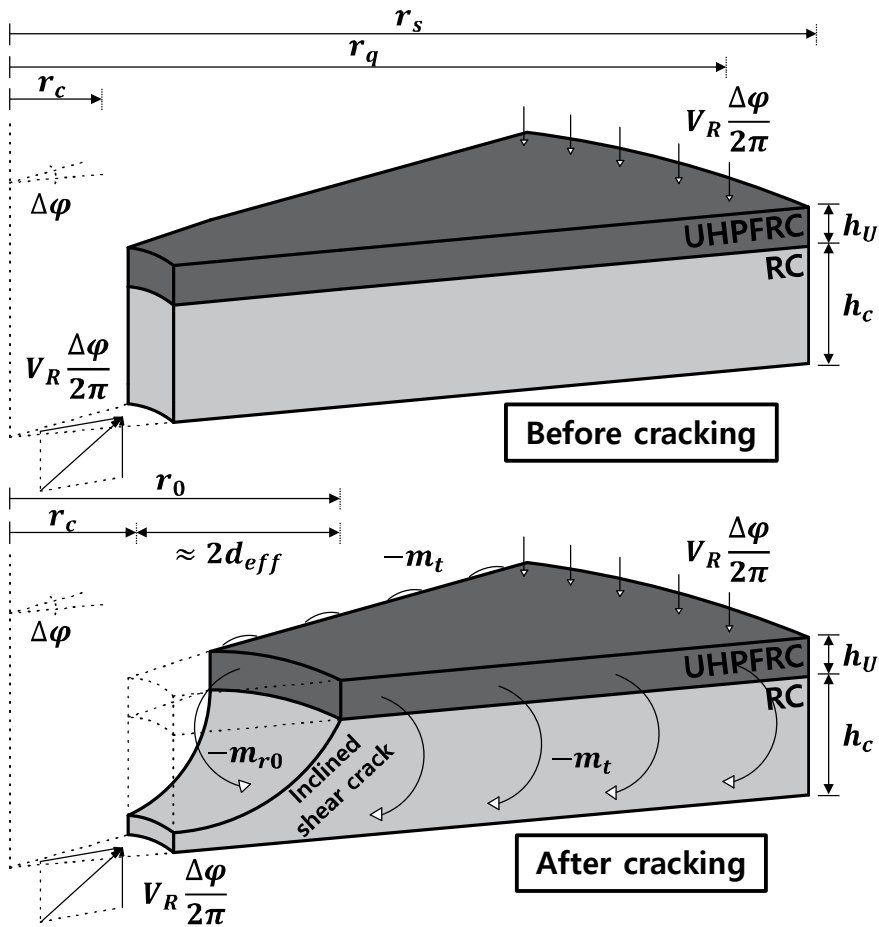


Fig 6-11. Uncracked and cracked stage of UHPC-RC composite slab portion

However, since there are no forces activated at the UHPC overlay around the column in the longitudinal direction due to the discontinuity, the longitudinal moment at the radius r_0 is sure to be different, or rather, smaller than that calculated by the original sector model method. Furthermore, there is no term regarding to the contribution of the UHPC overlay. Thus, in this study, a design method is proposed to derive the load-rotation behavior of the composite slabs through two free body diagrams from a slab portion including the regions inside and outside the critical shear crack, as shown in Fig 6-12, considering the retrofitting condition.

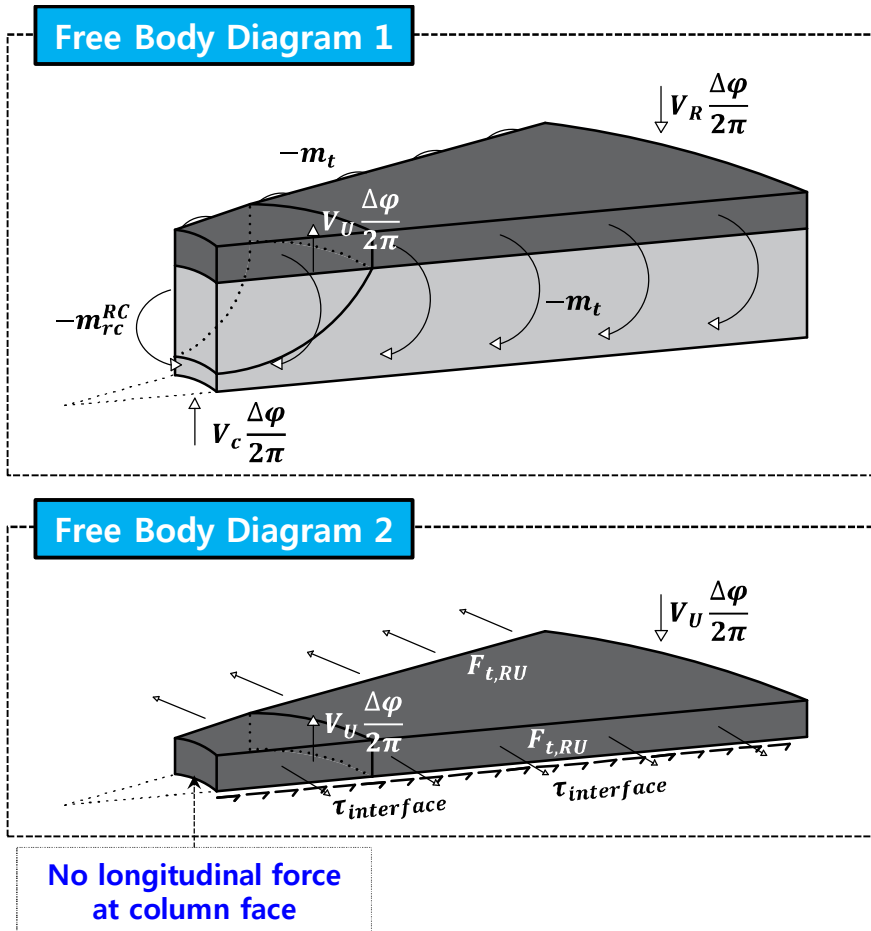


Fig 6-12. Two sets of free body diagram of UHPC-RC composite slab

On the basis of the two sets of free body diagram the moment equilibrium equations Eq.(6-37) and Eq.(6-38) can be derived, which are formulated from the free body diagram 1 and free body diagram 2, respectively. Since the two equilibrium equations were established, each contribution V_c and V_U can be computed as a function of the slab rotation through solving the simultaneous equations

$$V_c \frac{\Delta\varphi}{2\pi}(r_q - r_c) + V_U \frac{\Delta\varphi}{2\pi}(r_q - r_0) = -m_{r_c}^{RC}(\psi) \cdot r_c \cdot \Delta\varphi - \Delta\varphi \cdot \int_{r_c}^{r_s} m_t(\psi, r) dr \quad (6-37)$$

$$V_U \frac{\Delta\varphi}{2\pi}(r_q - r_0) = \Delta\varphi \cdot \frac{h_U}{2} \cdot \int_{r_c}^{r_s} F_{t,RU}(\psi, r) dr \quad (6-38)$$

Meanwhile, as can be seen in free body diagram 2, the contribution of the UHPC overlay V_U is also expressed in terms of the interface shear stress $\tau_{interface}$, which potentially delimits the maximum contribution of the UHPC overlay. In this study, it is assumed that the interface shear stress is uniformly distributed over the entire interface. Additionally, it should be considered that the interface shear stress is activated in two-dimensional stress as described in **Fig 6-13**. Thus, the term V_U can be also expressed as Eq.(6-39).

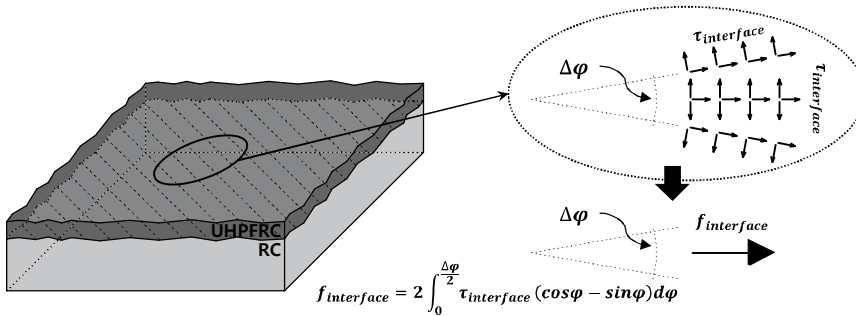


Fig 6-13. Computation of two-dimensional interface shear stress under pure shear

$$\begin{aligned}
 & V_U \frac{\Delta\varphi}{2\pi} (r_q - r_0) \tag{6-39} \\
 &= \frac{h_U}{2} \cdot 2 \cdot \int_{r_c}^{r_s} \int_0^{\Delta\varphi/2} \tau_{interface} (\cos\varphi - \sin\varphi) r d\varphi dr \\
 &= \frac{h_U}{2} \cdot \tau_{interface} \cdot (r_s^2 - r_c^2) \cdot \left(\sin \frac{\Delta\varphi}{2} + \cos \frac{\Delta\varphi}{2} - 1 \right) \\
 &\cong \Delta\varphi \cdot \frac{h_U}{4} \cdot (r_s^2 - r_c^2) \cdot \tau_{interface}
 \end{aligned}$$

As the Eq.(6-38) and Eq.(6-39) are essentially the same equation, the interface shear stress is also expressed as a function of the slab rotation. Thus, the following expression results

$$\tau_{interface} = \tau_{interface}(\psi) \tag{6-40}$$

Finally, the load-rotation behavior of the UHPC-RC composite slab and each contribution of the UHPC overlay and the RC substrate can be calculated as follows. The moment terms in Eq.(6-41) can be computed by Eq.(6-44) and Eq.(6-45). The force term in Eq.(6-42) can be computed by Eq.(6-47).

$$\begin{aligned}
 & V_c(\psi) \tag{6-41} \\
 &= \frac{2\pi}{r_q - r_c} \left(-m_{r_c}^{RC}(\psi) \cdot r_c - \int_{r_c}^{r_s} m_t(\psi, r) dr \right) \\
 &\quad - V_U(\psi) \cdot \frac{r_q - r_0}{r_q - r_c}
 \end{aligned}$$

$$\begin{aligned}
 & V_U(\psi) \tag{6-42} \\
 &= \frac{\pi}{r_q - r_0} \cdot h_U \cdot \int_{r_c}^{r_s} F_{t,RU}(\psi, r) dr \\
 &= \frac{\pi}{r_q - r_0} \cdot \frac{h_U}{2} \cdot (r_s^2 - r_c^2) \cdot \tau_{interface}(\psi)
 \end{aligned}$$

$$V_R(\psi) = V_c(\psi) + V_U(\psi) \tag{6-43}$$

Where, the longitudinal moment of section at radius of r_c is,

$$\begin{aligned}
 -m_{r_c}^{RC}(\psi) &= \frac{m_{cr}^{RC}}{\chi_{cr}} \cdot \left(\frac{\psi}{r_0} \right) && \left(\frac{\psi}{r_0} \leq \chi_{cr} \right) \\
 &= m_{cr}^{RC} && \left(\chi_{cr} < \frac{\psi}{r_0} \leq \chi_1 \right) \\
 &= \frac{m_R^{RC} - m_{cr}^{RC}}{\chi_{sy} - \chi_1} \cdot \left(\frac{\psi}{r_0} - \chi_1 \right) + m_{cr}^{RC} && \left(\chi_1 < \frac{\psi}{r_0} \leq \chi_{sy} \right) \\
 &= m_R^{RC} && \left(\chi_{sy} < \frac{\psi}{r_0} \right)
 \end{aligned} \tag{6-44}$$

and the integration of unit tangential moment along the section is expressed as follows,

$$\begin{aligned}
 -\int_{r_c}^{r_s} m_t dr &= -(r_0 - r_c) \cdot m_{rc}(\psi) + && (6-45) \\
 &\int_{r_0}^{r_{end}} m_{end} dr + && (r_{end} \leq r_s) \\
 &\int_{r_{end}}^{r_{sy}} EI_3 \cdot \left(\frac{\psi}{r} - \chi_{sy} \right) + m_{sy} dr + && (r_{sy} \leq r_s) \\
 &\int_{r_{sy}}^{r_{Ut}} EI_2 \cdot \left(\frac{\psi}{r} - \chi_{Ut} \right) + m_{Ut} dr + && (r_{Ut} \leq r_s) \\
 &\int_{r_{Ut}}^{r_1} EI_1 \cdot \left(\frac{\psi}{r} - \chi_1 \right) + m_1 dr + && (r_1 \leq r_s) \\
 &\int_{r_1}^{r_{cr}} m_{cr} dr + && (r_{cr} \leq r_s) \\
 &\int_{r_{cr}}^{r_{sh}} EI_{0,1} \cdot \left(\frac{\psi}{r} - \chi_{sh} \right) + m_{sh} dr + && (r_{sh} \leq r_s) \\
 &\int_{r_{sh}}^{r_s} EI_0 \cdot \frac{\psi}{r} dr
 \end{aligned}$$

$$-m_{r_c}(\psi) = EI_0 \cdot \left(\frac{\psi}{r_0} \right) \quad \left(\frac{\psi}{r_0} \leq \chi_{sh} \right) \tag{6-46}$$

$$\begin{aligned}
 &= EI_{0,1} \cdot \left(\frac{\psi}{r_0} - \chi_{sh} \right) + m_{sh} && \left(\chi_{sh} < \frac{\psi}{r_0} \leq \chi_{cr} \right) \\
 &= m_1 && \left(\chi_{cr} < \frac{\psi}{r_0} \leq \chi_1 \right) \\
 &= EI_1 \cdot \left(\frac{\psi}{r_0} - \chi_1 \right) + m_1 && \left(\chi_1 < \frac{\psi}{r_0} \leq \chi_{Ut} \right) \\
 &= EI_2 \cdot \left(\frac{\psi}{r_0} - \chi_{Ut} \right) + m_{Ut} && \left(\chi_{Ut} < \frac{\psi}{r_0} \leq \chi_{sy} \right) \\
 &= EI_3 \cdot \left(\frac{\psi}{r_0} - \chi_{sy} \right) + m_{sy} && \left(\chi_{sy} < \frac{\psi}{r_0} \leq \chi_{end} \right) \\
 &= m_{end} && \left(\chi_{end} < \frac{\psi}{r_0} \right)
 \end{aligned}$$

$$\begin{aligned}
 \int_{r_c}^{r_s} F_{t,RU}(\psi, r) dr &= (r_0 - r_c) \cdot F_{t,RU}(\psi, r_0) + && (6-47) \\
 &\int_{r_0}^{r_{end}} \beta f_{sU, sy} \rho_{sU} d_{sU} dr + && (r_{end} \leq r_s) \\
 &\int_{r_{end}}^{r_{sy}} \beta f_{sU, sy} \rho_{sU} d_{sU} dr + && (r_{sy} \leq r_s) \\
 &\int_{r_{end}}^{r_{sy}} \left[E_{Uss}^{RU} (\varepsilon_U - \varepsilon_{Utu}^{RU}) + f_{Utu} \right] h_U dr + \\
 &\int_{r_{sy}}^{r_{Ut}} \beta f_{sU, sy} \rho_{sU} d_{sU} dr + && (r_{Ut} \leq r_s) \\
 &\int_{r_{sy}}^{r_{Ut}} \left[E_{Uss}^{RU} (\varepsilon_U - \varepsilon_{Utu}^{RU}) + f_{Utu} \right] h_U dr + \\
 &\int_{r_{Ut}}^{r_1} \beta E_{sU} \varepsilon_{sU} \rho_{sU} d_{sU} dr + && (r_1 \leq r_s) \\
 &\int_{r_{Ut}}^{r_1} \left[E_{Ush}^{RU} (\varepsilon_U - \varepsilon_{Ute}) + f_{Ute} \right] h_U dr + \\
 &\int_{r_1}^{r_{cr}} \beta E_{sU} \varepsilon_{sU} \rho_{sU} d_{sU} dr + && (r_{cr} \leq r_s) \\
 &\int_{r_1}^{r_{cr}} \left[E_{Ush}^{RU} (\varepsilon_U - \varepsilon_{Ute}) + f_{Ute} \right] h_U dr + \\
 &\int_{r_{cr}}^{r_{sh}} \beta E_{sU} \varepsilon_{sU} \rho_{sU} d_{sU} dr + && (r_{sh} \leq r_s) \\
 &\int_{r_{cr}}^{r_{sh}} \left[E_{Ush}^{RU} (\varepsilon_U - \varepsilon_{Ute}) + f_{Ute} \right] h_U dr +
 \end{aligned}$$

$$\int_{r_{sh}}^{r_s} \beta E_{sU} \varepsilon_{sU} \rho_{sU} d_{sU} dr +$$

$$\int_{r_{sh}}^{r_s} E_U \varepsilon_U h_U dr$$

Where,

$$\varepsilon_U = \frac{\psi}{r} (d_U - x(\psi, r)) \quad (6-48)$$

Since all the terms expressed in Eq.(6-47) are formulated from different depths of compression zone, which is function of ψ and r , the force acting at the UHPC overlay have to be expressed in a very verbose manner as above. However, it is not a difficult concept because it just computes the tangential directional forces acting at the UHPC overlay.

6.2.4 Proposed capacity curves

1) Diagonal shear failure (Mode 1)

Mode 1 failure is a proposed failure mode which is triggered by the diagonal shear crack developed from the RC section, in other words, it is the case that the load carried by the RC section reaches the maximum load carrying capacity. Thus, the capacity curve for Mode 1 can be obtained as Eq.(6-49) by modifying Eq.(2-3) to Eq.(6-50). $V_U(\psi)$ can be obtained from Eq.(6-42).

$$V_{model}(\psi) = V_{c,C SCT}(\psi) + V_U(\psi) \quad (6-49)$$

$$\frac{V_{c,C SCT}(\psi)}{b_{0,eff}d_{eff}\sqrt{f'_c}} = \frac{3/4}{1 + 15\frac{\psi d_{eff}}{d_{g0} + d_g}} \quad (6-50)$$

Where, $b_{0,eff} = 4C + \pi d_{eff}$, C is side length of column and d_{eff} is effective flexural depth considering the effect of the UHPC overlay, f'_c is specified compressive strength of concrete, d_{g0} is reference size set at 16mm and d_g is maximum aggregate size.

2) Debonding failure (Mode 2)

Mode 2 failure is a proposed failure mode governed by the debonding at the interface between the UHPC overlay and concrete due to NIC (Near Interface Cracking), in other words, it is the case that the load carried by the interface reaches the maximum load carrying capacity. Thus, the capacity curve for Mode 2 can be obtained as Eq.(6-51). $V_c(\psi)$ can be obtained from

Eq.(6-41) and Eq.(6-42).

$$V_{mode2}(\psi) = V_c(\psi) + V_{U\max} \quad (6-51)$$

$$V_{U\max} = \frac{\pi}{r_q - r_0} \cdot \frac{h_U}{2} \cdot (r_s^2 - r_c^2) \cdot \tau_{interface,\max} \quad (6-52)$$

Where, $\tau_{interface,\max}$ is the maximum two-dimensional interface shear strength between the UHPC overlay and concrete under pure shear.

In the case of the two-way slabs, as is already referred, the in-plane interface shear stress acts as biaxial stress at the interface. As previously corroborated by Kupfer et al. (Kupfer, 1969), the performance of materials under biaxial stresses is significantly different from that of uniaxial stress. Therefore, the experimental results of the previous studies on the performance of the interface between the UHPC and concrete cannot be directly applied. In the present study, to estimate the two-way interface shear capacity of sand-blasted surface between the UHPC and concrete, the interface is assumed as a type of material which is governed by the Mohr-Coulomb failure criterion. According to this criterion, it is possible to determine the failure envelope given three material constants; 1) cohesion c , 2) coefficient of friction μ , and 3) separation resistance f_A . Then, the failure envelope of the Mohr-Coulomb material can be illustrated as combination of three linear envelopes in $\sigma - \tau$ coordinate system through the obtained parameters. In the stress state inside the failure envelope, the material is in unbroken state, however, when the stress state reaches the envelope, the material will be failed. Thus, the stress state outside the envelope cannot be existed. It should be notified that this linear envelope provides a good approximation for the failure of brittle-ductile materials like concrete in the intermediate stress level.

To determine the maximum biaxial shear strength of the interface, experimental results from four literatures on the interface performance between UHPC and concrete were referred (Lim & Hong, 2016, Tayeh et al., 2011, Muñoz et al., 2014, Li & Rangaraju, 2016). **Table 6-2** shows the collected test data from the four references performed under similar material and interface conditions with the present study. Based on the collected data, Mohr-Coulomb failure criterion of the sand-blasted interface between the UHPC and concrete is induced.

Table 6-2. Collected test data from four literatures on interface performance

Ref.	Test method	I.D.	Material			Test results	
			f'_c	f_t	f_{cU}	$\frac{\sigma}{f_t}$	$\frac{\tau}{f_t}$
			(MPa)	(MPa)	(MPa)	-	-
Lim and Hong (2016)	Slant shear	SC2V0.5	30.5	3.31	141.2	-1.924	3.332
		SC2V1	30.5	3.31	132.2	-1.645	2.849
		SC2V1.5	30.5	3.31	147.6	-1.449	2.509
		SC2V2	30.5	3.31	133.4	-1.962	3.398
		SC6V0.5	83.8	5.49	141.	-3.660	6.338
		SC6V1	83.8	5.49	132.2	-2.280	3.950
		SC6V1.5	83.8	5.49	147.6	-1.848	3.201
		SC6V2	83.8	5.49	133.4	-2.722	4.714
Tayeh et al. (2011)	Slant shear	SB1	38	3.70	170	-2.181	3.777
		SB2	38	3.70	170	-2.501	4.332
		SB3	38	3.70	170	-2.282	3.953
Muñoz et al. (2014)	Slant shear	Sb-60	55.9	4.49	126.5	-2.742	4.837
		Sb-70	55.9	4.49	126.5	-1.115	3.255
	Pull-off	Sb	55	4.5	126.5	0.517	0
Li and Rangaraju (2016)	Slant shear	UHPC2	49.1	4.0	158.2	-3.564	6.173
		UHPC2	49.1	4.20	158.2	0.550	0

$$k = \left(\mu + \sqrt{1 + \mu^2} \right)^2 \quad (6-53)$$

$$k\sigma_1 - \sigma_3 = 2c\sqrt{k} \quad (6-54)$$

$$\sigma_1 = f_A \quad (6-55)$$

Thus, based on the analyzed results, the biaxial interface shear strength under pure shear of sand-blasted interface between the UHPC and concrete is proposed as follows.

$$\tau_{interface,max} = f_A = 0.55f_t \quad (6-56)$$

Where, $f_t = 0.6 \cdot \sqrt{f_c}$ (MPa), as defined in KCI 2012.

In summary, load-rotation behavior and two capacity curves determine the performance point and governing the failure mode of the UHPC-RC composite slab as schematically described in **Fig 6-15**.

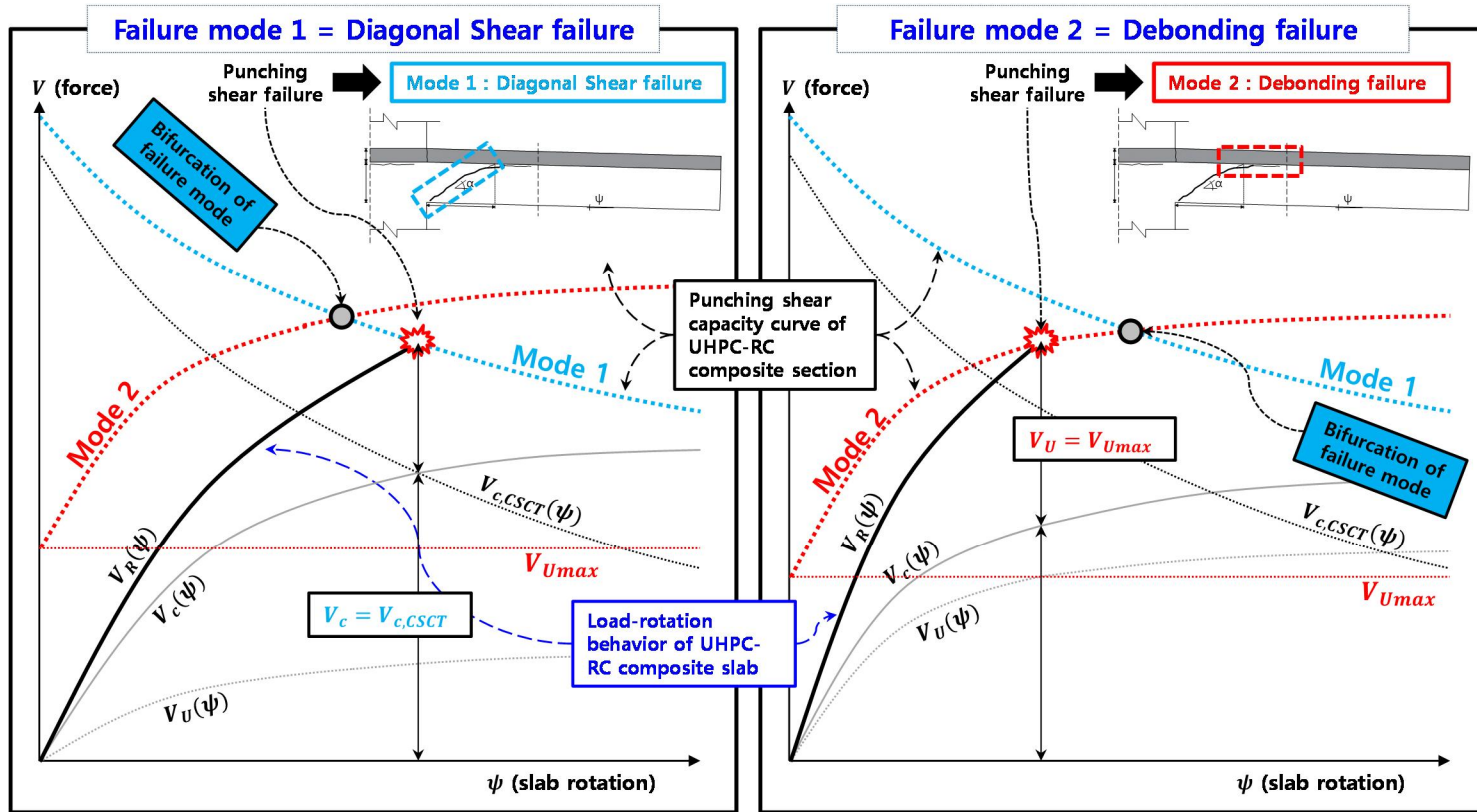


Fig 6-15. Typical load-rotation behavior and capacity curves depending on governing failure modes

6.3 Validation of the Proposed Method

The predicted failure mode and maximum punching shear resistance are determined by the intersection point of the demand curve (load-rotation behavior) and one of the capacity curves (failure criterion) occurring at smaller slab rotation. If the demand curve is not coincided with any of the capacity curves, the specimens would be failed in flexural failure mode. Comparisons between the test results and the predicted results are summarized in **Table 6-3**. The predictions by the proposed method shows a good agreement with the test results with a small value of COV (=2.26%) and the closest average to 1.0 (=1.003). As a result of comparison, the load-rotation behavior of the UHPC-RC composite slabs are quite accurately predicted. Furthermore, all the retrofitted specimens are predicted to be failed in Mode 1 failure as shown in **Fig 6-16**.

Table 6-3. Comparison between experimental test results and predictions

I.D.	Test results			Predicted results by proposed method				Strength ratios		
	ψ_{test}	V_{test}	Failure mode	$\psi_{pred.}$	V_c	V_U	$V_{pred.}$	Failure mode	$\frac{\psi_{test}}{\psi_{pred.}}$	$\frac{V_{test}}{V_{pred.}}$
	(‰)	(kN)	-	(‰)	(kN)		-			
R	21.3	644	FS	19.2	626	-	626	FS	1.11	1.03
U30	15.1	758	S/DB	15.7	712	49	761	S	0.96	1.00
U50	16.2	909	S/DB	14.3	781	143	924	S	1.13	0.98
U50S	14.2	984	S/DB	13.6	824	183	1007	S	1.04	0.98
U50L	15.5	1171	S/DB	12.5	906	229	1135	S	1.24	1.03
Average									1.10	1.00
St.Dev									0.09	0.02
COV(%)									8.49	2.26
Min									0.96	0.98
Max									1.24	1.03

Note) FS=flexure-shear failure, S=shear failure, DB=debonding failure

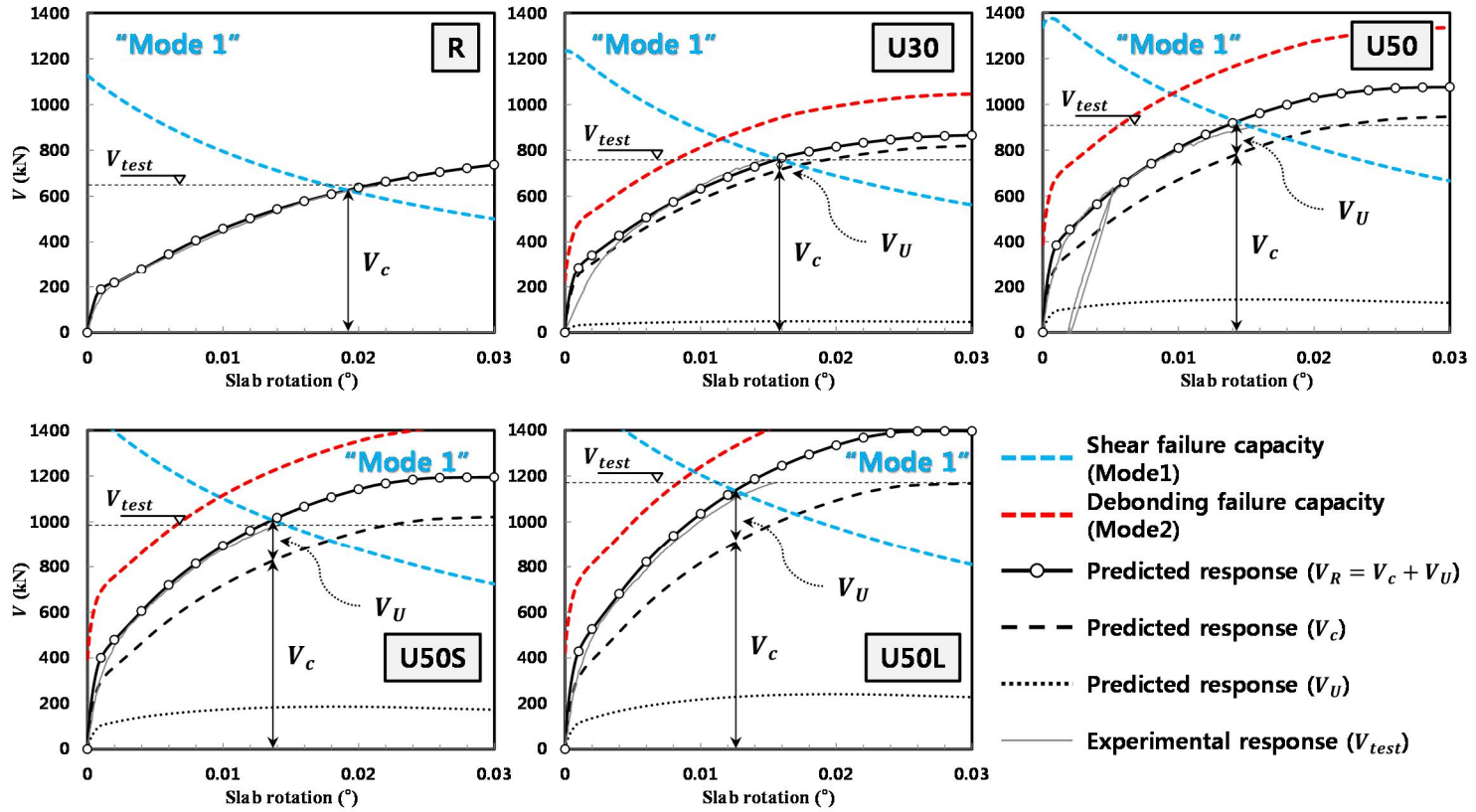


Fig 6-16. Comparison between load-rotation curves and predictions

6.4 Limitation of the Proposed Method

Actually, after cracking due to bending, shear can be transferred in reinforced concrete members by a number of potential actions, whose activation depends much on the shape and kinematics of the critical crack leading to failure. According to Fernandez Ruiz et al. (Fernandez Ruiz et al., 2015), the CSCT failure criterion can be explained by various potential shear-transfer action, where the development of a critical shear crack limits the capacity of the shear-transfer actions. The results show that the contributions of all shear-transfer actions decrease for increasing openings of the critical shear crack and that their decay follows a similar trend. The most critical shear transfer actions are as follows:

- 1) contribution of the top part of the critical shear crack
- 2) contribution of the bottom part of the critical shear crack
- 3) contribution of dowelling action
- 4) contribution of compression chord/arching action

Especially about the dowelling action, this action has shown to be efficient in regions if concrete were cannot develop spalling cracks. This situation can be achieved and further strengthened through adding FRP sheets or a thin layer of concrete overlay on the tension side. Thus, the proposed capacity curves should actually be interpreted by the combined action of the load-transfer mechanisms of the UHPC overlay and the above four actions.

In the present study, in order to exploit the CSCT, the specimens used in this study were assumed virtually as circular slabs having simply supported

condition along the contraflexure line. This assumption provided a fairly good prediction of the load-rotation behavior of the control specimen. Nevertheless, the proposed method should be evaluated against actual test results of UHPC-RC composite slab with simply supported condition for validation of the proposed method.

Applicable range of the proposed method also should be notified. As the model is formulated based on the UHPC-RC slab-column connection with column on top, there should be some modification in the proposed model for applying to the structures such as slab deck of a bridge with no discontinuity at top surface. In such a case, as the longitudinal force acts on the UHPC overlay in the vicinity of the column face as illustrated in **Fig 6-17**, the moment-curvature relationship of UHPC-RC composite section can be used at that section. This would lead to increases of shear resistance as well as flexural rigidity.

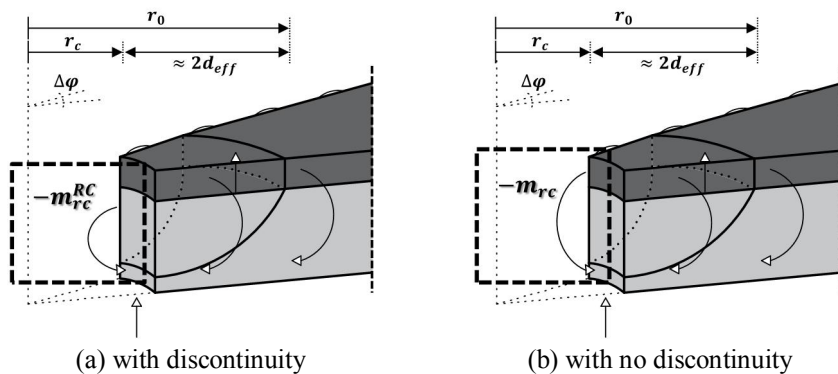


Fig 6-17. Moment at column face depending on discontinuity

Chapter 7. Concluding Remarks

In the present study, RC slab-column connections retrofitted by UHPC overlay on the top surface were experimentally and analytically studied, to evaluate the effects of the UHPC overlay to the punching shear resistance of the composite slabs. A set of test was performed with total of 5 UHPC-RC composite slabs under monotonic loading, focusing on the punching shear strength. All the specimens were failed abruptly in punching shear mode accompanying debonding at the interface. An analytical method to predict load-rotation behavior and capacity curves of the UHPC-RC composite slab was proposed based on the critical shear crack theory (CSCT), while being slightly modified considering the condition of the test specimens. Based on the test results and theoretical analysis, the following conclusions are made:

1. Concentric Loading Test of UHPC-RC Composite Slab

- 1) By adding a thin layer of UHPC, the normalized punching shear resistance increases at least 22% for 30mm UHPC overlay and up to 82 % for 50mm UHPC overlay with steel in it. This confirms that the UHPC overlay acts as a two-dimensional reinforcement.
- 2) The use of steel re-bars in the UHPC overlay has a significant influence on the resistance and deformation of the composite slab, which is different outcome from that of previous research performed by Bastien-Masse (2015). This experimental result directly implies that the load transfer mechanism of the UHPC-RC composite slab should be reconsidered from a slightly different point of view from

the previous study.

- 3) Due to bending efforts, many microcracks are generated in the UHPC overlay, which tend to be more predominant as the reinforcement ratio in the UHPC overlay becomes increased. In addition, the inclined shear cracks generated in the RC section cannot penetrate the UHPC overlay during the test, but rather rotate at the interface and developed to NIC. Therefore, the punching cone shaped cracks on the surface of the UHPC overlay can hardly be distinguished with naked eyes.
- 4) At cut sections, two governing failure modes were observed; (1) diagonal shear failure due to inclined shear cracks in the RC section, and (2) debonding failure at the interface due to NIC. These two failure modes were thoroughly investigated in the theoretical analysis stage, being recognized as major failure mechanisms of the composite slabs.
- 5) Regarding to the deformability, the deformation capacity of the retrofitted specimens turned out to be maintained above a certain level even though the retrofitting level increased, which is unmatched with the conventional sense. Considering the cracking pattern, the out-of-plane bending in the UHPC overlay probably allows the RC section to deform further, leading to comparatively larger deformation and crack opening of the RC section. This implies the additional contribution of the UHPC overlay to shear resistance.
- 6) Near the column, the UHPC layer deflects slightly upward by the force acting at the tip of the inclined shear crack propagated from the RC section, leaving limited horizontal cracking at tension side of RC

section near the column due to geometrical compatibility. This also explicitly means that the layer of UHPC provides additional shear resistance to the cracked RC section.

- 7) A design procedure using several current design code expressions is presented to account for the retrofitting effect of the UHPC overlay on the maximum resistance of a slab by two strategies. As a result, the predictions from ACI, KCI, EC2 and JSCE design expressions do not correctly estimate the punching shear capacity of the UHPC-RC composite slab, but with comparatively high correlation. This clearly means that due to the thin layer of UHPC overlay, not only the punching shear capacity corresponding to the improved flexural capacity is increased, but also the additional shear resistance can be obtained through the additional load transfer mechanism at the interface between RC section and UHPC overlay.

2. Theoretical Analysis

- 1) Aimed at precisely analyzing the structural behavior and failure mechanisms, this study applies the CSCT with slight modification to the RC slab-column connections retrofitted by the UHPC overlay with or without steel re-bars in it. The validity of the proposed method was confirmed by means of comparing the experimental results with the predicted results.
- 2) A multilinear moment-curvature relationship of the UHPC-RC composite section is used with the slightly modified sector model regarding to the two sets of free body diagram to predict the load-rotation behavior of a slab subjected to a point force. By using the proposed method, each contribution of the RC section and the UHPC

overlay to the total punching shear resistance is calculated.

- 3) The contribution of the UHPC overlay is calculated by solving the simple differential equations set up from the new free body diagram. As the contribution of the UHPC overlay depends on not only the thickness of the layer, but also the function of the interface shear strength, the maximum value of the contribution depends on the performance level of the interface. Thus, for better performance, the UHPC overlay must provide a good bond with the RC section.
- 4) Based on the two failure modes observed through the experimental test, two capacity curves corresponding to each failure mode are proposed as failure criterion of the UHPC-RC composite slab; 1) diagonal shear failure in RC section: $V_{model1}(\psi) = V_{c,C SCT}(\psi) + V_U(\psi)$, and 2) debonding failure at interface : $V_{model2}(\psi) = V_c(\psi) + V_{Umax}$. The performance point and corresponding failure mode are determined by the point at which the demand curve crosses one of the capacity curves occurring at smaller slab rotation.
- 5) It is noteworthy that the proposed method directly reflects the materialistic and geometric characteristics of the UHPC overlay. In addition, it appears that by increasing the thickness of the UHPC overlay and the amount of steel re-bars in it, the load-carrying capacities of the layer of UHPC as well as the RC substrate become greater, ultimately leading to higher shear resistance.
- 6) The proposed method predicts well the load-rotation behavior and the maximum punching shear resistance of the UHPC-RC composite slab with a good agreement, with a small value of COV (=2.27%) and the closest average to 1.0 (=1.003).

References

1. ACI Committee 318. (2011). Building Code Requirements for Structural Concrete (ACI 318-11) and Commentary (pp. 503). Farmington Hill, MI: American Concrete Institute.
2. Bastien-Masse, M., and Brühwiler, E., (2016). Experimental investigation on punching resistance of R-UHPFRC–RC composite slabs. *Materials and Structures*, 49(5), 1573-1590.
3. British Standards Institution. (2004). Eurocode 2: Design of Concrete Structures – Part 1-1: General Rules and Rules for Building (pp. 225). Bruxelles, Belgium: European Standard EN-1992-1-1:2004:E, European Committee for Standardization.
4. Carbonell Muñoz, M. A., Harris, D. K., Ahlborn, T. M., and Froster, D. C. (2013). Bond performance between ultrahigh-performance concrete and normal-strength concrete. *Journal of Materials in Civil Engineering*, 26(8), 04014031.
5. Choi, K. K., and Park, H. G. (2004). Strength model for punching shear of flat plate-column connections. *Journal of the Korea Concrete Institute*, 16(2), 163-174.
6. Fehling, E., Schmidt, M., Walraven, J., Leutbecher, T., and Fröhlich, S. (2013). BetonKalender: Ultra-High Performance

-
- Concrete UHPC, Fundamentals Design, Examples (pp. 188). *Ernst & Sohn*.
7. Graybeal, B. A. (2006). *Material property characterization of ultra-high performance concrete* (No. FHWA-HRT-06-103).
 8. Guandalini, S., Burdet, O. L., and Muttoni, A. (2009). Punching tests of slabs with low reinforcement ratios. *ACI Structural Journal*, 106(1), 87.
 9. Habel, K., Denarié, E., and Brühwiler, E. (2006). Structural response of elements combining ultrahigh-performance fiber-reinforced concretes and reinforced concrete. *Journal of Structural Engineering*, 132(11), 1793-1800.
 10. Habel, K., Denarié, E., and Brühwiler, E. (2007). Experimental investigation of composite ultra-high-performance fiber-reinforced concrete and conventional concrete members. *ACI Structural Journal*, 104(1), 93.
 11. Harries, K. A., Zeno, G., and Shahrooz, B. (2012). Toward an improved understanding of shear-friction behavior. *ACI Structural Journal*, 109(6), 835.
 12. Japan Society of Civil Engineers. (2010). *Standard Specifications for Concrete Structures-2007 'Design'* (pp. 469). Tokyo, Japan: Japan Society of Civil Engineers.
 13. Jungwirth, J., and Muttoni, A. (2004). Structural behavior of

- tension members in Ultra High Performance Concrete. In *International symposium on ultra high performance concrete* (No. EPFL-CONF-111692). International Symposium on Ultra High Performance Concrete.
14. Kinnunen, S., and Nylander, H. (1960). *Punching of concrete slabs without shear reinforcement* (p. 112). Elander.
15. Korea Concrete Institute. (2012). Korean Structural Design Code (KCI 2012) (pp. 342). Seoul, Korea. (in Korean)
16. Kupfer, H., Hilsdorf, H. K., and Rusch, H. (1969, August). Behavior of concrete under biaxial stresses. In *Journal Proceedings* (Vol. 66, No. 8, pp. 656-666).
17. Li, Z., and Rangaraju, P. R. (2016). Effect of Surface Roughness on the Bond Performance Between Ultra-High Performance Concrete and Precast Concrete in Bridge Deck Connections. In *Transportation Research Board 95th Annual Meeting* (No. 16-6355).
18. Lim, W. Y., and Hong, S. G. (2016). Slant Shear Tests for Determining the Interfacial Shear Strength of Concrete Strengthened with Ultra-High Performance Fiber Reinforced Concrete. *Journal of Korea Concrete Institute*, 28(6), 637-646.
19. Marí, A., Bairán, J., Cladera, A., Oller, E., and Ribas, C. (2015). Shear-flexural strength mechanical model for the design and assessment of reinforced concrete beams. *Structure and*

-
- Infrastructure Engineering*, 11(11), 1399-1419.
20. Muttoni, A. (2008). Punching shear strength of reinforced concrete slabs without transverse reinforcement. *ACI structural Journal*, 105(EPFL-ARTICLE-116123), 440-450.
21. Muttoni, A., and Fernández Ruiz, M. (2008). Shear strength in one-and two-way slabs according to the Critical Shear Crack Theory. In *fib Symposium, Amsterdam 2008* (No. EPFL-CONF-121522). fib Symposium, Amsterdam 2008.
22. Muttoni, A., and Schwartz, J. (1991). Behavior of beams and punching in slabs without shear reinforcement. In *IABSE colloquium* (Vol. 62, No. EPFL-CONF-111612, pp. 703-708). IABSE Colloquium.
23. Nielsen, M. P., and Hoang, L. C. (1999). *Limit analysis and concrete plasticity*. CRC press, pp. 21-32.
24. Noshiravani, T., and Brühwiler, E. (2013). Analytical model for predicting response and flexure-shear resistance of composite beams combining reinforced ultrahigh performance fiber-reinforced concrete and reinforced concrete. *Journal of Structural Engineering*, 140(6), 04014012.
25. Noshiravani, T., and Brühwiler, E. (2013). Experimental investigation on reinforced ultra-high-performance fiber-reinforced concrete composite beams subjected to combined bending and shear. *ACI Structural Journal*, 110(2), 251.

26. Park, H. G., Choi, K. K., and Chung, L. (2011). Strain-based strength model for direct punching shear of interior slab–column connections. *Engineering Structures*, 33(3), 1062-1073.
27. Rocha, D. W. (2012). *Flexural strengthening by means of a rc overlay in the tension zone* (Doctoral dissertation, Faculdade de Ciências e Tecnologia).
28. Ruiz, M. F., Muttoni, A., and Sagaseta, J. (2015). Shear strength of concrete members without transverse reinforcement: A mechanical approach to consistently account for size and strain effects. *Engineering structures*, 99, 360-372.
29. Tayeh, B. A., Bakar, B. A., and Johari, M. M. (2013). Characterization of the interfacial bond between old concrete substrate and ultra high performance fiber concrete repair composite. *Materials and structures*, 46(5), 743-753.
30. Wuest, J. (2007). *Comportement structural des bétons de fibres ultra performants en traction dans des éléments composés* (Doctoral dissertation, Ecole Polytechnique Fédérale de Lausanne). (in French)
31. Yoo, D. Y., and Yoon, Y. S. (2016). A Review on Structural Behavior, Design, and Application of Ultra-High-Performance Fiber-Reinforced Concrete. *International Journal of Concrete Structures and Materials*, 10(2), 125-142.

국 문 초 록

무량판 구조시스템의 슬래브-기둥 접합부는 시스템 내에서 부모멘트와 전단력에 의한 가장 큰 조합응력이 작용하는 부위로, 무량판 구조의 붕괴를 일으킬 수 있는 취약적인 파괴 모드 중 하나인 뚫림전단파괴에 굉장히 취약한 곳이다. 최근 고층 건물의 활성화와 가변형 건축평면 및 교량 슬래브 상판 보강에 대한 수요가 증가하고 있는 추세로, 시공성 및 경제성 측면에서 효율적인 슬래브-기둥 접합부의 보강 방법에 대한 연구가 필요한 실정이다.

초고성능 콘크리트 (Ultra-High Performance Concrete, 이하 UHPC)는 1990년대 중반에 개발된 신재료로서, 내구성, 압축 및 인장 강도와 같은 역학적 특성에서 고성능을 발휘하여 차세대 건설재료로 각광받아 연구자 및 시공기술자들로부터 많은 연구가 이루어져 왔다. 특히 단면중타 공법, 오버레이 공법 등 기존 철근콘크리트 구조물의 보수보강에 사용되어 휨 및 전단 내력 등 구조적 성능을 크게 향상시키는 것이 연구를 통해 다수 보고되었다. 하지만, 상용화가 다수 진전된 상황에도 불구하고 이러한 합성 부재의 뚫림전단강도에 대한 연구는 미비한 실정이다.

따라서 본 연구에서는 UHPC 오버레이가 뚫림전단내력 향상에 기여하는 기제를 분석하기 위하여, UHPC-RC 합성 슬래브의 집중단조가력 실험을 수행하였다. 실험변수는 UHPC 오버레이의 두께와 오버레이 내에 배근되는 철근량이며, 무보강 실험체 포함 총

5 매의 실험체가 제작되었다. 또한 계면에서의 효율적인 하중 전달을 위해 샌드블라스팅 공법으로 계면을 처리한 후 UHPC 를 타설하였다. 실험 결과는 보강을 통해 최대전단내력과 구조적 강성이 증대됨을 보였으며, 특히 두 가지 파괴모드에 의해 거동이 지배되는 것으로 나타났다: 1) 대각전단균열에 의한 RC 단면의 전단파괴와 2) UHPC 와 RC 계면의 균열에 의한 계면분리파괴. 현행설계기준의 적용가능성을 평가하기 위해 두 가지 전략을 통해 UHPC-RC 합성 슬래브의 예측강도를 산정하였다. 하지만 UHPC 오버레이가 뿔립전단내력을 향상시키는 메커니즘을 잘 반영하지 못하여 예측결과와 실험결과는 큰 편차를 보였다.

실험 결과에 근거하여, UHPC-RC 합성 슬래브의 거동과 전단내력을 평가하기 위해 수정된 CSCT 에 기반한 분석 모델을 제안하였다. 제안된 방법을 통해 UHPC-RC 합성 슬래브 거동에 대한 RC 슬래브와 UHPC 오버레이의 기여분을 각각 산정 가능하고, 이를 토대로 요구 곡선 (하중-회전각 거동) 및 역량 곡선 (파괴 기준) 작성이 가능하다. 본 연구의 실험결과를 제안된 방법의 검증에 사용한 결과, 제안된 방법은 UHPC-RC 합성 슬래브의 거동과 파괴 모드를 잘 예측할뿐 아니라, 낮은 변동계수와 1.0 에 근접한 평균값을 보이며, 기존 예측식들보다 균일한 예측결과를 보였다.

주요어 : CSCT; 뿔립전단강도; 보강; 슬래브-기둥 접합부; UHPC 오버레이

학 번 : 2015-22846